SEPARATION OF CESIUM FROM SIMULATED HIGH LEVEL WASTE USING ELECTRODIALYSIS ION EXCHANGE

By

MAHENDRA CHINTHALA

(ENGG02201004009)

Indira Gandhi Centre for Atomic Research, Kalpakkam

A thesis submitted to the
Board of Studies in Engineering Sciences
In partial fulfillment of requirements
for the Degree of

DOCTOR OF PHILOSOPHY

of

HOMI BHABHA NATIONAL INSTITUTE

July, 2015

Homi Bhabha National Institute

Recommendations of the Viva Voce Committee

As members of the Viva Voce Committee, we certify that we have read the dissertation prepared by **Mahendra Chinthala** entitled "**Separation of Cesium from simulated High Level Waste using Electrodialysis Ion exchange**" and recommend that it may be accepted as fulfilling the thesis requirement for the award of Degree of Doctor of Philosophy.

Chairman – Dr. M. Sai Baba		**Date:**	22/3/16
Guide / Convener – Dr. P.M. Satya Sai	PM Satya Sai	**Date:**	22/3/16
Examiner – Prof. P.S.T. Sai		**Date:**	22/03/16
Member 1 – Dr. S. Rangarajan		**Date:**	22/03/2016
Member 2- Dr. N. Sivaraman	N. Sivaraman	**Date:**	22/3/16

Final approval and acceptance of this thesis is contingent upon the candidate's submission of the final copies of the thesis to HBNI.

I hereby certify that I have read this thesis prepared under my direction and recommend that it may be accepted as fulfilling the thesis requirement.

Date: 22/3/16

Place: Kalpakkam

PM Satya Sai
(Guide)

STATEMENT BY AUTHOR

This dissertation has been submitted in partial fulfillment of requirements for an advanced degree at Homi Bhabha National Institute (HBNI) and is deposited in the Library to be made available to borrowers under rules of the HBNI.

Brief quotations from this dissertation are allowable without special permission, provided that accurate acknowledgement of source is made. Requests for permission for extended quotation from or reproduction of this manuscript in whole or in part may be granted by the Competent Authority of HBNI when in his or her judgment the proposed use of the material is in the interests of scholarship. In all other instances, however, permission must be obtained from the author.

(Mahendra Chinthala)

DECLARATION

I, hereby declare that the investigation presented in the thesis has been carried out by me. The work is original and has not been submitted earlier as a whole or in part for a degree at this or any other Institution /University.

(Mahendra Chinthala)

List of Publications arising from the thesis

Journal

1. "Separation of cesium by Electrodialysis-Ion exchange using AMP-PAN", Ch. Mahendra, Suranjen Bera, C. Anand Babu, K.K. Rajan, Separation Science and Technology, 2013, 48, 2473-2478.

2. "Current -Voltage characteristics in EDIX for separation of cesium from AMP-PAN", Ch. Mahendra, P.M. Satya Sai, C. Anand Babu, Desalination, 2014, 353, 8-14.

3. "Analysis and modeling of fixed bed sorption of cesium by AMP-PAN", Ch. Mahendra, P.M. Satya Sai, C. Anand Babu, K. Revathy, K.K. Rajan, Journal of Environmental Chemical Engineering, 2015, 3, 1546–1554.

4. "Transport phenomena in electrodeionization of cesium from AMP-PAN", Ch. Mahendra, P.M. Satya Sai, C. Anand Babu, K. Revathy, K.K. Rajan (Manuscript under preparation).

Book Chapter

1. "Application of Thomas Model for ion exchange of cesium on AMP-PAN", Ch. Mahendra, P.M. Satya Sai, C. Anand Babu, K. Revathy, K.K. Rajan, Chemical and bioprocess Engineering; Trends and Development, Apple Academic Press, Taylor and Francis Group (Chapter-12).

Conferences

1. "Separation of cesium from simulated High Level Waste using Electrodialysis Ion exchange", Ch. Mahendra, Suranjen Bera, C. Anand Babu, K.K. Rajan, SESTEC12, Mithibai College, Mumbai, Feb 27, 2012.

2. "Application of Thomas Model for ion exchange of cesium on AMP-PAN", Ch. Mahendra, P.M. Satya Sai, C. Anand Babu, K. Revathy, K.K. Rajan, International Conference on Chemical and Bioprocess Engineering, NITW, Warangal, Nov 23, 2013.

3. "Electrodeionization of cesium from AMP-PAN", Ch. Mahendra, P.M. Satya Sai, C. Anand Babu, K. Revathy, K.K. Rajan, CHEMCON13, ICT, Mumbai, Dec 27, 2013.

4. "Intergration of Ion exchange and Electrodialysis for the separation of cesium form simulated High Level Waste", Ch. Mahendra, P.M. Satya Sai, C. Anand Babu, K. Revathy, K.K. Rajan, Interenational Conference on Innovative Technologies and Management for Water Security, NIOT, Chennai, Feb 12, 2014.

5. "Effect of electrolytes concentration on recovery of cesium from AMP-PAN by Electrodialysis- Ion exchange (EDIX)", Ch. Mahendra, P.M. Satya Sai, C. Anand Babu, K. Revathy, K.K. Rajan, "SESTEC 14, BARC, Mumbai, Feb 25-28, 2014.

(Mahendra Chinthala)

Dedicated to

My Parents

ACKNOWLEDGEMENT

I express my sincere gratitude towards Dr. P.M. Satya Sai, Deputy General Manager, Nuclear Recycle Board, Bhabha Atomic Research Centre Facilities, for granting me the privilege to carry out this dissertation work under his guidance. I acknowledge his valuable insight and persistent support.

I am very thankful to Dr. C. Anand Babu, former Associate Director, Component Development Group, for providing me exciting and challenging research problems with excellent research facilities.

I am grateful to Dr. M. Sai Baba, Chairman, Doctoral Committee and Associate Director, Resources Management Group, for his continuous encouragement. I am thankful to my other doctoral committee members: Dr. N. Sivaraman, Head, Solution Chemistry and Separation Science Section, Chemistry Group and Dr. S. Rangarajan, Water and Steam Chemistry Division, BARC Facilities, for their constructive suggestions. I would like to thank my former doctoral committee member Dr. S.V. Narasimhan, Associate Director, Chemistry Group, BARC Facilites, for giving valuable suggestions during our interactions.

I am extremely grateful to Shri. K.K.Rajan, Director, Fast Reactor Technology Group, for his constant support and encouragement. I take immense pleasure in thanking Shri. G. Padma Kumar, Head, Chemical Technology Division, FRTG, for providing facilities to carry out my experiments. I thank Shri. G. Mohanakrishnan, Head, Chemical Engineering Services Section, FRTG for great support and help during my research.

My sincere thanks are due to Dr. B.K. Sharma, Manager, Demonstration Facility for Metal Fuel Fabrication, for his valuable suggestions and cooperation during the research work. I wish to record my sincere thanks to Shri. Muralidaharan, Shri. Murugappa, Mrs. K. Revathy, Mrs. M. Mythili, Shri. S.Sujish, Shri. Sourabh Agarwal, Mrs. Jinimol Joy, Shri. Asif Ahmad Bhat, Shri. Suresh, Shri. Jobey Joseph, Shri. Nagaraj, Shri. Marikumaran, Shri. Nandakumar, Shri. Kannan, Shri. Srinivasan, Shri. Anbaraasan, Shri. Sridharan, Shri. Alaghar, Shri.Venkatachalam, Shri. Radha, Smt. Priya and Smt. Maragatham for their kind help and support. I wish to thank Suranjen Bera, Chemistry Group and Rahul Trika, Reprocessing Group, for their unforgettable support. I profoundly thank all the technical and non-technical members of chemical technology division for their valuable co-operation during my research work.

I feel extremely fortunate to have friends like Dhanasekaran, Srihari, Deepak, Pradeep, Sadu, Ramana, Avinash, Kalyan, Bendict, Prasana, Hari Prasad, Samba, Siva Kesava Reddy, Maasilamani and Yadgiri who were always with me in any situation. I would like to thank all my school and college friends who have encouraged me in all the ways.

I heartfelt gratitude to my parents, Shri. Malakondaiah and Smt. Tirupathamma, grandmother Smt. Atchamma, sisters Smt. Srilakshmi, Smt. Madhavi, brother T. Srinivasulu, brothers-in-law Shri. K. Sreedhar and Shri. B. Ashok and other relatives for their endless love, affection, support, and encouragement.

(Mahendra Chinthala)

CONTENTS

Title **Page No.**

Synopsis

Energy is essential for the survival and growth of modern human civilization and is a vital factor in nation's economic development. In view of the growing demand for energy in developing countries like India, the quest for new resources of energy is ever increasing. Combustion of fossil fuels (oil, gas and coal) emits greenhouse gases and there is an inadequate availability of fossil fuels to sustain the future demand. The life cycle emissions (from mining of ore to waste disposal) of nuclear power are very low, between 2.5 and 5.7 gCeq/kWh (grams of Carbon Equivalent per unit of electricity) as against 206 to 357 gCeq/kWh in case for coal and 106 to 188 gCeq/kWh for gas technologies [1]. Every unit of nuclear power generated saves 1 kg of CO_2 emissions [2]. 10,000 MWe nuclear power plant needs only about 300–350 tons of enriched fuel per annum, as against 35–50 million tons of coal needed for a coal fired thermal power station of the same capacity, thus requiring about a shipload or 20 trainloads per day to transport the coal [2]. In view of this, nuclear energy is accepted as a no green-gas emitting alternative to burning of fossil fuels. Presently about 15-20 % of the world's electricity requirement is fulfilled by the 441 nuclear power plants installed in over 31 countries [3].

In nuclear power plants, controlled nuclear fission is carried out in nuclear reactors and the liberated energy during fission is used for electricity production. The three-stage nuclear power programme of India has been planned based on a closed fuel cycle concept, requiring reprocessing of spent fuel from every reactor. The objective is to judiciously utilize mined uranium and thorium resources of the country to a maximum extent. In the closed nuclear fuel cycle, U and Pu are recovered from the spent fuel by the well known PUREX process. After reprocessing of the spent fuel, the challenging aspect is the safe management of nuclear waste. The nuclear waste contains heat emitting fission products like ^{137}Cs, ^{90}Sr, minor actinides (^{241}Am, ^{243}Am, ^{245}Cm and ^{237}Np), along with the structural elements like Fe, Cr, Zr.

^{135}Cs and ^{137}Cs are the main fission products from thermal fission of ^{235}U, along with ^{90}Sr.Increased operation of nuclear reactors results in the production of radioactive Cs isotopes. Due to the half life of cesium isotopes ^{134}Cs ($t_{1/2}$= 2.06 y), ^{135}Cs ($t_{1/2}$= 2×10^{6} y), and 137 Cs ($t_{1/2}$= 30.2 y), these need to be isolated from the environment for several hundreds of years. ^{137}Cs is the major source of decay heat in High Level Waste (HLW) due to its large heat output (0.42 W/g). Along with this, the chemical similarity of Cs with Na can lead to serious problem of interference of these nuclides in the biological system of human beings. Separation of ^{137}Cs from High Level Liquid Waste (HLLW) would markedly reduce the radiation fields in subsequent operations and provides a significant heat source reduction in the repository. Besides these, long half life and high energy gamma rays emitted from ^{137}Cs make this radionuclide a viable alternative source for gamma irradiators to replace the commonly used ^{60}Co ($t_{1/2}$=5.2 y, γ = 1173 keV and 1332 keV) for the sterilization of medical accessories, food preservation, brachytherapy, blood irradiation, hygienization of sewage sludge etc [4, 5].

Several methods like co-precipitation [6, 7], solvent extraction [8-10], and ion exchange [11-15] have been used to separate ^{137}Cs from HLLW. Among these techniques, ion exchange is one of the most promising processes on account of its compactness of operation, capability to achieve decontamination factors of several orders of magnitude by employing selective ion exchangers and amenability for remote operation. Inorganic ion exchange materials like natural zeolite [11, 12, 15], hexacyanoferratecomplexes [13, 14], phosphates [16-18], silicotitanates [19, 20], AMP based sorbents [21-29] have been extensively investigated for cesium removal from aqueous waste. Resorcinol formaldehyde is employed for treatment of Cs bearing in Indian nuclear programme [30-32].

Among the ion exchangers studied, ammonium molybdophosphate (AMP) was shown to be highly selective for Cs in acidic medium. The main disadvantage of AMP is its microcrystalline structure, which makes the column operation difficult. To improve the column properties of AMP, several researchers tried different combinations of AMP with different organic polymers, silica gel, Al_2O_3 and zirconium phosphate. Sebesta [21] developed AMP–PAN by immobilizing ammonium molybdophosphate (AMP) on polyacrylonitrile (PAN) polymer support. AMP–PAN has been extensively reported for removing ^{137}Cs from acidic and high salted radioactive waste stream [22, 24-26] . Since cesium replaces ammonium ion on the exchanger, regeneration of AMP-PAN or recovery of sorbed cesium should be carried out with ammonium salt solutions of high concentrated ions. This not only reduces the life of the ion exchange material but also results in a solution of Cs high in concentration of ammonium ions making the recovery of Cs from these solutions difficult.

In view of these difficulties, a hybrid electro-dialysis ion exchange (EDIX) process has been investigated for the separation of cesium from simulated high level liquid waste, with a view to minimize the waste generation and to reduce the steps involved in the process. In this process, a simulated waste solution containing Cs in 4N HNO_3 was passed through AMP-PAN packed in a column, for selective sorption of Cs on the resin. Cs composition in HLLW depends on the type of reactor, burn-up and concentration effected prior to storage. Based on these factors, ^{137}Cs content in these wastes varies from 10 to several thousands of ppm [19, 31, 33, 34]. Based on literature review, 750 ppm Cs^+ in 4N HNO_3 is used for Cs sorption studies on AMP-PAN which gives a column loading capacity of around 32 mg/g of resin. After loading Cs^+ on AMP-PAN, it is kept in the middle compartment of a three compartment electrodialysis cell. The eluant (ammonium sulphate) is passed through the anode compartment and electrolytes (dilute HNO_3) through the other two compartments. On application of potential, ammonium ions form the anode compartment migrate towards cathode through the middle compartment. Cs (on AMP-PAN) in the middle compartment gets replaced with ammonium ion from anode compartment and the replaced Cs starts migrating towards cathode, where it gets concentrated. Consequently, Cs is separated from waste using AMP-PAN and the separated Cs is recovered from the ion exchange resin in cathode compartment of an electrodialysis cell.

Cs is concentrated in a small volume in the cathode compartment, along with some ammonium hydroxide, which is generated due to migration of small amounts of ammonium ions and generation of hydroxyl ions at the cathode. Ammonia gas can be easily removed with simple distillation by recirculating the contents of the cathode compartment. Thus, pure Cs can be obtained with minimum steps of operations by EDIX. Various parameters affecting the Cs recovery in EDIX system have been studied in the present study. A mathematical model (Nernst-Plank) was applied to investigate the transport phenomena of metal ions through the packed bed (AMP-PAN) in electro-dialysis system.

This thesis is organized into six chapters.

The first chapter gives the details of India’s nuclear programme towards meeting the energy demand in the country and consequent inventory of HLLW. Different types of nuclear fuel cycle options available are presented and the rationale for opting for a closed fuel cycle for future energy security is explained. Various processing steps involved in aqueous and non-aqueous processes are briefly summarized. The classification of waste as low level liquid waste (LLW), intermediate level waste and high level waste (HLW) and treatment philosophy for different categories is elaborated. The need for removal of Cs-137 from radioactive waste and its important applications have also been described.

Various methods and materials have been proposed for the separation of cesium from acidic as well as basic solutions. The solvent extraction methods involving crown ethers, calixarenes and calix-crowns [35] reported for separation of cesium from acidic waste solutions are discussed. Various transition metal ferrocyanides like copper and nickel ferrocyanides which are widely used for co-precipitation are also indicated. Ion exchangers like Ferro cyanides, AMP-based materials, Zeolites and other materials are listed. Other methods like precipitation co-flotation, chromatographic extraction, and electrochemical separations like Electrodialysis- Ion exchange / electrodeionization are also briefly explained. The chapter also lists the aims and objective of the present work.

Chapter-2 gives a general outline about materials, different experimental techniques and instrumentations, used throughout the work. The properties of AMP-PAN and ion exchange membranes used are presented. The preparation of simulated HLW is also reported. The details of Scanning electron microscope (SEM), X-ray diffraction (XRD) and Fourier Transform Infra Red (FTIR) used for characterization of AMP-PAN are given and their working principles are also explained. Usage of Atomic Absorption spectrophotometer (AAS) for the determination of concentration of cesium, strontium and sodium is reported. Other details of instruments used in this work are briefly elaborated. Equilibrium studies carried out by equilibrating known volumes of organic and aqueous phases in stoppered glass tubes at constant temperature are presented. Batch kinetic studies of cesium ion exchange on AMP-PAN are also investigated. The details of the column performance of Cs ion-exchange on AMP-PAN studied for different parameters are elaborated. Experimental set up, and the procedure adopted for the investigation of EDIX process are also given.

Chapter-3 is about cesium ion exchange studies on AMP-PAN. Studies on selectivity of Cs by AMP-PAN, investigated using batch and column experiments, are presented in this chapter. Cesium ion exchange on AMP-PAN is studied for different operating conditions and is found to follow Langmuir isotherm model. Ion exchange kinetics of Cs on AMP-PAN are also explained for different parameters. Pseudo second order kinetic model predicted the kinetics of Cs on AMP-PAN well. Separation of Cs from simulated acidic solution carried out in packed bed columns is reported. Various parameters affecting the column dynamics of Cs sorption by AMP-PAN are elaborated. Uptake of Cs by AMP-PAN increased with increase in initial feed concentration due to increase in concentration gradient and also increased with bed height due to increase in number of sorption sites. Uptake decreased with increase in feed flow rate due to decrease in residence time of solute. Different mathematical models like Thomas, Yoon-Nelson and Bohart Adam models are applied for predicting the breakthrough and uptake capacity. Thomas and Yoon-Nelson models predicted the breakthrough well. Regeneration of AMP-PAN in glass column is also reported for different eluant concentrations.

In chapter-4, current–voltage characteristics in a hybrid electrodialysis–ion exchange system for the recovery of cesium ions from AMP-PAN are explained. The occurrence of concentration polarization in EDIX process and its effects are discussed. Limiting current density occurring on account of concentration polarization is experimentally determined in this chapter with current-voltage curves. Influence of operating parameters like flow rate, anolyte concentration on I-V characteristics are elaborated. Limiting currents increased with increase in electrolyte flow rates and anolyte concentrations due to decrease in concentration polarization. The onset of concentration polarization is predicted by observing the catholyte pH which jumps to more than 7 from less than 1. Determination of empirical constants predicting limiting current density as a function of electrolytes' flow rates and concentration is presented. The effect of operation of EDIX process at over limiting currents is compared with operation at under limiting currents. Operating the cell at 80 % value of the limiting current resulted in maximum recovery.

Chapter-5 is about the investigation of EDIX for recovery of Cs from AMP-PAN. Different modes of operation of the cell are detailed. In mode-I, eluant (ammonium sulphate) is passed as anolyte and in mode-II, eluant is passed directly through the ion exchange resin in the middle compartment of the electrodialysis cell. The transport of ions in the packed bed of electrodialysis cell is explained based on the Porous plug model. Nernst- Plank ion transport model is applied to study the ionic movement in the EDIX process in terms of convection, diffusion and migration.

The effect of process parameters like current density, eluant concentration and loading capacity on recovery of Cs from AMP-PAN in EDIX is discussed. Recovery of Cs from AMP-PAN in electrodialysis setup by migration increased with increase in current density and eluant concentration in mode-I. High recovery of more than 80% is observed for loading capacity of 8.82 mg/g of resin for the operating conditions investigated. The variation in the electrolytes' properties during the operation of the cell is also presented. In mode-II, migration of Cs into cathode compartment increased with increase in current density and decreased with increase in eluant concentration. Increase in catholyte concentration did not show any effect on Cs migration.

Ohmic resistance and potential gradient of the packed bed in the electrodialysis cell for the recovery of Cs from AMP-PAN are calculated. Migration term of Nernst-Plank equation is applied to find an empirical equation for the transport of ions on application of electric field. Determination of apparent diffusion coefficient of Cs in electrodialysis cell is reported in this chapter. The apparent diffusion coefficient of Cs is found to decrease with time for all the parameters studied.

Chapter-6 summarizes the scope of Cs recovery from AMP-PAN using EDIX .Optimization of the parameters in the EDIX process is also discussed. Scope of future studies is also elaborated.

References

1. IAEA 2000: Nuclear Power and sustainable development. 2000: .
2. S.A. Bharadwaj. Indian nuclear power programme – Past, present and future. Sadhana, 2013. **38**: p. 775-794.
3. IAEA Nuclear Technology Review 2009, I., Vienna, 3.
4. http://www.epa.gov/radiation/source-reduction-management/applications.html.
5. IAEA Technical Report Series.
6. K. Shakir, M. Sohsah, M. Soliman, Removal of cesium from aqueous solutions and radioactive waste simulants by coprecipitateflotation. Sep. Sci. Technol., 2007. **54**: p. 373–381.
7. P.A. Hass, A review of infomation on ferrocyanide solids for the removal of cesium from solutions. Sep. Sci. Technol., 1993. **28**: p. 2479-2506.
8. X. Chai, J. Wang, J. Chen, Solvent extraction of strontium and cesium: A review of recent progress, Solvent Extr. Ion Exch., 2012. **30**: p. 623-650.
9. P.V. Bonnesen, L.H. Delmau, B.A. Moyer, R.A. Leonard, A robust alkaline-side CSEX solvent suitable for removing cesium from Savannah River high level waste. Solvent Extr. IonExch., 2000. **18**: p. 1079-1107.
10. J.D. Law, R.S. Hersbt, D.R. Peterman, R.D. Tillotson, T.A. Todd, Development of a cobalt dicarbollide/polyethylene glycol solvent extraction process for separation of cesium and strontium to support advanced aqueous reprocessing. Nuclear Technology, 2004. **147**: p. 284-290.

11. P. Rajec, K. Domianová, Cesium exchange reaction on natural and modified clinoptilolite zeolites. Journal of Radioanalytical and Nuclear Chemistry, 2008. **275**(3): p. 503-508.

12. B. Yıldız, H.N. Erten, and M. Kış, The sorption behavior of Cs + ion on clay minerals and zeolite in radioactive waste management: sorption kinetics and thermodynamics. Journal of Radioanalytical and Nuclear Chemistry, 2011. **288**(2): p. 475-483.

13. J. Narbutt, J. Siwinski, B. Bartos, A. Bilewicz, Studies on new titanium hexacyanoferrate sorbents for radiocesium removal from primary coolant of pressurized water reactors. Journal of Radioanalytical and Nuclear Chemistry Articles, 1986. **101**(1): p. 41-49.

14. C. Loos-Neskovic, S. Ayrault, V. Badillo, V. Jimenez, B. Garnier, E. Fedoroff, M. Jones, D. J. Merinov, Structure of copper-potassium hexacyanoferrate (II) and sorption mechanisms of cesium. Journal of Solid State Chemistry, 2004. **177**(6): p. 1817-1828.

15. M. Panagiotis, Application of natural zeolites in environmental remediation: a short review. Microporous Mesoporous Materials, 2011. **144**: p. 15–18.

16. V.N. Lebedev, N.A. Melnik, A.V. Rudenko, Sorption of cesium on titanium and zirconium phosphates. Radio Chemistry, 2003. **45**: p. 149-151.

17. G.S. Murthy, M.V. Sivaiah, S.S. Kumar, V.N. Reddy, R.M. Krishna, S. Lakshminarayana, Adsorption of cesium on a composite inorganic exchanger zirconium phosphate-ammonium molybdophosphate. Journal of radioanalytical and nuclear chemistry, 2004. **260**(1): p. 109-114.

18. Bin Ma, Sanghwa Oh, Won Sik Shin , Sang-June Choi, Removal of Co2+, Sr2+ and Cs+ from aqueous solution by phosphate-modified montmorillonite (PMM). Desalination, 2011. **276**(1-3): p. 336-346.

19. K.A. Venkatesan, V. Sukumaran, M.P. Antony, T.G. Srinivasan , Studies on the feasibility of using crystalline silicotitanates for the separation of cesium-137 from fast reactor high-level liquid waste. Journal of Radioanalytical and Nuclear Chemistry, 2009. **280**(1): p. 129-136.

20. T. A. Tood, V.N. Romanovskiy, A comparison of crystalline silicotitanate and ammonium molybdo-phospahte-polyacrylonitrile composite sorbent for the separation of cesium from acidic waste. Radiochemistry 2005. **47**: p. 398-402.

21. F. Sebesta, Composite ion exchanger with ammonium molybdophosphate and its properties. J. Radioanal. Nucl. Chem. , 1990. **140**: p. 15-21.

22. T..J. Tantaer, R.S. Herbst, T.A. Todd, A.L. Olson, H.B. Eldregdge, Evaluation of ammonium molybdophosphate-polyacrylonitrile AMP-PAN as a cesium selective sorbent for the removal of 137 Cs from acidic nuclear waste solutions. 2002. **6**: p. 107-121.

23. T. J. Tranter, R.S. Herbst, T. A. Todd, Determination of a solid phase mass transfer coefficient for modeling an asorption bed system using ammonium molybdophospahte-polyacrylonitrile (AMP-PAN) as a sorbent for the removal of 137 Cs from acidic nuclear waste solutions. Adsorption 2002. **8**: p. 291-299.

24. T.A. Todd, N.R. Mann, T.J. Tranter, F. Sebesta, J. John, A. Motl, Cesium sorption from concentrated acidic tank wastes using ammonium molybdophosphate-polyacrylonitrile composite sorbents. Journal of radioanalytical and nuclear chemistry, 2002. **254**(1): p. 47-52.

25. T.J. Tranter, R.S. Herbst, T.A. Todd, A.L. Olson, H.B. Eldredge, Application of a second order kinetic model for the preliminary design of an adsorption bed system using ammonium molybdophosphate–polyacrylonitrile for the removal of 137 Cs from acidic nuclear waste solutions. Advances in Environmental Research, 2003. **7**(4): p. 913-923.

26. T. A. Todd, K.N. Brewer, D. J. Wood, P. A. Tullock, N. R. Mann, L. G. Olson, Evaluation and Testing of Inorganic Ion Exchange Sorbents for the removal of Cesium-137 from Idaho Chemical Processing Plant Acidic Tank Waste. Sep. Sci. Technol., 2001. **36**: p. 999-1016.

27. Y. Park, Y.C. Lee, W.S. Shin, S.J. Choi, Removal of cobalt, strontium and cesium from radioactive laundry wastewater by ammonium molybdophosphate–polyacrylonitrile (AMP–PAN). Chemical Engineering Journal, 2010. **162**(2): p. 685-695.

28. Y. Xiushen , W. Zhijian , L. Wu, L. Haining, L. Quan, Q. Binju, G. Min , G. Fei, Rubidium and cesium ion adsorption by an ammonium molybdophosphate–calcium alginate composite adsorbent. Colloids and Surfaces A: Physicochemical and Engineering Aspects, 2009. **342**(1-3): p. 76-83.

29. H. Mimura, Y. Onodera, Selective Uptake and Recovery of Cesium Ions by Composite Columns of Ammonium Molybdophosphate (AMP)-Calcium Alginate. Journal of Nuclear Science and Technology, 2002. **39**(3): p. 282-285.

30. Dwivedi, Charu Kumar, Amar Ajish, Juby K.Singh, Krishan Kant Kumar, Manmohan Wattal, Piaray Kishen Bajaj, Parma Nand, Resorcinol-formaldehyde coated XAD resin beads for removal of cesium ions from radioactive waste: synthesis, sorption and kinetic studies. RSC Advances, 2012. **2**(13).

31. C. Dwivedi, S. K.Pathak, M. Kumar, S.C. Tripathi, P.N. Bajaj, Removal of cesium by spherical resorcinol–formaldehyde resin beads: Sorption and kinetic studies. Journal of Radioanalytical and Nuclear Chemistry, 2013. **297**(1): p. 1-8.

32. S.A. Shady, Selectivity of cesium from fission radionuclides using resorcinol–formaldehyde and zirconyl-molybdopyrophosphate as ion-exchangers. Journal of Hazardous Materials, 2009. **167**(1-3): p. 947-952.

33. A.K. Deepa, A.P. Jakhete, D. Mehta, N. Singh, C.P. Kaushik, K. Singh, Estimation of the heat generation in vitrified waste product and shield thickness for the transportation of vitrified waste product using Monte Carlo technique. Indian J. Pure & App. Physics 2012. **50**: p. 867-869.

34. I.W. Donald, B.L Metcalfe, R.N.J. Taylor, Taylor, Review- The immobilization of high level radioactive wastes using ceramics and glasses. Jounal of membrane science, 1997. **32**: p. 5851–5887.

35. P.K. Mohapatra, S.A. Ansari., A. Sakar, A. Bhattacharyya, V.K. Manchanda, Evaluation of calix-crown ionphores for selective separation of radio-cesium from acidic nuclear waste solution, Analytica chimica Acta 2006. p. 308-314.

LIST OF FIGURES

List of Tables

LIST OF ABRREVATIONS

AAS	Atomic Absorption Spectrophotometer
AEM	Anion Exchange Membrane
AMP	Ammonium molybdophosphate
APE	Average percentage error
CCD	Chlorinated Cobalt Dicarbollide
CEM	Cation Exchange Membrane
CST	Crystalline Silicotitanates
DAE	Department of Atomic Energy
ED	Electrodialysis
EDI	Electrodeionization
EDIX	Electrodialysis- Ion exchange
EW	Exempt Waste
FBR	Fast Breeder Reactor
FTIR	Fourier Transform Infrared Spectroscopy
GDP	Gross domestic product
HLW	High Level Waste
ILW	Intermediate Level Waste
LCD	Limiting current density
LLW	Low Level Waste
MTZ	Mass Transfer Zone
PAN	Polyacrylonitrile
RF	Resorcinol Formaldehyde
RPM	Revolutions per minute
RTIL	Room Temperature Ionic Liquid
XRD	X-ray diffraction
ZrHP	Zirconium mono Hydrogen Phosphate

LIST OF SYMBOLS

$\boldsymbol{\delta}$	bed thickness, (m);
ΔE_{bed}	bed potential drop, (V);
Gradφ	bed potential gradient, (V/m);
τ	time required for 50% sorbate breakthrough, (min);
a	Coefficient for the limiting current density calculation, $As^{b}m^{1-b}/keq$;
b	Coefficient for the limiting current density calculation;
b	Langmuir constant, (L/mg);
$i_{\text{lim,emp}}$	empirical limiting current density, (A/m^2);
$\overline{u}_i.$	mobility of ion in solid phase, ($m^2/s/V$);
n	Freundlich parameter;
q_e	equilibrium solute concentration in solid phase, (mg/g);
q_m	maximum solute conc. in solid phase, (mg/g);
q_t	solute concentration in solid phase at time t, (mg/g);
t_e	exhaustion time, (min);
t_b	breakthrough time, (min);
t_z	time required for the movement of MTZ down its own length, (min);
m	amount of resin in the column, (g);
z	valence,
t_s	ion transport numbers in the solution;
t_m	ion transport numbers in the membrane;
u	linear velocity, (m/s);
$n_{\text{Cs,max}}$	maximum amount of Cs present in the catholyte, ($moles/m^2/s$)
k_m	mass transfer coefficient, a model parameter, (s^{-1});
A_s	membrane surface in direct contact with solution, (m^2);
A_t	total surface of membrane, (m^2);
C_o	initial solute concentration in the solution phase, (mg/L);
C_e	equilibrium metal concentration in the solution phase, (mg/L);

C_i	initial concentration of the solute, (mg/L);
C_f	final equilibrium concentration of the solute, (mg/L);
C	effluent concentration, (mg/L);
$\bar{C}_{Cs}^{0}$	concentration of Cs in solid phase at time t=0, (moles);
$\bar{C}_i$	solute concentration in solid phase, (moles);
D	diffusion coefficient, (m^2/s);
$\bar{D}_i$	diffusion coefficient of species i in solid phase, (m^2/s);
$\bar{D}_{Cs,eff}$	effective diffusion coefficient of Cs in solid phase, (m^2/s);
E_a	anode electrode potential, (V);
E_c	cathode electrode potential, (V);
E_m	membrane potential, (V);
E_{cell}	cell potential, (V);
F	Faraday constant, (C/mole);
H	height of the ion exchange bed, (m);
H_{MTZ}	height of the mass transfer zone, (m);
I	thickness of the boundary layer, (m);
K_1	rate constant for pseudo-first-order adsorption, (min^{-1});
K_2	rate constant of the second-order sorption process, (g/mg/h);
K_d	distribution coefficient, (L/g),
K_{id}	intra-particle diffusion rate constant, ($mg/g\ min^{0.5}$);
K_{BA}	Bohart Adam model rate constant, (L/ mg/h);
K_F	Freundlich constant, ($mg^{1-1/n}L^{1/n}/g$);
K_{Th}	Thomas rate constant (L/min.mg);
K_{YN}	Yoon Nelson model rate constant, (h^{-1});
N	number of experimental data;
N_0	sorption capacity, (mg/L);
$\bar{N}_{Cs}^{0}$	possible flux of Cs in solid phase at time t=0, ($moles/m^2/s$);
V_{eff}	effluent volume, (L);
R	gas constant, (J/mol/K);
R_{cell}	cell resistance, (Ω);
R_a	anolyte resistance, (Ω);
R_c	catholyte resistance, (Ω);

R_m	membrane resistance, (Ω);
R_e	eluant resistance, (Ω);
Q	flow rate, (L/min);
T	temperature, (K);
V	volume of solution, (L);
W	dry weight of the resin used, (g);
Z	bed height, (m)

Introduction

1

This chapter introduces the need of nuclear power and the nuclear programme of India towards meeting the energy demand in the country. An overview of fuel reprocessing of the spent fuels is preserved. Various processing steps and the challenges involved in the reprocessing are briefly explained. The advantages and necessity of closed fuel cycle for future energy security are detailed. The main focus of this chapter is on the need for removal of Cs-137 from High Level Waste for lowering the activity of the waste to be disposed.

1.1. Perspective of nuclear power in India

Energy is essential for the survival and growth of modern human civilization and is vital for a nation's economic development. The demand for energy increases with increase in population and rise in economic growth. There is an ever- increasing need to generate more power as all the industrial, agriculture and other sectors are sustained by power.

Developing countries generally have higher growth rates of population compared to developed countries. India is economically growing in terms of GDP at a rate of about 6–8 % a year. Sustaining the economic growth at the current rate is essential for improving the quality of life [1]. For its growing population, increased attention needs to be paid by India to provide energy, especially supply of electricity. All available sources of energy, therefore, must be optimally developed and deployed to meet the short as well as long term energy needs of our country.

The present power scenario in the world is presented in Table 1.1. India has the lowest average power per capita consumption among the top ten power consuming countries and significantly below the world's average. As GDP growth accelerates to an ambitious 8 to 10 %, shortage of power will become more severe.

Table 1.1 Power scenario of different countries in 2012 [2, 3]

Rank	Country	Electricity consumption (TWh)	Population (million)	Per capita energy consumption (KWh/year)
	World	21016.3	7137	2945
1	China	4724	1350	3499
2	USA	4052	314	12904
3	Russia	1002	143	7007
4	Japan	964	128	7531
5	India	931	1260	739
6	Canada	646	35	18457
7	Germany	578	82	7049
8	Brazil	536	194	2763
9	France	531	64	8297
10	S. Korea	496	49	10122

The resources used for power generation in India presently are illustrated in Figure 1.1.

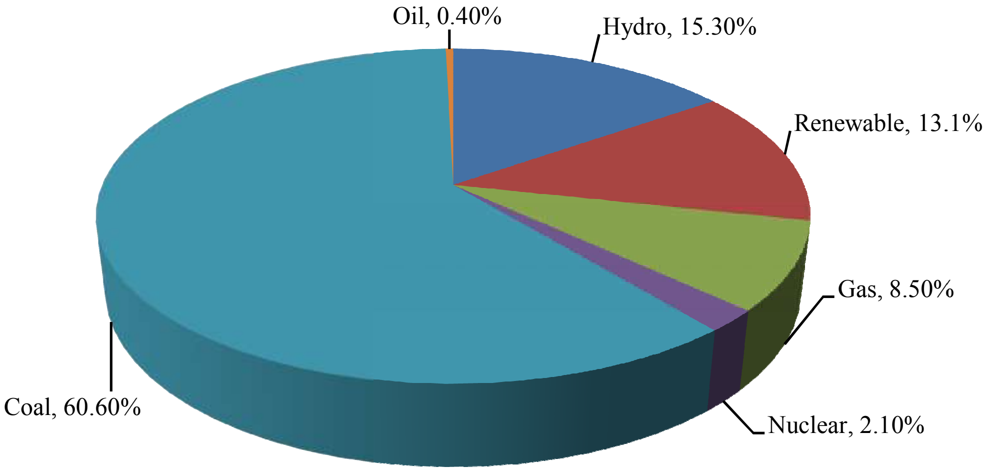

Figure 1.1 Breakup of installed power capacity in India as on April 31, 2015 [4]

Coal is the main resource at present and coal-fired plants will continue to be the primary source of electricity production in the country for quite some time to come. Figure 1.2 shows the availability of energy resources in India and the possible electricity generation with the available resources. The Integrated Energy Policy [5] indicates that at a growth rate of 5 % in domestic production, currently extractable coal resources will be exhausted in about 45 years. Nearly 80 per cent of the oil is imported in the country, which is an area of concern for the Government with regard to energy security in the near future.

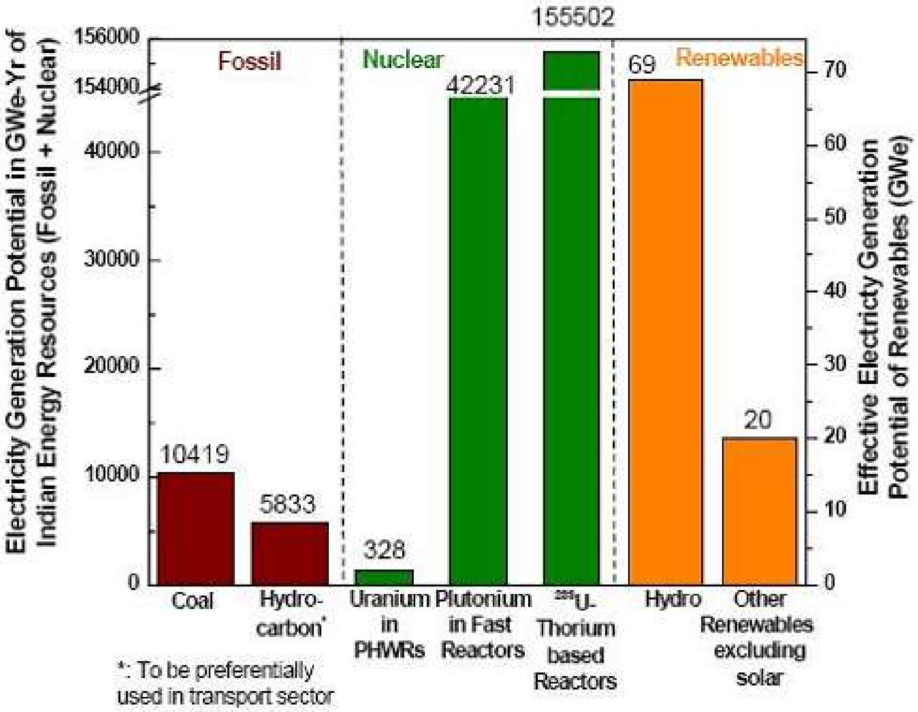

Figure 1.2 Current Indian energy resources [6]

Potential for hydro is limited by rainfall and topography of the location of water sources. Other renewable energy sources like wind have similar limitations of growth and energy supply. A renewable energy source like solar energy also holds promise as a possible inexhaustible energy source for a tropical country like India. Use of extensive solar energy may call for changes in pattern of energy consumption and urbanization. Compared to the other resources, nuclear energy could provide the most energy availability in terms of electricity generation with the available resources.

Currently, the nuclear energy share in electricity generation is about 2.1 %. The nuclear share in total primary energy mix is expected to grow, as the installed nuclear power capacity grows. The Integrated Energy Policy of India estimates the share of nuclear power in the total primary energy mix to be between 4.0 and 6.4 % in various scenarios in the year 2031–32 [5].

Thus, Nuclear energy, in view of its huge potential and techno-commercial viability, will play an increasingly important role in the future. The rate of growth of nuclear share at the primary level is expected to be rapid as conventional fossil fuel sources, particularly coal, approach exhaustion, or their extraction tends to become uneconomical.

1.2. India's Nuclear Programme

For the optimum utilization of the indigenous nuclear resource profile of modest Uranium and abundant Thorium in the country, India has adopted the unique sequential three-stage nuclear power programme [7]. The three-stage power programme of Department of Atomic Energy (DAE) has been planned based on a closed fuel cycle concept, requiring reprocessing of spent fuel from every reactor as shown in Figure 1.3. The objective is to judiciously utilize mined uranium and thorium resources of the country to a maximum extent.

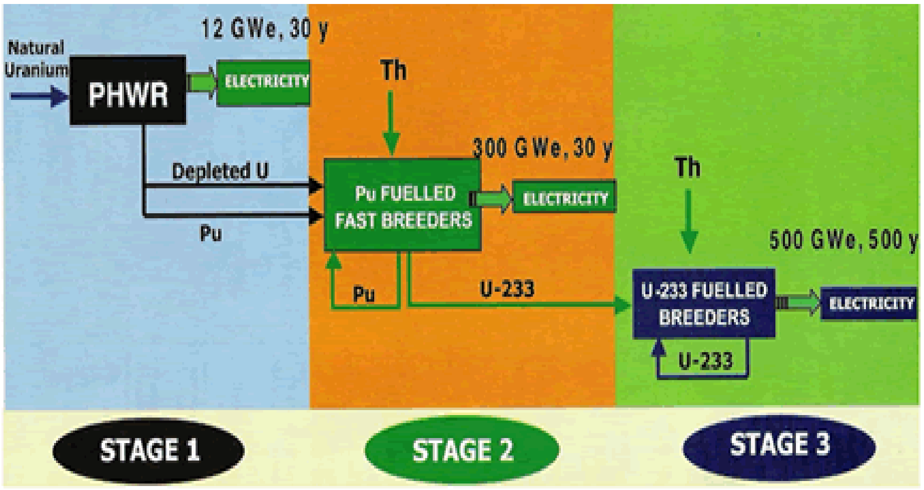

Figure 1.3 India's three stage Nuclear Programme [7]

Uranium has just 0.7 % fissionable ^{235}U isotope, while ^{238}U, the dominant isotope of uranium is a fertile material. It needs to be converted to fissile ^{239}Pu for further use. The process of this conversion takes place in a nuclear reactor where uranium fuel is used. Fisson of ^{235}U produces excess neutrons over and above those required for maintaining a steady fission chain reaction. Some of these excess neutrons invariably get absorbed in the major isotope ^{238}U and result in production of ^{239}Pu. By suitable reactor physics design of a nuclear reactor, the production of Pu can be optimized. Thus the spent fuel from thermal reactors contains a small quantity of ^{239}Pu, along with residual uranium (predominantly ^{238}U). The spent fuel can be reprocessed chemically to separate plutonium, residual uranium and the fission products.

Pu^{239} is a fissile material and when used in Fast Reactors, where neutron energies are kept high (by not slowing them through use of a moderator as in thermal reactors), is more efficient in producing excess neutrons during fission chain reaction. These excess neutrons are used by proper reactor physics design to convert ^{238}U into additional Plutonium. By suitable choice of fuel type and reactor configuration, the Fast Reactors can produce a little more Pu than they consume, thus the name 'Breeder' Reactors. Similarly, thorium is a fertile material and has to be converted to a fissile material, viz. ^{233}U, to be used for power production.

A closed fuel cycle approach as mentioned above, involving reprocessing of spent fuel to separate the useful fissile and fertile isotopes from spent fuel and reusing them in nuclear reactors, has been adopted as a guiding principle for India's nuclear energy programme to ensure long term energy security for the country.

Fast Breeder Reactors (FBRs) are operated with fuels based on Plutonium mixed with reprocessed Uranium, recovered by reprocessing of the first stage spent fuel. In FBRs, Plutonium-239 undergoes fission, producing energy and at the same time, producing

Plutonium-239 by transmutation of Uranium-238. Thorium-232 is not fissile and has to be converted to Uranium-233 by transmutation in a reactor for use as a fissile material. In the second stage, once sufficient nuclear power capacity is built through Plutonium-based FBRs, Thorium-232 will be introduced as a blanket material to be converted to Uranium 233. The third stage of the programme will be using a Thorium-232-Uranium 233 fuel cycle in the reactors. Direct use of Thorium-232 as a fuel will thus be in the third stage reactors. Thorium-232-Uranium-233 fuel cycle does not permit attractive breeding characteristics like that of Pu–U cycle but would facilitate the nuclear power capacity built during second stage of the programme to be sustained for as long as Thorium, which is quite large in the country, is available.

1.3. Nuclear Fuel Cycle

There are two fuel cycle options for long-term nuclear power production that are of relevance and under consideration at the present juncture, i.e., the once through cycle with disposal of spent fuel as such and the closed fuel cycle with reprocessing and recycle of uranium and plutonium. Both the options require efficient and safe waste management strategies.

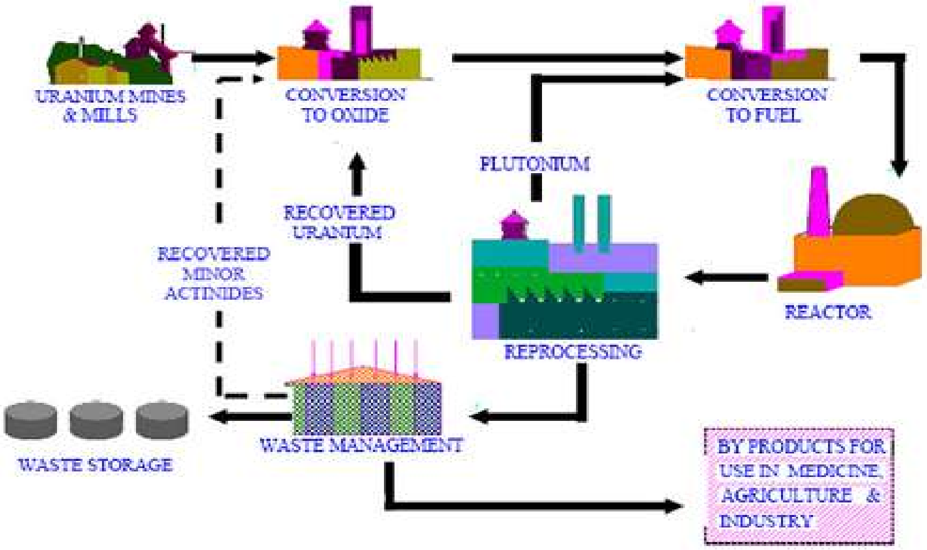

Figure 1.4 Closed Nuclear Fuel Cycle [8]

The known Indian sources of uranium are insufficient to support the long-term Indian nuclear energy program, if once-through option is adopted. Closing the nuclear fuel cycle by reprocessing the spent fuel and recycle of uranium and plutonium back into reactor systems as shown in Figure 1.4 helps in exploiting the full potential of nuclear power and maximizes the resource utilization [9].

1.4. Overview of spent fuel reprocessing

Used fuel from light water reactors (33GW/t burn-up levels, 10y cooling) contains about 96% of its original uranium, of which the fissionable U-235 content has been reduced to less than 1%. Figure 1.5 shows about 3% of the used fuel comprises waste products and the remaining 1% is plutonium (Pu) produced while the fuel was in the reactor and not 'burned' then [10].

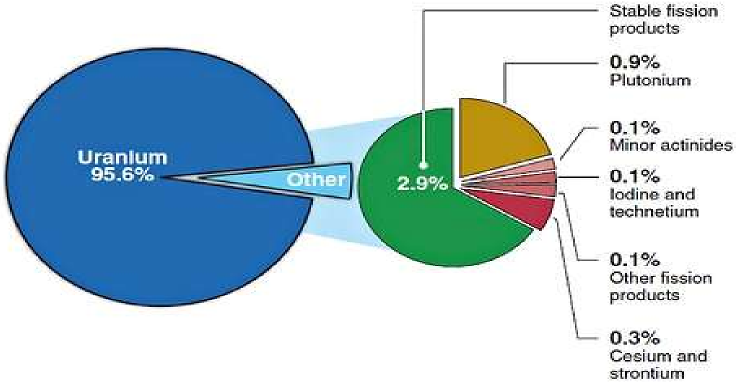

Figure 1.5 Composition of spent nuclear fuel [10]

The aim of reprocessing is to recover uranium and plutonium from the spent fuel for recycle in reactors and to concentrate the fission product wastes in a form suitable for long term storage. The reprocessing waste contains mainly fission products and small amounts of transuranium elements, which are immobilized in a specially formulated glass matrix, sealed in metal canisters designed for long-term storage [11].

There are two types of processes available for reprocessing of spent nuclear fuel based on its hydrous nature.

1.4.1. Aqueous Reprocessing

Aqueous reprocessing is a hydrometallurgical process. India adopted PUREX process, a solvent extraction process using 30% TBP in an inert diluent mixture of paraffins with 12–14 carbon atoms or pure n-dodecane, totally amenable for automation and remote handling. The PUREX process has been the workhorse of fuel reprocessing for the last few decades and no other process developed before or after can claim its versatility. Many modifications for the PUREX process have been made and named as UREX+, TRUEX, DIAMEX, SANEX, etc.

An overview of PUREX process was shown in Figure 1.6.

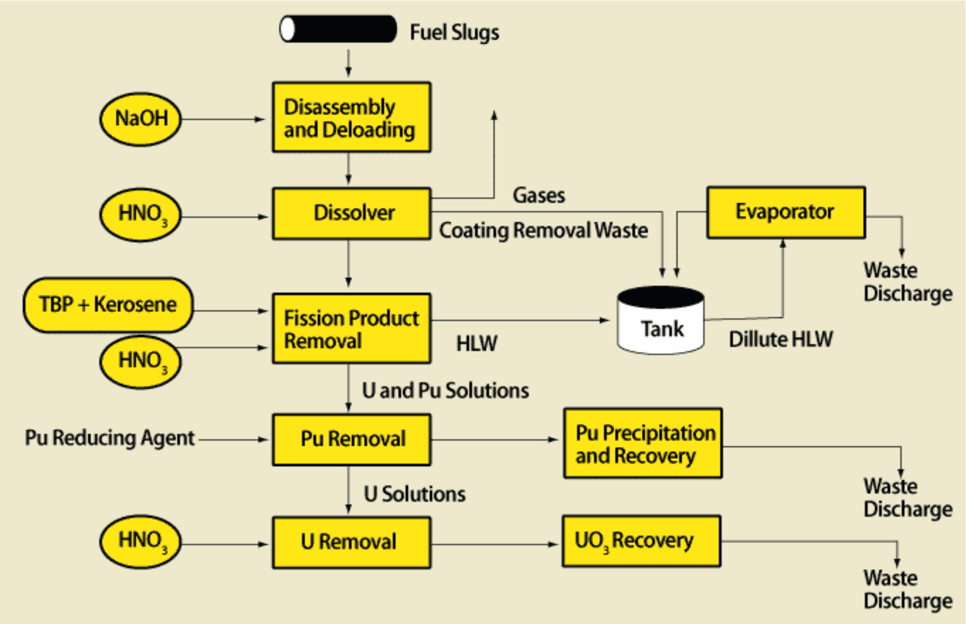

Figure 1.6 Overview of reprocessing of spent fuel [12]

The basic steps involved in the process are:

1. Head-end treatment involving chemical or mechanical decladding followed by dissolution of fuel in nitric acid, feed clarification and adjustment of chemical conditions of the solution for solvent extraction.

2. Co-decontamination involving extraction of uranium (as U(VI)) and of plutonium (as Pu(IV)) leaving bulk of the fission products in aqueous phase, which goes as high active waste.

3. Washing/scrubbing of organic stream with nitric acid, sometimes using two nitric acid scrubs of different HNO_3 concentration to backwash fission products co-extracted with uranium and plutonium.

4. Partitioning of U and Pu by selective reduction of Pu(IV) in the organic phase to Pu(III) which goes to the aqueous phase, and back extraction of U(VI) with dilute HNO_3.

5. Further purification of uranium and plutonium streams to obtain U and Pu of desired purity.

6. Treating the used solvent for its recycle.

7. Waste management.

1.4.2. Non-aqueous reprocessing

Many process for non-aqueous reprocessing of spent nuclear fuel have been proposed based on volatilization, halide volatility, partial oxidation, electrochemical nature of spent fuel. Pyrochemical processes for reprocessing of spent nuclear fuel are investigated worldwide as an alternative to the traditional hydro-metallurgical methods [13].

Electrochemical (pyro chemical) reprocessing is particularly suitable for reprocessing fast reactor spent fuel [14]. The new types of fuels planned for these reactors (e.g. metallic, oxide, carbide) might be difficult to process by hydrometallurgical methods due to their limited solubility in aqueous media. A simplified scheme of the pyrochemical reprocessing flow sheet is shown in Figure 1.7.

The pyrochemical reprocessing is based on electrorefining of spent fuel in a molten LiCl-KCl bath using reactive solid aluminium cathodes [15]. In this process, the fuel is electrochemically dissolved in the carrier melt forming a mixture of actinides (An) and fission products (FP). All actinides are selectively recovered from the melt by electro-deposition on solid aluminium cathodes in the form of solid actinide-aluminium (An-Al) alloys.

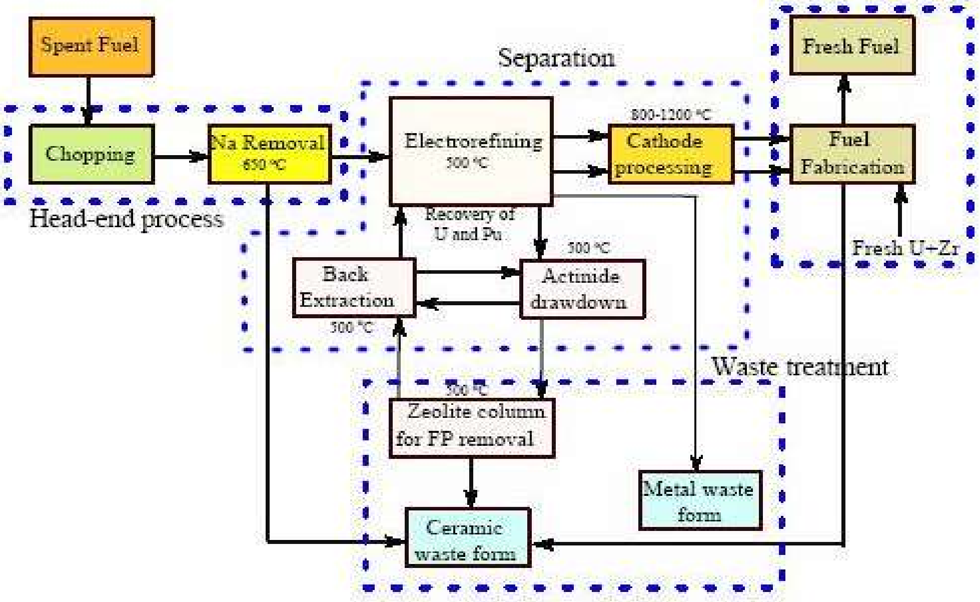

Figure 1.7 Pyrochemical reprocessing flow sheet[16]

1.5. Radioactive waste management

Radioactive wastes are generated during various operations of the nuclear fuel cycle viz. mining and milling, fuel fabrication, power generation and reprocessing. Additionally, radioactive wastes are generated from non fuel cycle sources such as application in industry, healthcare and research. The primary objective of radioactive waste management is protection of human health, environment and future generation.

Effective management of waste involves characterization, treatment, conditioning, storage and monitoring prior to final disposal [8]. Various processes followed in the management of radioactive wastes are presented in Figure 1.8.

1.5.1. Classification of radioactive waste

Radioactive wastes arise in different forms viz; solid, liquid and gas with variety of physical and chemical/radiochemical characteristics. Wastes can be classified as long-lived short lived based on the half-life of the isotopes present. For operational convenience, the wastes can also be classified on treatability. Depending on the level and nature of radioactivity, radioactive wastes can be classified as exempt waste, Low &

Intermediate level waste and High Level Waste [17]. Classification of radioactive waste, as recommended by International Atomic Energy Agency (IAEA) [18] is shown in Figure 1.9.

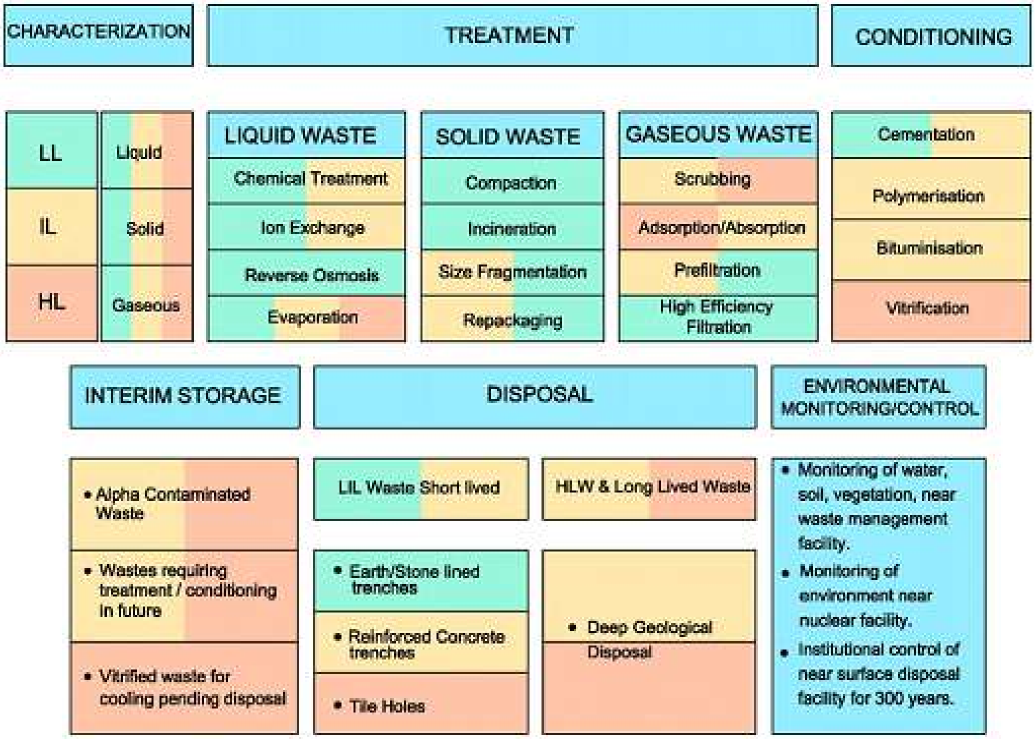

Figure 1.8 Management of radioactive waste [8]

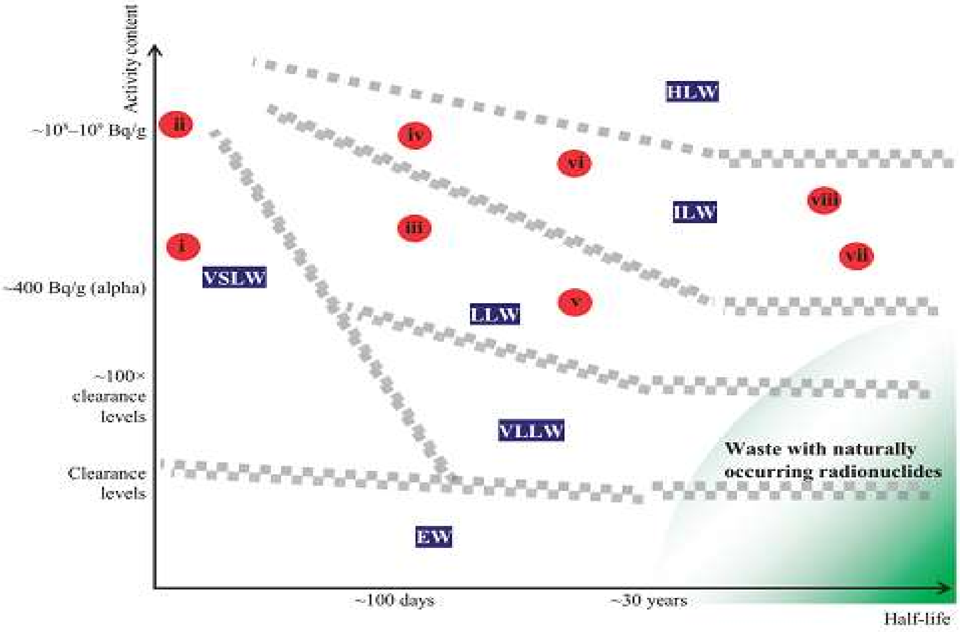

Figure 1.9 Radioactivity classification system (IAEA)[18]

(1) *Exempt waste (EW):* Exempt wastes have levels of radioactivity too low to warrant any concern from the regulators. These can be disposed of to the environment and are not likely to cause any adverse impact.

(2) *Low level waste (LLW)* (37–3.7×10^{6} Bq/L): Waste that is above clearance levels, but with limited amounts of long lived radionuclides. Such waste requires robust isolation and containment for periods of up to a few hundred years and is suitable for disposal in engineered near surface facilities. This class covers a very broad range of waste. LLW may include short lived radionuclides at higher levels of activity concentration, and also long lived radionuclides, but only at relatively low levels of activity concentration.

(3) *Intermediate level waste (ILW)* (3.7×10^{6} - 3.7×10^{11} Bq/L): ILW because of its content, particularly of long lived radionuclides, requires a greater degree of containment and isolation than that provided by near surface disposal. However, ILW needs no provision, or only limited provision, for heat dissipation during its storage and disposal. ILW may contain long lived radionuclides, in particular, alpha emitting radionuclides that will not decay to a level of activity concentration acceptable for near surface disposal. Therefore, waste in this class requires disposal at greater depths, of the order of tens of meters to a few hundred meters.

(4) *High level waste (HLW)* ($> 3.7 \times 10^{11}$ Bq/L): Waste with levels of activity high enough in concentration to generate significant quantities of heat by the radioactive decay process or waste with large amounts of long lived radionuclides that need to be considered in the design of a disposal facility for such waste. Disposal in deep, stable geological formations usually several hundred meters or more below the surface is the generally recognized option for disposal of HLW.

1.5.2. Storage

Storage of radioactive waste involves maintaining the radioactive waste such that: (i) isolation, environmental protection and monitoring are provided, and (ii) actions involving treatment, conditioning and disposal are facilitated. In some cases, storage may be practiced for primarily technical considerations, such as storage of radioactive waste containing mainly short lived radionuclides for decay or storage of high-level radioactive waste for thermal considerations prior to geological disposal.

1.5.3. Treatment

Pre-treatment of waste is the first step in waste management after characterization. It consists of collection, segregation, chemical adjustment and decontamination and may include a period of interim storage. The wastes are treated based on their physical or chemical characteristics, radioactivity levels and amenability to treatment methods using the process depicted in Figure 1.8. Treatment of liquid wastes results in two streams, one high in volume and low in activity, to be disposed into environment and other high in activity and low in volume, to be contained. Solid wastes are treated for volume reduction.

1.5.4. Conditioning

Conditioning of radioactive waste involves immobilizing the radioactive waste into a solid form suitable for handling, transportation, storage and disposal. Common immobilization methods include solidification of low and intermediate level radioactive waste in cement or polymer, and vitrification of high-level liquid waste in a glass matrix.

1.5.5. Disposal

Disposal is the final step in the radioactive waste management system. It consists mainly of the emplacement of radioactive waste in a disposal facility with reasonable assurance for safety, without the intention of retrieval and without reliance on long term surveillance and maintenance. The safety is mainly achieved by isolation, by use of different barriers around the radioactive waste in what is termed a ‘Multi barrier concept‘. Liquid and gaseous wastes are treated to remove most of the activity, thus achieving high decontamination factors. The treated streams are disposed into environment.

1.6. Need for removal of Cesium-137 from HLW

Cesium-137 does not exist in the natural environment and is an important fission product in the nuclear fission of U^{235}. The amount of any particular isotope produced per fission is called its yield, typically expressed as percent per parent fission. Figure 1.10 shows the percentage yield of atoms resulting from the thermal fission of uranium, which results in the largest yields at mass numbers 95 and 137. Table 1.2 shows the yield of different fission products from nuclear fission[19].

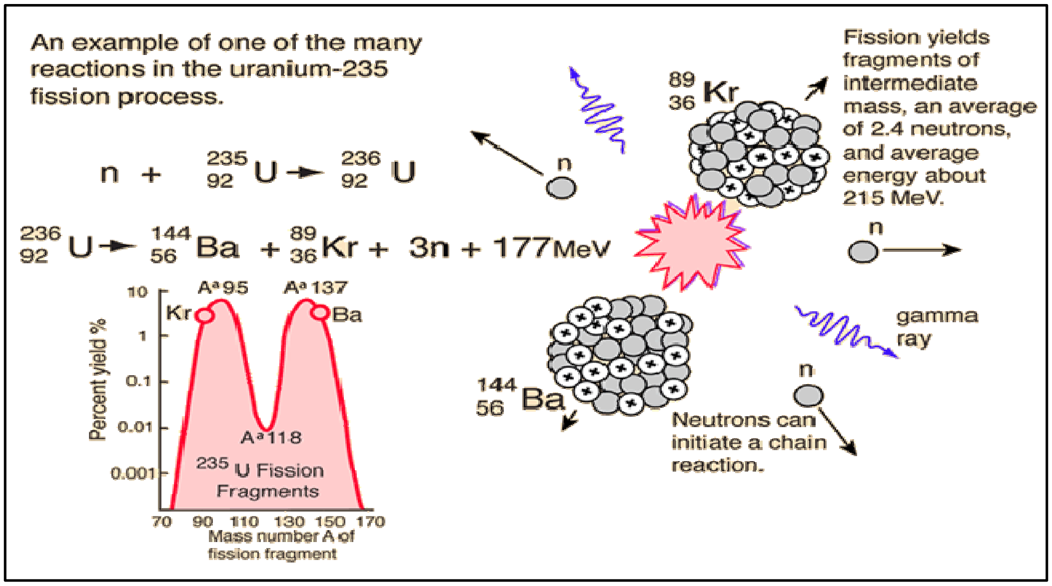

Figure 1.10 Percentage yield of fission products

Fission of various isotopes of thorium, uranium, and plutonium all yield about 6% Cs-137 and 6.7 % Cs-135 with half lifes of 30.2 and 2×10^{6} years, respectively. Even though ^{135}Cs is having very high half life compared to Cs-137, it is only a β emitter with decay energy of 0.209 MeV whereas ^{137}Cs is both β and γ emitter with 1.173 MeV. Since γ rays are more powerful and penetrable than β rays, ^{137}Cs is more radioactive than Cs-135. This high fission yield results in an abundance of ^{137}Cs in spent nuclear fuel, as well as in regions contaminated by fission byproducts after nuclear accidents [20].

Table 1.2 Main fission products in nuclear fission reactions

Nuclide	Yield (%)	Half life (years)	Maximum Decay Energy (MeV)
^{135}Cs	6.7	2.3×10^{6}	0.209
^{93}Zr	6.4	1.53×10^{6}	0.09
^{137}Cs	6.23	30.17	1.173
^{99}Tc	6.1	2.13×10^{5}	0.291
^{90}Sr	5.9	28.6	0.546+2.279
^{144}Ce	5.45	0.78	0.3182+2.996
^{87}Rb	2.56	4.8×10^{10}	0.2733
^{147}Pm	2.26	2.6234	0.2247
^{85}Kr	1.33	10.72	0.687
^{129}I	0.9	1.57×10^{7}	0.189

Cesium-137 undergoes high-energy beta decay, primarily to an excited nuclear isomer of Barium-137, which in turn undergoes gamma decay with a half-life of about 150 seconds [21]. In addition, cesium is much more chemically reactive than many of the transition metal fission products. As a group-I alkaline metal, elemental cesium is quite electropositive, and is readily oxidized by water, forming highly soluble Cs^{+} [22]. For this reason, elemental cesium-137 may contaminate large volumes of water during nuclear accidents, which are difficult to contain or process [23].

Increased operation of nuclear reactors results in the production of radioactive Cs isotopes which are the major source of radiation in HLW generated after the reprocessing of spent nuclear fuel. HLW accounts for about 99 percent of the total radioactivity produced in the process of nuclear electricity generation. Separation of ^{137}Cs from HLW would markedly reduce the radiation fields in subsequent fuel cycle processing streams and provides a significant heat source reduction in the repository.

Many radio-nuclides find application in medicine where their radioactive nature is exploited for diagnostic nuclear medicine. Cs-137 is used in medical radiation therapy devices for treating cancer; in industrial gauges that detect the flow of liquid through pipes; and in other industrial devices to measure the thickness of materials, such as paper, photographic film, or sheets of metal. It is also used for calibration of radiation-detection equipment, such as Geiger-Mueller counters. In addition, ^{137}Cs can be used as a radiation source for food preservation, sterilization of medical products, hygienization of sewage sludge etc.

1.7. Cs separation methods

Precipitation, solvent extraction and ion exchange are the most common methods for the separation of cesium from acidified waste solutions. Apart from these, many other technologies like electrodialysis, ultra filtration, reverse osmosis, have been developed for the separation of cesium from acidic waste solutions. Co precipitation, solvent extraction and ion exchange are presented here briefly.

1.7.1. Co-precipitation

Radioactive Cs-137 may be removed from nuclear waste aqueous solutions by co-precipitation. Among the alkali metal salt, Cs^+ salts have the largest range of solubility [24]. Most of the precipitation agents are ineffective in separating alkali metal ions from solution, since most alkali metal salts are water soluble.

Two Cs salts that are insoluble in water are cesium tetraphenylborate (CsTPB), $Cs^+[B(C_6H_5)_4]^-$ and cesium cobaltdicarbollide (CsCDC), $Cs^+[Co(B_9C_2H_{11})_2]^-$ CsTPB is less soluble than Cs_2PtCl_6 the most insoluble Cs compound found [24], and CsCDC is slightly more soluble than Cs_2PtCl_6. From the solubility relationships of the Cs compounds, it was found that precipitating anion for Cs^+ should have the following properties [25] :

(a) -1 charge; (b) hydrophobic character; (c) relatively high symmetry; (d) volume of approximately 300 A^3; (e) weak base character.

Then, in order to serve as an ideal precipitating agent for the radioactive Cs in a large-scale process, the anion should also (a) be chemically inert, (b) produce a precipitate with a high percentage of Cs, (c) generate a solubility order of Na ≈ K≫Cs, and (d) be easy and inexpensive to prepare and/or obtain.

A number of precipitation compounds were tried for the removal of cesium from aqueous waste streams, they are transition metal ferrocyanides, phosphor molybdates or phospotungstates, tetraphenyl borate. Among the transition metal ferrocyanides copper and nickel ferrocyanides are widely used. Copper ferrocyanides have better mechanical characteristics and radiation stability. Their composition fairly remains constant and does not vary with the change in mole ratios of the reactants.

An isotope dilution–precipitation process was developed to remove Cs-137 from radioactive wastewater. It involves addition of stable cesium chloride to wastewater and then allows both the stable and radioactive Cs^+ to be precipitated together using sodium tetraphenylborate. This process was investigated for treating LLW [26].

1.7.2. Solvent extraction

For separation of cesium from acidic waste solutions, solvent extraction methods involving cobalt dicarbollide, crown ethers, calixarenes and calix-crowns were extensively studied [27].

Cobalt dicarbollide has been studied as a cesium extractant from acidic High Level Waste (HLW) [28] which is having good chemical and radiation stability [29]. Chlorinated cobalt dicarbollide (CCD), shown in Figure 1.11 has also been extensively studied as an extractant for cesium by Czech scientists [30].

Dicarbollide is a very lipophilic anion and can selectively interact with certain cations through ion pairing. Cesium, with good ion pairing ability with CCD, is found to be the most efficiently extracted cation by CCD.

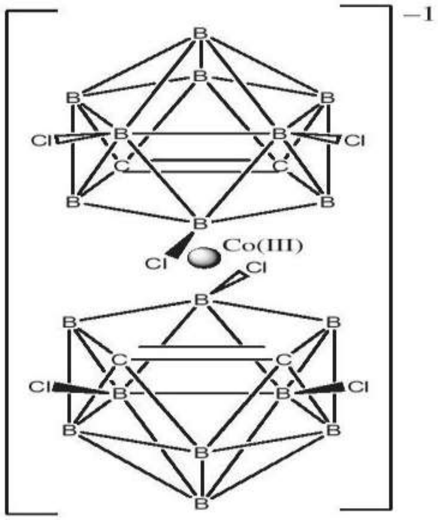

Figure 1.11 Chlorinated cobalt dicarbollide

Novel crown ether substituted cobalt bis(dicarbollide) ion has been used as a selective reagent for cesium extraction [31]. New anion derivatives of the closo-decaborate $[B10H10]^{2-}$ bearing amine or phosphine groups were tested as extractants for separating cesium from acidic medium, too, where cesium cations are complexed by these anions to form neutral compounds which can be extracted by organic solvents of medium polarity [32]. Makrlik et al. also carried out several studies by using combined extractants to extract cesium, mainly with hydrogen dicarbollylcobaltate and crown ethers or PEG [33-36].

One deterrent to using cobalt dicarbolide for the separation of cesium is the requirement for nitrobenzene as a solvent. Nitrobenzene is on the EPA "Extremely Hazardous" list [37] because of its toxicity and potential for explosion in strong acids and bases. The high cost of cobalt dicarbolide may be a drawback, although material costs are generally a minor concern relative to the total plant operating cost.

Macrocyclic polyethers, or crown ethers have been found to be effective for extracting cesium from aqueous streams [38, 39]. Researchers at ANL developed a derivative of dibenzo-18-crown-6 (CSEX) that had good cesium distributions and high selectivity of cesium over sodium, but the extractant molecule was not stable in acid media [40, 41]. Russian researchers focused on dibenzo-21-crown-6 extractant molecules, but with limited success [42]. Crown ethers containing seven or eight oxygen atoms may also have good size compatibility for cesium. For example, bis[1-hydroxyalkylbenzo]-21-crown-7 (Figure 1.12), [43] 4,5-bis(tertoctylbenzo)- dibenzo-24-crown-8 (Figure 1.13), [44] have been selected as cesium extractants.

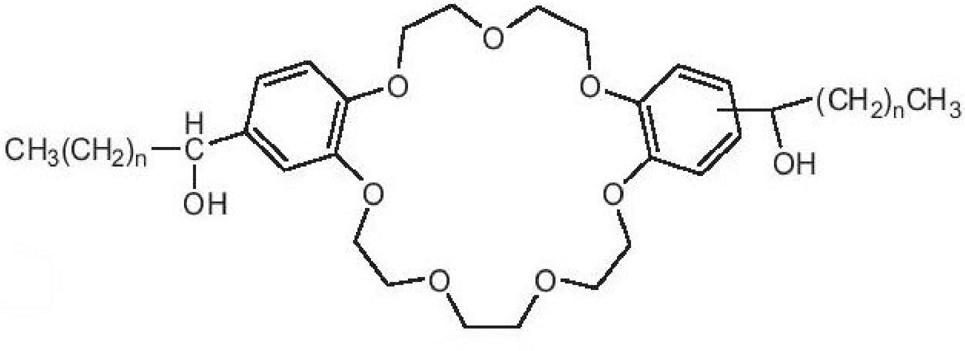

Figure 1.12 bis [1-hydroxyalkylbenzo]-21-crown-7

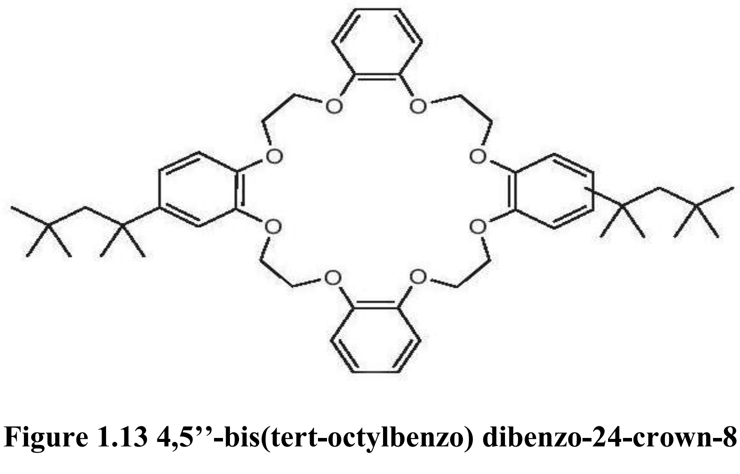

Figure 1.13 4,5’’-bis(tert-octylbenzo) dibenzo-24-crown-8

Crown ethers are stereospecific extractants because they have a cage structure that can be highly selective for the Cs^+. The primary disadvantages of the crown ethers have been chemical and radiolytic instability, tendency for third phase formation, and cost [45, 46].

In recent years, calixarenes, especially calixarene-crown ether derivatives, have been extensively studied as extractants for cesium [47]. Calixarenes are cyclic compounds constituted by four phenolic units linked by methylene groups (p-tert-butyl-calix[4]arene). Numerous calixarene-crown extractants were developed and determined that compounds with a polyethylene glycol chain containing six oxygen atoms were more efficient for cesium extraction and more selective for cesium over sodium than compounds containing five or seven oxygen atoms [48]. Calix[4]arene-crown ethers (Figure 1.14) were found to be highly effective at removing cesium from acidic media.

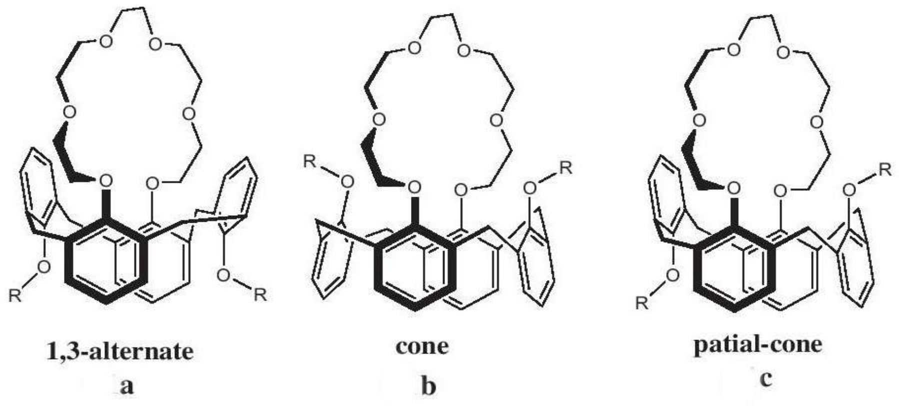

1,3-alternate **a** **cone** **b** **patial-cone** **c**

Figure 1.14 Calix [4] arene-crown ethers

Guillon et al. efficiently synthesized a series of calix arene-crown ethers with different conformations [49]. The extraction ability of calixarene-crown ethers for cesium is structure-sensitive. Minor modification on the main frame of calixarene-crown ethers can result in a significant change in extraction properties [50, 51].

Gorbunova and co-workers synthesized several functionalized calix[4]arene benzo-crown-6 ethers with primary amine groups in various positions [52]. These compounds retain good extraction ability for cesium when the amino group is neutral, but they show very poor extraction ability when the amino group is protonated, which will permit pH-switched back-extraction or stripping.

Tests on cesium extraction employing one of the developed amine-derivatized calixarenes, 5-amino methyl calix[4] arene-bis[4-(2-ethylhexyl)-benzo-crown-6] depicted in Figure 1.15, have shown potential application in cesium removal from radioactive wastes [53, 54]. Mohapatra et al. studied cesium extraction by three calixarene-crown ethers, calyx [4] arene-bis (crown-6), calyx [4] arene-bis (benzocrown-6), and calix[4] arene- bis (napthocrown-6). It was found that calix [4] arene-bis(napthocrown-6) shown in Figure 1.16 is the best for cesium extraction [27].

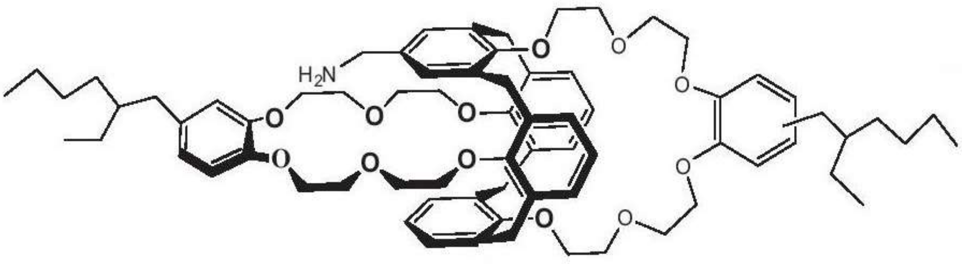

Figure 1.15 5-aminomehtyl calix [4] arene-bis [4-(2-ethylhexyl)-benzo-crown-6]

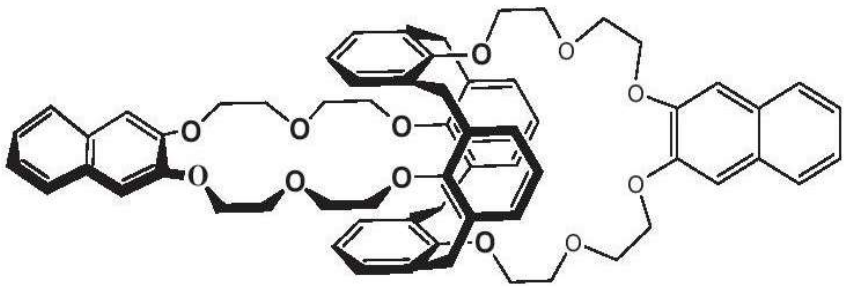

Figure 1.16 Calix [4] arene-bis(napthocrown-6)

Calixarenes appear to be stable in acidic media, however, they are still relatively expensive extractants. The major advantage of calixarenes over other cesium extractants, such as cobalt dicarbollide, is that cesium can be easily stripped from the solvent using water or dilute nitric acid solutions. The use of Room Temperature Ionic Liquids (RTIL) as a medium for cesium extraction has also been great interest in recent years [55-59].

1.7.3. Ion exchange

Extensive research and development has been performed on the application of ion exchange and extraction chromatography technologies for the separation of cesium from acidic HLW. Separation of cesium from acidic streams has been demonstrated with many ion exchange and fixed extractant media.

Insoluble transition metal hexacyanoferrates have been known for decades as effective agents for the removal of radioactive cesium from solution. Cesium removal from acidic solutions utilizing transition metal cyanoferrate sorbents has been widely demonstrated. Much work has been done with metal (cobalt, zinc, nickel and titanium) cyanoferrates for the removal of cesium from nuclear waste streams [60-67]. One of the most promising cesium-selective hexacyanoferrates is potassium nickel hexacyanoferrate (KNiFC) and its preparation methods have been developed by Kourim [66, 68]. The use of potassium, nickel hexacyanoferrate ($KNiFe(CN)_6$) for Cs removal over a pH range of 1-10 was also reported [69]. Numerous cyanoferrates with Cu, Co, Ni and Zn transition metals in polyacrylonitrile (PAN) matricies for the removal of Cs were developed and tested [70].

There has been a significant amount of work in the development of titanates and silicotitanates for removal of cesium [71, 72]. While the majority of research for crystalline silicotitanates (CST) has been with alkaline media, much work has also been done with acidic waste simulants or actual wastes [63, 73].

Resorcinol Formaldehyde (RF) is another ion exchange material to be mentioned which is highly selective for Cs in alkaline medium. The high affinity of RF for Cs is attributed due to the presence of -OH group, which ionizes under high alkaline condition [74, 75].

Ammonium molybdophosphate (AMP) has also been extensively investigated and found to be highly effective for the removal of cesium from acidic liquids. Ammonium molybdophosphate becomes soluble in solutions with pH >4, and therefore, is only applicable to acidic solutions. The main disadvantage of AMP is its microcrystalline structure, which makes column operation difficult. In order to improve the column properties of AMP, several researchers tried different combinations of AMP with different organic polymers, silica gel, Al_2O_3 and zirconium phosphate. Sebesta [76] made an engineered form of AMP by immobilizing it on Polyacrylonitrile (PAN) support, making it amenable for column operations. Tranter et al [77] reported that AMP–PAN has high Cs ion exchange capacity of 32 g Cs/kg sorbent. Todd et al [63, 78] reported the batch equilibrium data for AMP–PAN from which cesium adsorption followed the classical Langmuir isotherm. Cesium can be eluted from AMP-PAN with concentrated ammonium salt solutions (NH_4NO_3, NH_4Cl, etc.) or the cesium and ammonium molybdophosphate complexes can be dissolved in caustic to separate the active exchanger material from an inert binder material, such as PAN [79].

Other ion exchange materials based on titanium and zirconium phosphate [80], antimony pentoxide, titanium dioxide, and various other metal oxides [81-84], and zirconium monohydrogen phosphate (ZrHP) sorbent embedded with AMP have been developed and tested for the removal of cesium from acidic media [85, 86].

1.8. Scope of the present work

The environmental concerns as well as the potential applications of radioactive Cs would make separation of Cs from HLW an attractive proposition. Many techniques and materials have been studied for the separation of Cs from HLW.

Ion exchange (IX) is widely used for Cs-137 separation from radioactive wastes. Ammonium MolybdoPhospahte Polyacrylonitrile (AMP-PAN) was reported to be having high affinity for Cs from acidic waste. Due to its high affinity for cesium, regeneration of AMP-PAN to obtain Cs in pure form is a multistep process and various options have been studied to achieve this.

In an attempt to get Cs in pure form in a single step operation, a hybrid Electrodialysis-Ion exchange (EDIX) process was investigated in this work. In this technique, Cs sorbed ion exchange resin (AMP-PAN) is filled in the middle compartment of a three compartment electrodialysis cell and is separated from anode and cathode compartments using ion exchange membranes. This process is similar to electrodeionization process, which was initially developed for ultra pure water production by Glueckauf [87]. The difference between EDI and the present EDIX is that in the former the ion exchange resin is regenerated by ions due to water splitting at the bipolar interface, whereas in the later, the regeneration is due to the eluant ions (ammonium ions) circulating in the ED cell. The desorption of cesium is carried out by passing an eluant (NH_4^+ containing solution) through the anode/middle compartment and the desorbed Cs is recovered in the cathode compartment where it had migrated under the application of electric current. Thus, ion exchange and electrodialysis are combined to produce an effective process for the selective separation of Cs^+. This process recovers Cs in pure form and concentrates it with minimum number of operations.

The objective of the present work is to study the hybrid EDIX process for recovery of Cs from HLW using AMP-PAN. This study includes

(i) Batch and column experiments for recovery of Cs from HLW by AMP-PAN. Investigation of mechanisms of the exchange operation.

(ii) Regeneration of Cs loaded AMP-PAN by EDIX. Investigation of current-voltage characteristics and determination of limiting currents.

(iii) Studies on different modes of operation of the electrodialysis cell for maximum recovery of Cs from AMP-PAN,

(iv) Analysis of the transport phenomena of Cs in the electrodialysis setup.

Materials and methods

2

This chapter lists the details of the properties of various materials and chemicals used in the work. Technical details and principles of instruments used for characterizing AMP-PAN such as FT-IR and XRD are presented. Principals of analytical instruments made use of, such as Atomic Absorption spectrophotometer, pH meter, conductivity meter are explained.. Experimental procedures used for batch ion exchange studies, kinetic studies, column loading and regeneration of Cs on AMP-PAN are detailed. Various methods employed for the investigation of EDIX process for the recovery of Cs from AMP-PAN are explained.

2.1. Materials and chemicals

2.1.1. Chemicals and reagents

All the chemicals and reagents used in this study were of analytical grade and were used as received unless otherwise mentioned.

2.1.2. AMP-PAN

Ammonium molybdophosphate $(NH_4)_3[PMo_{12}O_{36}]\cdot 3H_2O$–polyacrylonitrile (AMP-PAN). Ion-exchange resin was supplied by M/s. Thermax Ltd, Pune (India). The properties of the resin are given in the Table. 2.1.

Table 2.1 Properties of AMP-PAN ion exchange resin

Properties of AMP-PAN	
Nature	Cationic resin
Particle Size	0.4-0.5 mm
Shape	Spherical
Porosity	Macro porous
Bulk density	1.5 g/cm³
AMP loaded on resin	65%
Moisture	55%

2.1.3. CMI-7000 and AMI-7000 ion exchange membranes

The cation exchange membrane (CMI-7000) and anion exchange membrane (AMI-7000) were procured from Membranes International, USA. The properties of the cation and anion exchange membranes are presented in Table 2.2 and Table 2.3 respectively.

Table 2.2 Properties of CMI-7000

Technical Specification	**CMI-7000S**
Functionality	Strong Acid Cation Exchange Membrane
Polymer Structure	Gel polystyrene cross linked with divinylbenzene
Functional Group	Sulphonic Acid
Standard Thickness (mils)	18±1
Total Exchange Capacity (meq/g)	1.3±0.1
Water Permeability(ml/hr/ft^2)@5psi	<10
Mullen Burst Test strength (psi)	>80
Thermal Stability (C°)	90
Chemical Stability Range (pH)	1-10

Table 2.3 Properties of AMI-7000

Technical Specification	**AMI-7001S**
Functionality	Strong Base Anion Exchange Membrane
Polymer Structure	Gel polystyrene cross linked with divinylbenzene
Functional Group	Quaternary Ammonium
Standard Thickness (mils)	20±1
Total Exchange Capacity (meq/g)	1.0±0.1
Water Permeability(ml/hr/ft^2)@5psi	<20
Mullen Burst Test strength (psi)	>80
Thermal Stability (C°)	90
Chemical Stability Range (pH)	1-10

2.1.4. Preparation of simulated HLW

CsCl, SrCl and NaCl salts were used for the preparation of simulated HLW solution in 4N HNO_3. Other elements present in the actual waste are not simulated as their concentrations are much lower.

2.1.5. Eluant preparation

Ammonium Sulphate salt was used for the preparation of eluant with Demineralized water as solvent.

2.2. Instrumentation

2.2.1. pH meter

All pH measurements were made with Elicho LI 120 pH meter. The meter was calibrated at 298 K with standard buffers of pH 4, 7 and 10.

2.2.2. Ion conductivity meter

The sample conductivities were made with Radiometer Analytical CDM 230 ion conductivity meter. The meter was calibrated at 298 K with 0.1D KCL.

2.2.3. Atomic Absorption Spectrophotometer (AAS)

Cs, Sr and Na in all samples were analyzed by Atomic Absorption Spectrophotometer (novAA 300, Analytik jena). Atomic absorption spectroscopy is an analytical technique used for quantitative determination of chemical elements using the absorption of optical radiation (light) by free atoms in the gaseous state.

Atoms of different elements absorb characteristic wavelengths of light. Analysing a sample for a particular element requires a light from that element. For example, to analyze a sample for the presence of lead, a lamp containing lead emits light from excited lead atoms that produce the right mix of wavelengths to be absorbed by any lead atoms from the sample [88].

The quantity of interest in atomic absorption measurements is the amount of light at the resonant wavelength, which is absorbed as the light passes through a cloud of atoms. As the number of atoms in the light path increases, the amount of light absorbed increases in a predictable way. By measuring the amount of light absorbed, a quantitative determination of the amount of analyte element present can be made. The use of special light sources and careful selection of wavelength allow the specific quantitative determination of individual elements in the presence of others. It requires standards with known analyte content to establish the relation between the measured absorbance and the analyte concentration and relies therefore on the Beer-Lambert Law.

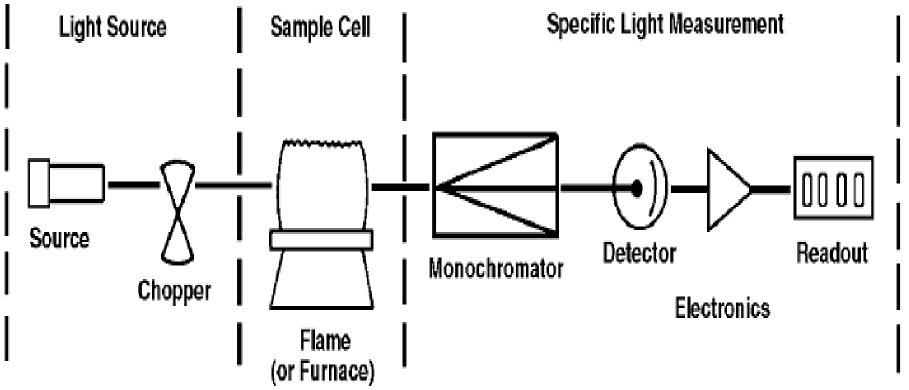

Figure 2.1 Atomic absorption spectrometer block diagram

In order to analyze a sample for its atomic constituents, it has to be atomized. The atom cloud required for atomic absorption measurements is produced by supplying enough thermal energy to the sample to dissociate the chemical compounds into free atoms. The oldest and most commonly used atomizers in AAS are flames, principally the air-acetylene flame with a temperature of about 2300 °C and the nitrous oxide system (N_2O)-acetylene flame with a temperature of about 2700 °C. The latter flame, in addition, offers a more reducing environment, being ideally suited for analytes with high affinity to O_2. Other atomizers, such as electrothermal (graphite tube), glow-discharge atomization, hydride atomization, or cold-vapor atomization might be used for special purposes.

The atoms should then be irradiated by optical radiation, and the radiation source could be an element-specific line radiation source or a continuum radiation source. The radiation then passes through a monochromator in order to separate the element-specific radiation from any other radiation emitted by the radiation source, which is finally measured by a detector.

The ease and speed at which precise and accurate determinations can be made with this technique have made atomic absorption one of the most popular methods for the determination of metals.

2.2.4. X-Ray Diffraction

X-ray diffraction (XRD) is a unique method in determination of crystallinity of a compound. The atomic planes of a crystal cause an incident beam of X-rays to interfere with one another as they leave the crystal. The phenomenon is called X-ray diffraction.

XRD analysis is based on constructive interference of monochromatic X-rays and a crystalline sample. The X-rays are generated by a cathode ray tube, filtered to produce monochromatic radiation, collimated to concentrate, and directed toward the sample. The interaction of the incident rays with the sample produces constructive interference (and a diffracted ray) when conditions satisfy Bragg's Law ($n\lambda=2d \sin \theta$). This law relates the wavelength of electromagnetic radiation to the diffraction angle and the lattice spacing in a crystalline sample [89]. The characteristic x-ray diffraction pattern generated in a typical XRD analysis provides a unique "fingerprint" of the crystals present in the sample. When properly interpreted, by comparison with standard reference patterns and measurements, this fingerprint allows identification of the crystalline form.

A block diagram of the typical powder diffractometer, consisting of an X-ray source, a sample under investigation and a detector to pick up the diffracted X-rays is shown in the Figure 2.2. The X-ray beam passes through the soller and divergence slits and then fall on the sample which is spread uniformly over a rectangular area of a glass slide. The scattered X-rays from the sample pass through the soller and receiving slits and then fall on a monochromator before detection. The monochromator separates out the stray wavelength radiation as well as fluorescent radiation emitted by the sample. The output of the diffraction measurement is obtained as plot of intensity of diffracted x-rays versus Bragg angle. In the present study, STOE diffractometer based on the Bragg-Brentano reflection geometry, was used for the characterization of AMP-PAN ion exchange resin.

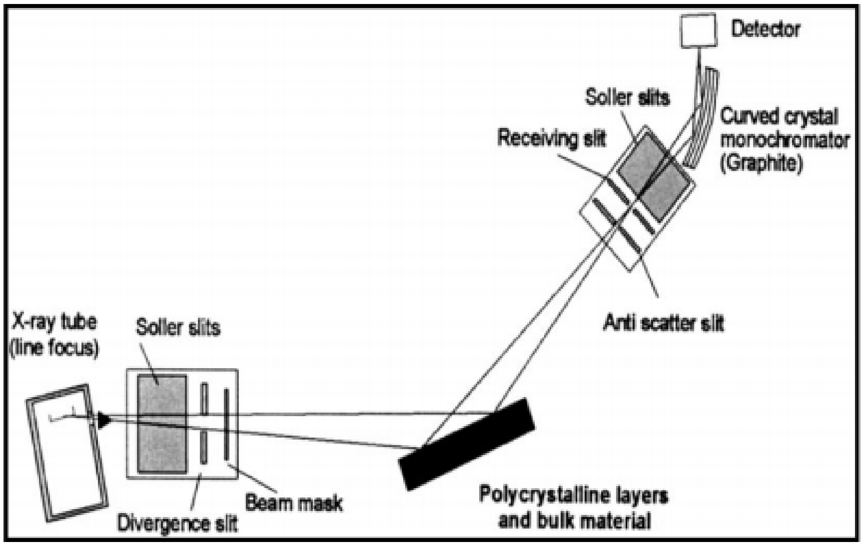

Figure 2.2 X-Ray diagram of a typical reflection mode diffractometer

2.2.5. Fourier transform infrared spectroscopy (FTIR)

ABB-MB 3000 FT-IR spectrometer with a range of 4000-400 cm^{-1} was used for the measurement of IR spectra.

FTIR is an effective analytical instrument for detecting functional groups and characterizing covalent bonding information by producing an infrared absorption spectrum. The spectra produce a profile of the sample, a distinctive molecular fingerprint that can be used to screen and scan samples for many different components. It offers quantitative and qualitative analysis for organic and inorganic samples [90].

A common FTIR spectrometer consists of a source, interferometer, sample compartment, detector, amplifier, A/D convertor, and a computer. The source generates radiation which passes the sample through the interferometer and reaches the detector. Then the signal is amplified and converted to digital signal by the amplifier and analog-to-digital converter, respectively. Eventually, the signal is transferred to a computer in which Fourier transform is carried out. Figure 2.3 is a block diagram of an FTIR spectrometer.

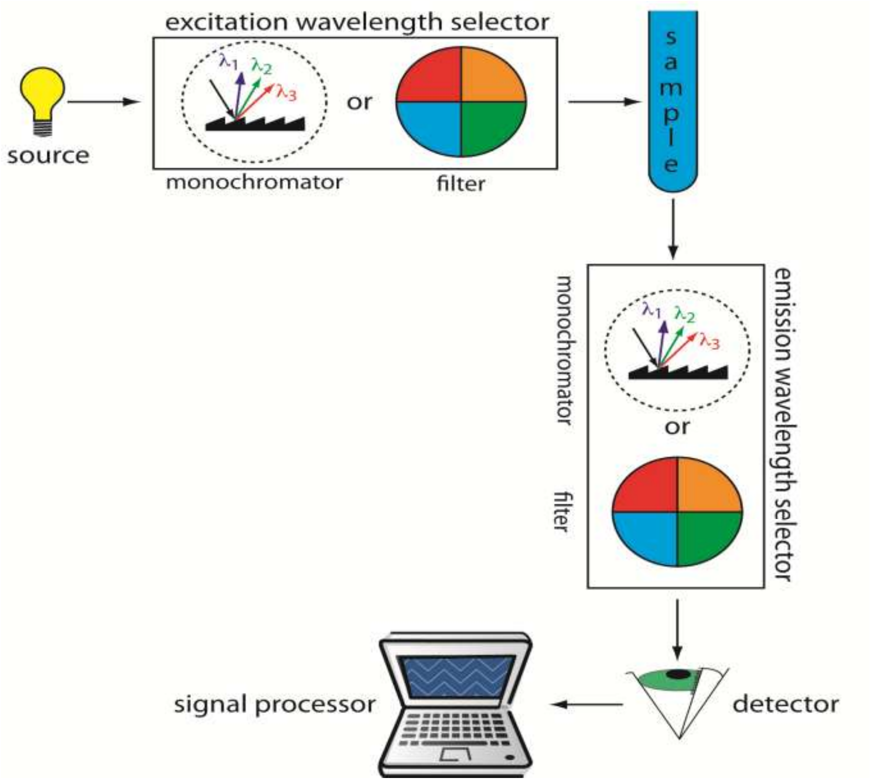

Figure 2.3 Block diagram of FTIR spectrometer

2.3. Experimental methods

2.3.1. Batch equilibrium studies

2.3.1.1. Equilibrium Isotherms

Equilibrium sorption studies were carried out by contacting 10 mL of synthetic waste solutions of different initial concentrations of Cs in 4N HNO_3 with ion exchange resin of 0.1 g. Vials containing the waste and resin were agitated using a water shudder maintained at 25 ^{0}C and agitation speed of 60 RPM. Contact time of 8 h was provided, which was sufficient for the system to reach equilibrium. The resin was separated from the solution by filtration and the equilibrium concentration of the solution was determined by Atomic Absorption Spectrophotometer. The uptake of cesium by the ion exchange resin, q_e (mg/g), was obtained as follows

$$q_e = \frac{(C_0 - C_e)V}{W} \tag{2.1}$$

where, C_o and C_e are the initial and equilibrium metal concentrations in the solution phase (mg/L), respectively; V is the volume (L); and W is the dry weight of the resin used (g).

2.3.1.2. Uptake of Cs by AMP-PAN

The selective uptake of Cs by AMP-PAN was tested with a simulated solution of Cs, Sr and Na in different concentrations of nitric acid medium. The initial concentrations of Cs, Sr and Na were 800, 100 and 1000 ppm, respectively. One gram of AMP-PAN was equilibrated in 20 mL of the simulated solution for 24 h in water shudder at 60 RPM.

2.3.2. Batch kinetic studies

Batch kinetic studies of cesium ion exchange on AMP-PAN were studied by adding 3 g of AMP-PAN ion exchanger resin of 0.5 mm average diameter, to 1L of cesium solution and stirring at 600 RPM. The solution was stirred with a mechanical stirrer and samples were withdrawn at several time intervals, total sampling volume being 2% of the solution volume. The batch studies were performed for different feed concentrations, particle sizes and stirring speeds.

2.3.3. Column dynamic studies

2.3.3.1. Cs loading on AMP-PAN

Fixed-bed column experiments were conducted at room temperature using a glass column with an internal diameter of 20 mm and a height of 55 cm. The column was packed with AMP-PAN ion-exchanger on supporting layers of glass-wool to prevent the loss of the resin. A schematic of the experimental setup for column study is shown in Figure 2.4.

Column performance of Cs ion-exchange on AMP-PAN was studied for different influent cesium concentrations (500-1000 mg/L), feed flow rates (5-15 mL/min) and bed heights (14.5-21.5 cm). The Cs solution was pumped into the column in a down-flow direction by a peristaltic pump. Samples were collected at regular intervals and were analyzed by Atomic Absorption Spectrophotometer (AAS).

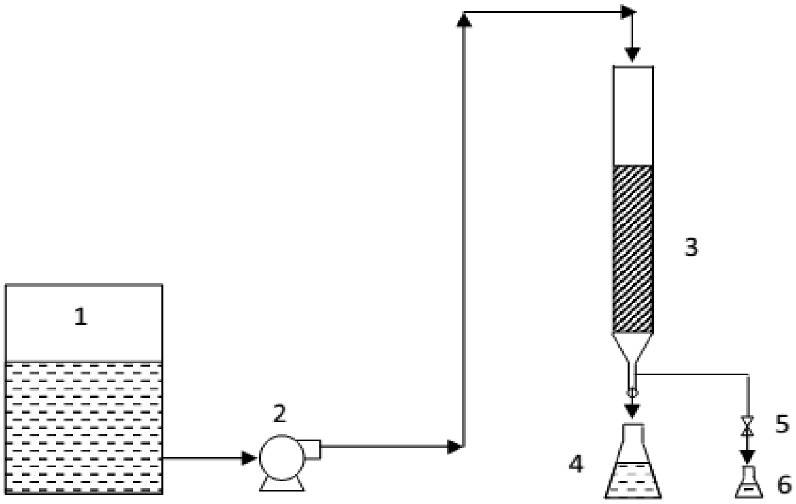

Figure 2.4 Schematic of column setup for fixed bed studies

1. Influent tank; 2. Peristaltic pump; 3. Ion exchange resin;
4. Effluent collection tank; 5. Valve; 6.Sampling bottle

2.3.3.2. Regeneration of AMP-PAN

A glass column with an inner diameter of 12 mm filled with approximately 5 g AMP-PAN exchanger was loaded with 750 ppm of Cs^+ in 4N HNO_3 at 5ml/min flow rate and calculated the break though capacity. For the elution of cesium from AMP-PAN, ammonium sulphate solutions of 3.7 M and 0.27 M were passed through the column at 5 mL/min and samples were collected from the outlet at regular intervals of time.

2.3.4. Electrodialysis-Ion exchange (EDIX)

2.3.4.1. Mode-I

The experimental set-up consists of three separate compartments: anode compartment, middle compartment and cathode compartment as shown in Figure 2.5.

After loading Cs on AMP-PAN resin in column, the loaded resin was transferred to the middle compartment of the electrodialysis cell through a funnel. The AMP-PAN loaded compartment was separated from the anode and cathode compartments by two cation exchange membranes having dimensions of 10 cm × 10 cm × 0.5 cm and an effective area 50 cm^2 each. The outer two electrode compartments had dimensions of 10 cm × 10 cm x 0.8 cm and each contained a platinum coated titanium electrode with effective area of 50 cm^2. A regulated D.C (direct current) power supply rated in amperes was used to provide a steady current. Both anolyte and catholyte were circulated at same flow rates of 200 mL/min and flow rate through middle compartment is maintained at 5 mL/min. Middle and cathode compartments were circulated with one litre of 0.1 N HNO_3. One litre of 0.27 M NH_4^+ made from $(NH_4)_2SO_4$ salt was circulated as eluant in the anode compartment.

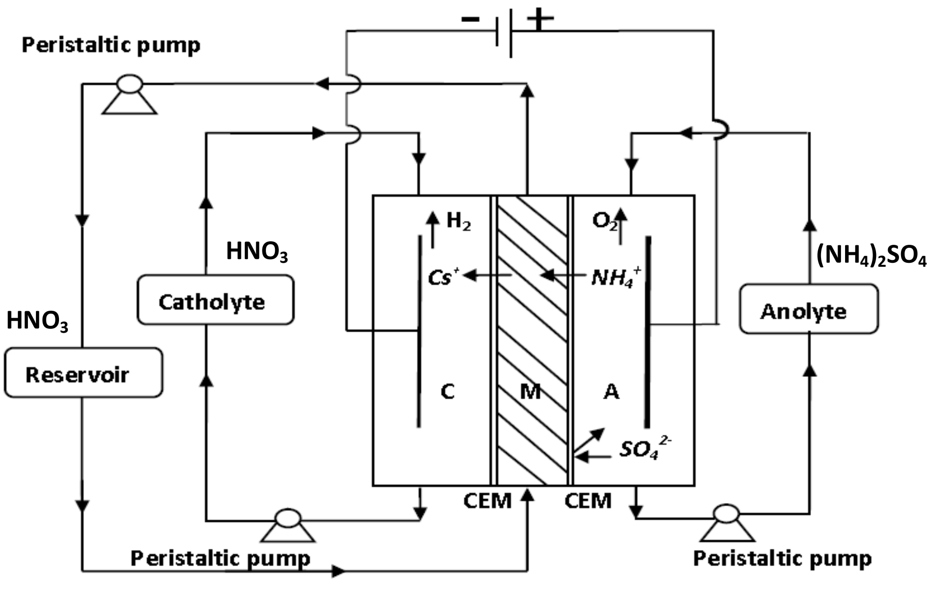

Figure 2.5 EDIX experimental setup for mode-I operation

2.3.4.2. Mode-II

In this mode of operation, the eluant ($(NH_4)_2SO_4$) is passed directly through the AMP-PAN loaded in the middle compartment of the three compartment electrodialysis cell. A schematic of experimental setup is shown in Figure. 2.6.

The central compartment containing AMP-PAN is separated from anode and cathode compartments using anion and cation exchange membranes, respectively.

Dilute nitric acid (0.1N) of 1000 mL was used as both electrolytes, and was circulated in the anode and cathode compartments at 200 mL/min using peristaltic pumps. Ammonium sulphate used as an eluant, was passed through the central compartment at 5 mL/min in once-through mode. The cell was operated varying the current density, concentrations of both eluant and catholyte and operating time. Samples were collected from all the compartments at regular intervals of time and analyzed for cesium concentration.

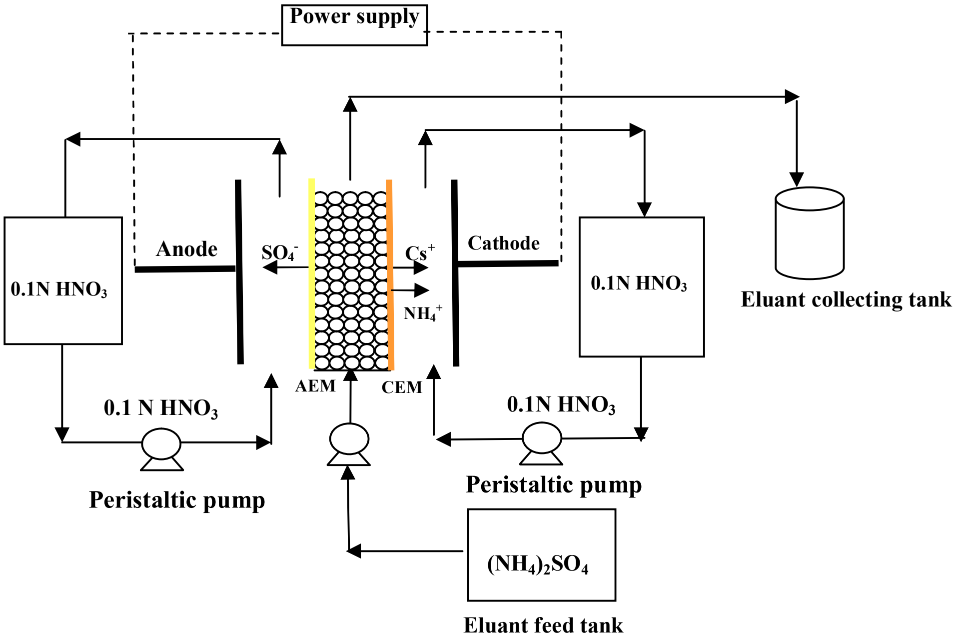

Figure 2.6 Schematic of experimental setup for mode-II operation

2.3.4.3. Experimental determination of Limiting current density

Figure 2.7 shows the schematic of the experimental setup used for the determination of current- voltage curves of the hybrid EDIX process.

Current-voltage curves were obtained by a stepwise increase of the current through the cell, at the rate of 0.2 A in 30 sec. The limiting current density is determined by the intersection of the first and the second slope of the current versus voltage curve.

Limiting currents can also be determined by transforming the I-V curves into Cowan plots [91]. Cowan plots are obtained by plotting the electrical resistance across the membrane stack against the reciprocal electric current. The limiting currents are obtained by drawing tangents to decreasing resistance and increasing resistance curves in Cowan plots and the limiting current is the current corresponding to the point of intersection of these two lines.

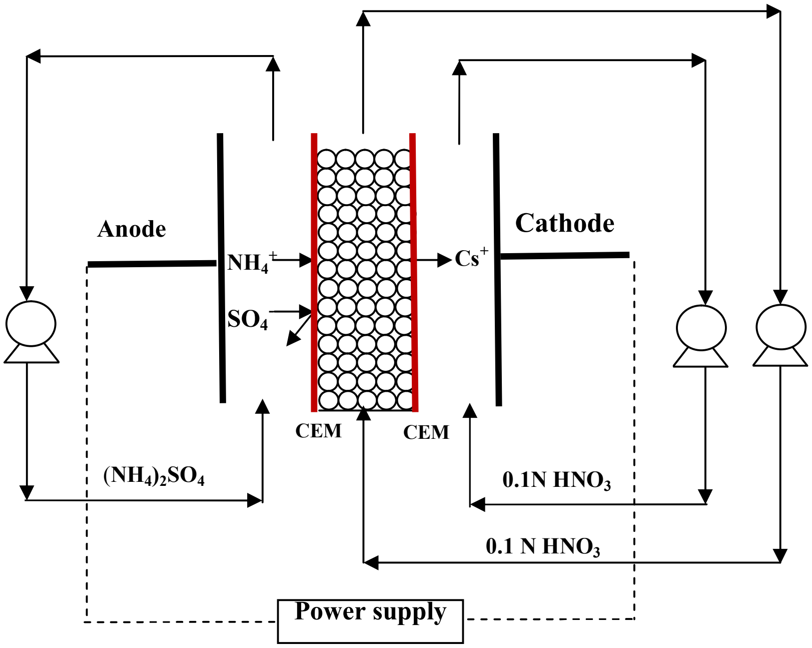

Figure 2.7 Experimental setup for limiting current determination

Cesium ion exchange studies on AMP-PAN

3

This chapter gives a detailed application of AMP-PAN for separation of Cs from acidic solutions. Batch equilibrium isotherms, kinetic studies and parameters affecting the kinetics are elaborated. Different kinetic models are applied to the experimental batch kinetic data and evaluated the kinetics. Column dynamic sorption of Cs on AMP-PAN is studied for different operating parameters. Column properties like mass transfer zone, saturation of bed, etc., are discussed. Various mathematical models are applied to predict the breakthrough of cesium from column for different parameters.

3.1. Introduction

Many methods have been proposed to separate ^{137}Cs from nuclear waste, including co-precipitation [92, 93], solvent extraction [94, 95], and ion exchange [96-98]. Though co-precipitation is widely practiced for treatment of low active wastes, ion exchange is the most promising for wastes with high concentration of Cs. Inorganic ion exchangers such as titanium phosphate, zirconium phosphate, ferrocyanide molybdates, hexacyanoferrate compounds, alumino-silicates and ammonium molybdophosphate were investigated for their application to cesium removal from acidic waste [77, 86, 99-105].

Of these, Ammonium Molybdophosphate-Polyacrylonitrile (AMP-PAN) was reported to be better than the other cesium sorbents. Sebesta [106] made an engineered form of AMP by immobilizing it on Polyacrylonitrile (PAN) support, making it amenable for column operation. Chemical and mechanical stability of the AMP-PAN in 3M HNO_3 is quite high and its stability is not adversely affected by a radiation dose of 10^4 Gy [107]. Park et al. [108] investigated the removal of cobalt, strontium and cesium from radioactive laundry wastewater by AMP–PAN in the presence of cationic and anionic surfactants and reported that AMP-PAN had high selectivity for Cs. Suss and Pfrepper also reported the selectivity for Cs over other cations and found excellent distribution coefficients in HNO_3 systems up to 10 N [109]. Further, AMP–PAN showed a high capacity for removal of Cs from feed solutions with high amount of salts at 23^oC and 50^0C [77]. Nilchi et al. [110] studied the stability of AMP-PAN and the effects of contact time, solution p^H, solution temperature, and interfering cations on cesium adsorption. AMP-PAN is thermally stable up to 190^oC and also chemically stable in mineral acids. It was observed that the increase of pH, temperature, and contact time have positive effects on cesium adsorption. However, limited studies are available in the literature regarding its kinetic behavior and the uptake of cesium from acidic waste solutions in column operations [78, 110-113].

Fixed-bed column performance is usually described through the concept of the breakthrough curve. Breakthrough is said to have occurred when the effluent concentration crosses a set value (typically 5% of influent concentration) and exhaustion of the bed occurs when the effluent concentration is equal to another set value (typically 95% of the influent concentration [114].Complete exhaustion occurs when the effluent concentration is equal to the influent concentration [114-116], which might take a long time. The area of the sorption bed in which sorption is occurring is called the mass transfer zone (MTZ) [114]. Time of breakthrough represents the saturated zone and the time period between breakthrough and exhaustion, the unsaturated zone. Breakthrough capacity and percentage utilization of the column depend strongly on the operating parameters of the column, in addition to the ion exchanger properties.

For Cs sorption on AMP-PAN, not much data were reported on the dependence of breakthrough curve on these parameters, such as bed height, flow rate and concentration of the feed solution. Effect of these operating parameters on the breakthrough characteristics of AMP-PAN column for removal of Cs from aqueous acidic cesium solutions is presented in this chapter.

Many mathematical models [114-116] were proposed for the prediction of breakthrough curves, such as Thomas model, Yoon-Nelson model, Bohart-Adam model. This chapter also examines the application of different models to the experimental breakthrough curves in order to assess the validity of the model and estimate the model coefficients.

3.2. Batch Studies

When a solute is introduced into a two-phase system, which may be gas/solid, gas/liquid, or gas/liquid, it will be distributed between the two phases, and when equilibrium is reached, the solute distribution will be defined by the distribution coefficient. The high affinity of the species by the sorbent is indicated by high distribution coefficient. The distribution coefficient, K_d, of a solute between two phases is defined as the ratio of the concentration of the solute in one phase to the concentration of the solute in the other phase under equilibrium conditions.

$$\boldsymbol{K_d} = \left(\frac{C_i - C_f}{C_f}\right)\left(\frac{V}{W}\right) \qquad (3.1)$$

where, K_d is the distribution coefficient (mL/g), C_i is the initial concentration of the solute (mg/L), C_f is the final equilibrium concentration of the solute (mg/L), W is the mass of the solid phase (g) and V is the volume of solution (L).

3.2.1. Selective uptake of Cs by AMP-PAN

The selectivity of AMP-PAN for Cs was tested with a simulated solution of Cs, Sr and Na in different concentrations of nitric acid medium as mentioned in 2.3.1.2. The variation of distribution coefficients of Cs, Sr and Na with acidity was shown in Figure 3.1. The distribution coefficients of Cs were in the range of 900-1500 mL/g for the studied concentration. The high distribution coefficient of Cs on AMP-PAN showed its greater ability for the separation of Cs from aqueous solution. The high affinity of AMP-PAN for Cs^+ is due to the similar hydration radii of Cs^+ and NH_4^+ (2.50 Å). Even though the distribution coefficients of Cs decreased with increase in acidity, the values were very high compared to the distribution of other ions (Sr and Na). The decrease in distribution coefficients with increase in acidity is due to increase in competition from protons for exchange sites which might have decreased the exchange of other ions.

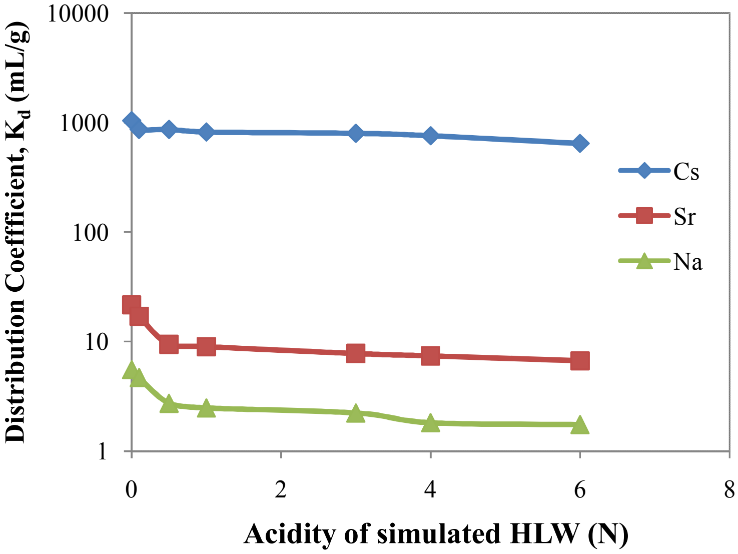

Figure 3.1 Distribution coefficients of important ions in HLW on AMP-PAN

3.2.2. Characterization studies of AMP-PAN

The FT-IR spectrum of unused AMP–PAN and Cs sorbed AMP-PAN were shown in Figure 3.2. From the spectrum, it can be seen that the broadness of the O–H stretching band in the region of 3,000–3,650 cm^{-1} is caused by the H-bonding between the adsorbed H_2O and N–H group. Maximum adsorption at 2250 cm^{-1} is due to the nitrile groups in the PAN [117-119]. The peak at 1,620 cm^{-1} corresponds to the bending vibration of water molecules [110]. The strong peak range of 1400–1500 cm^{-1} is due to the presence of NH_4^+. The broad peak existing in the region of 1,300–1,500 cm^{-1} is due to bending vibration of $-CH_2$ group [108, 110]. The vibrational bands of P–O, Mo O, and Mo–O–Mo in the AMP are observed from 1067, 963, and 870 cm^{-1} to 1061, 960 and 867 cm^{-1}, respectively. The peaks observed in the region of 730–970 cm^{-1} and at 1,100 cm^{-1} are attributed to MoO_4^- and PO_4^{3-} groups, respectively. The sorption of Cs^+ by AMP-PAN is due to the exchange of NH_4^+ for Cs^+. Thus in the spectrum of Cs sorbed resin, a shift in the transmittance was observed in the range of 1000-3000 cm^{-1}, which confirms NH_4^+ and vibration of water molecule were involved in the mechanism of Cs sorption.

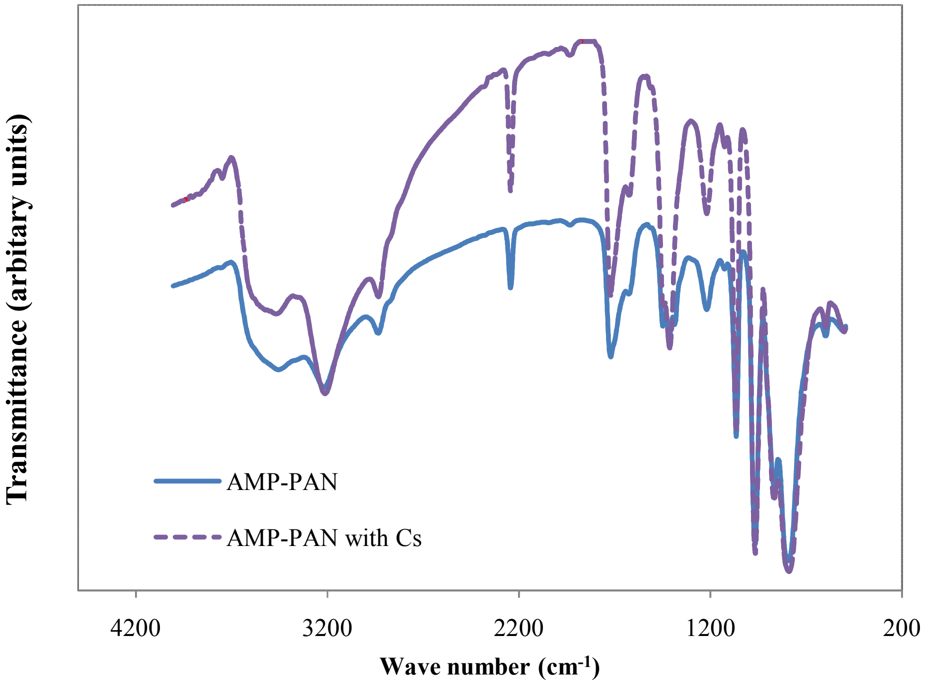

Figure 3.2 FTIR spectrum of AMP-PAN and Cs sorbed AMP-PAN

The XRD patterns of unused AMP–PAN and Cs sorbed AMP-PAN are shown in Figure 3.3. XRD is an effective method to investigate the existence of AMP in composites. From analyzing Figure 3.3, it was found that the XRD data of the synthetic AMP-PAN are in good agreement with the XRD pattern of reported data [110, 119]. The major reflections appear at 2θ=10.76, 21.62, 26.48, 30.68 and 36.14°, which suggests formation of crystalline AMP with the formula of $(NH_4)_3PO_4\ (MoO_3)12{\cdot}4H_2O$ (JCPDS Card No. 09-0412) [120]. The results indicate that AMP has been successfully loaded on PAN matrix.

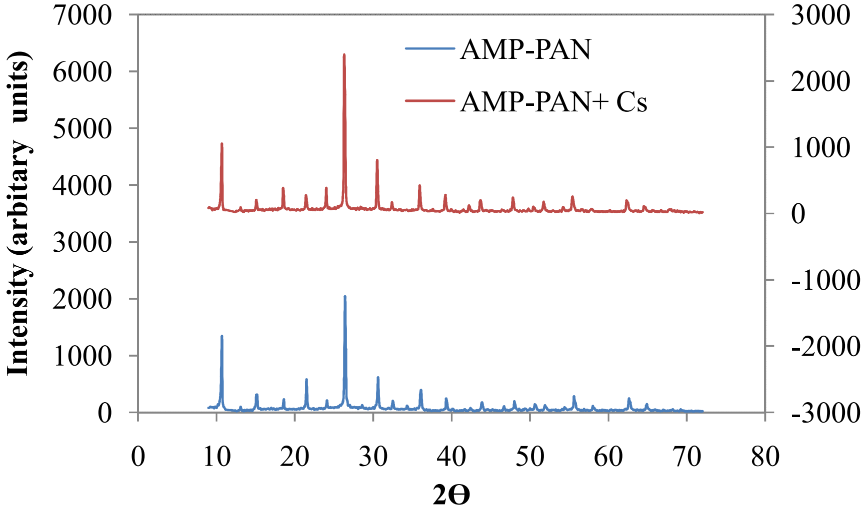

Figure 3.3 XRD patterns of AMP-PAN and Cs sorbed AMP-PAN

3.2.3. Equilibrium isotherms

Equilibrium sorption studies were conducted at different initial concentrations of cesium ranging from 0 to 1000 mg/L. The maximum equilibrium uptake capacity was observed to be 41.2 mg/g. The equilibrium isotherms of cesium ion-exchange on AMP-PAN were modeled by Freundlich and Langmuir models. These models are mathematically described by the equations:

$$q_e = K_F C_e^{1/n} \qquad (3.2)$$

$$\frac{q_e}{q_m} = \frac{bC_e}{1+bC_e} \qquad (3.3)$$

where C_e is the liquid-phase equilibrium metal concentration (mg/L); q_e the amount of metal exchanged at equilibrium (mg/g); q_m the maximum amount of metal exchanged (mg/g); K_F ($mg^{1-1/n}L^{1/n}/g$) and n are Freundlich constants and b the Langmuir constant (L/mg).

Freundlich model indicates the heterogeneity of the sorbent surface and considers multilayer sorption. The linear form of Freundlich model is expressed as follows:

$$\ln q_e = \ln K_F + \frac{1}{n}\ln C_e \qquad (3.4)$$

Langmuir model is based on monolayer sorption on uniform homogeneous surface with sites of identical nature. The linear form of Langmuir model is expressed by the following equation:

$$\frac{1}{q_e} = \frac{1}{q_m} + \frac{1}{q_m b C_e} \tag{3.5}$$

Constants of Freundlich and Langmuir models were determined from their linear plots and presented in Table 3.1.

Table 3.1 Freundlich and Langmuir isotherm constants for cesium uptake by AMP-PAN

Freundlich model			Langmuir model		
K_F(mg$^{1-(1/n)}$L$^{1/n}$g^{-1})	n	R^2	q_m(mg /g)	b (L/ mg)	R^2
11.48	4.69	0.923	41.20	0.054	0.996

The equilibrium isotherms based on the model constants are shown in Figure 3.4 along with the experimental data. As can be seen by the correlation coefficients (R^2), both models predict the experimental data well, but the Langmuir isotherm fits the equilibrium data better. This may be due to the uniform monolayer sorption on AMP-PAN.

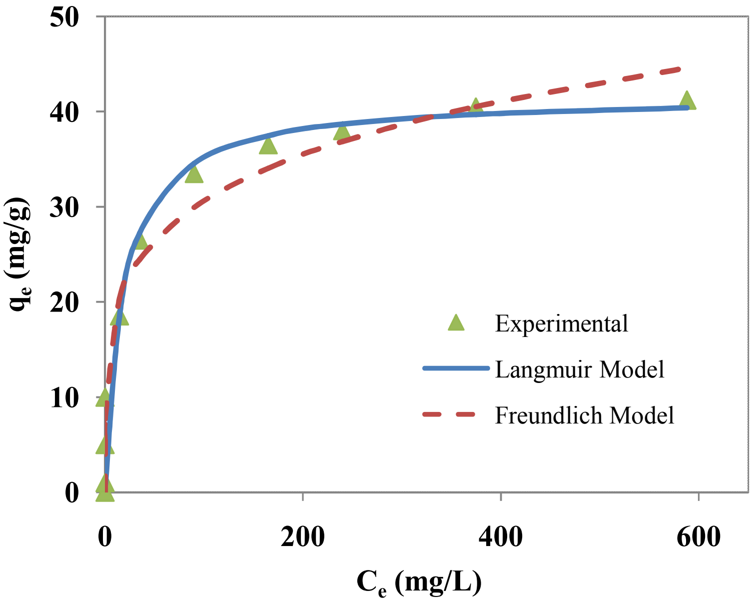

Figure 3.4 Equilibrium isotherms of Cs exchange on AMP-PAN

These experimental data are generally used in further studies concerning the dynamic sorption of solute in column studies for the prediction of breakthrough curves. However, equilibrium isotherms and constants determined in a fixed bed should be used for evaluating the breakthrough curves and kinetic constants to model such a system mathematically.

3.3. Kinetic studies

3.3.1. Effect of stirring

The effect of stirring on the uptake of cesium by AMP-PAN was studied by varying the stirring speed from 200 to 600 RPM and keeping the other variables constant as shown in the Figure 3.5.

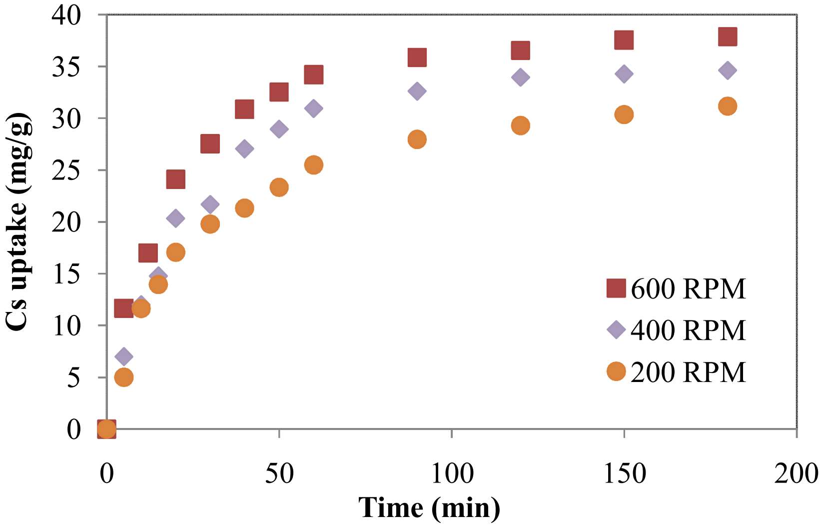

Figure 3.5 Cs uptake by AMP-PAN for different stirrer speeds
C_0= 300 mg/L, particle size= 0.5 mm

It was observed that with increase in the stirring speed from 200 to 600 RPM, the uptake of cesium increased from 31.17 to 37.86 mg/g and further increase resulted in no increase. As the stirring speed increases, the resistance to diffusion of ions to the surface of the ion-exchanger through the boundary layer decreases, which might have increased the uptake rate. It can be concluded that liquid film thickness decreases with increasing stirring speed. Similar results were available in the literature [121]. The increase in the uptake with improving turbulence indicates that the Cs uptake by AMP-PAN is film diffusion controlled at low stirring speeds. As increasing the speed beyond 600 RPM did not offer any advantage. All further kinetic experiments were carried out at a stirring speed of 600 RPM.

3.3.2. Effect of feed concentration

The initial concentration of the feed solution was varied from 100 to 500 mg/L to find the influence of concentration on cesium uptake of AMP-PAN. As shown in Figure 3.6, the uptake capacity of the ion-exchanger increased with increase in the initial feed concentration. The cesium uptake was found to be 18.99, 37.86 and 43.66 mg/g for 100, 300 and 500 mg/L, respectively. The increase in the initial concentration of the feed solution increases the concentration difference between the liquid and solid phase and this would have increased the uptake capacity of the resin.

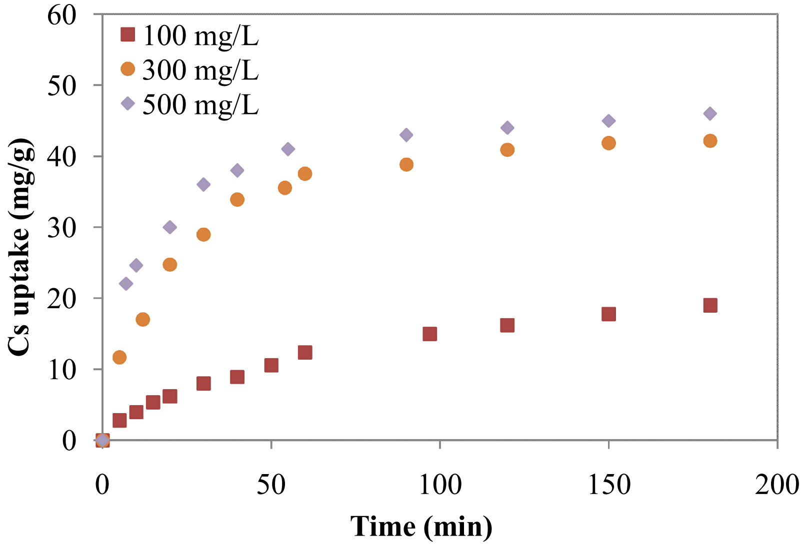

Figure 3.6 Cs uptake by AMP-PAN for different feed concentrations

3.3.3. Effect of particle size

Kinetic experiments were conducted with different sizes of resin particles, viz., 0.5, 0.7 and 1 mm and the results are shown in Figure 3.7. The uptake capacity of the resin increased with decrease in the particle sizes as observed from Figure 3.7. Decrease in the particle size increases the surface area available for the same amount of resin which had increased the uptake capacities of the resin [122, 123]. The uptake capacities were found to be 43.66, 42.47 and 35.20 mg/g, respectively for 0.5, 0.7 and 1 mm sizes of particles.

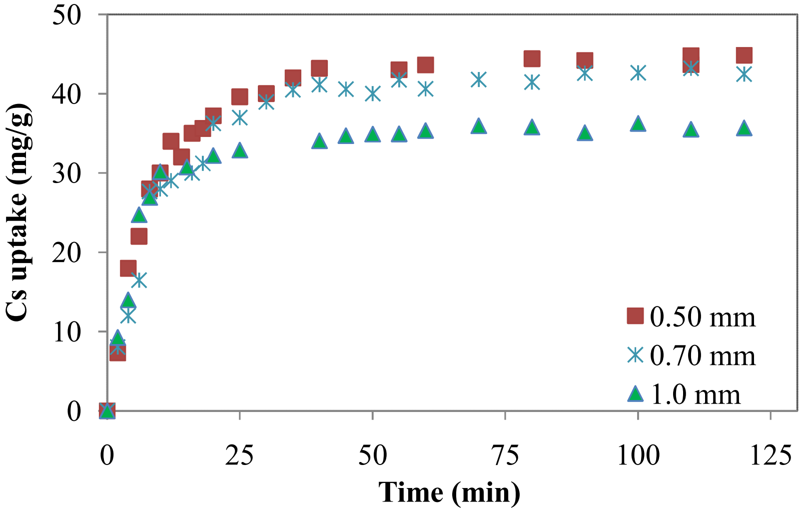

Figure 3.7 Cs uptake by AMP-PAN for different particle sizes
C_0=700 mg/L, RPM=600

3.4. Application of Kinetic models

It was observed that the uptake of cesium increased with time and then remained constant after 90 min for all the parameters studied. The rate of uptake was rapid in the first 40 min and approached equilibrium after 90 min. The time data generated for uptake of ions by sorbents can be used to determine the rate constants. The rate constants determine the sorption phenomenon on the active sites of the sorbent as well as its intra-particle diffusion within pores of the sorbent. Different kinetic models have been proposed for predicting the sorption kinetic behavior. In order to analyze the kinetic data for the sorption of cesium ions onto AMP-PAN resin, the pseudo first-order, pseudo second-order, and intraparticle diffusion models were used.

3.4.1. Pseudo-first order Lagergren model

The Lagergren first-order model [124] is given by the following equation.

$$\frac{dq_t}{dt} = K_1(q_e - q_t) \qquad (3.6)$$

where, K_1 (min^{-1}) is the rate constant for pseudo-first-order adsorption, q_e (mg/g) and q_t (mg/g) are the amounts of Cs exchanged at equilibrium and at time t, respectively.

The linear form of the pseudo-first-order equation is represented as:

$$\ln(q_e - q_t) = \ln q_e - K_1 t \qquad (3.7)$$

The plot of $\ln(q_e - q_t)$ versus t should give a linear relationship from which K_1 and q_e can be determined from the slope and intercept of the plot, respectively.

The parameters of pseudo first-order model determined for different parameters from Figures 3.8, 3.9 and 3.10 are summarized in Table 3.2.

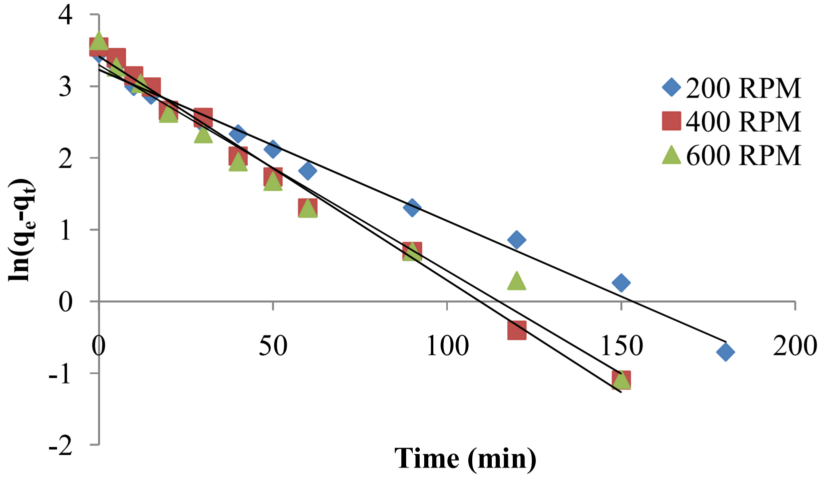

Figure 3.8 Pseudo-first order kinetic plots for Cs uptake by AMP-PAN for different stirring speeds

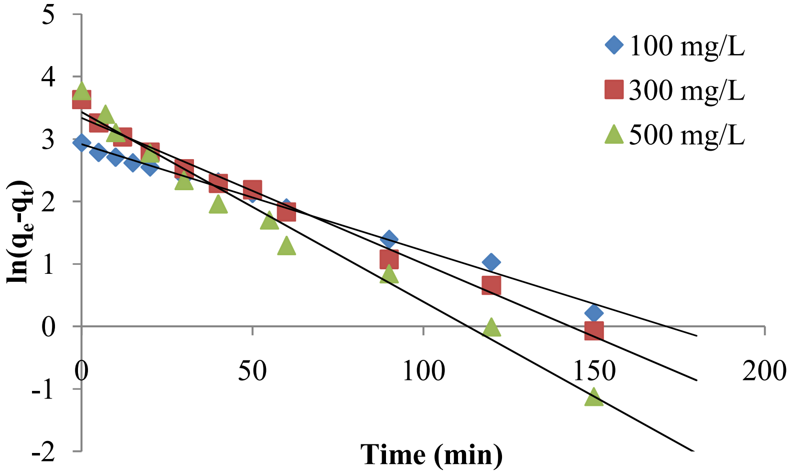

Figure 3.9 Pseudo-first order kinetic plots for Cs uptake by AMP-PAN for different feed concentrations

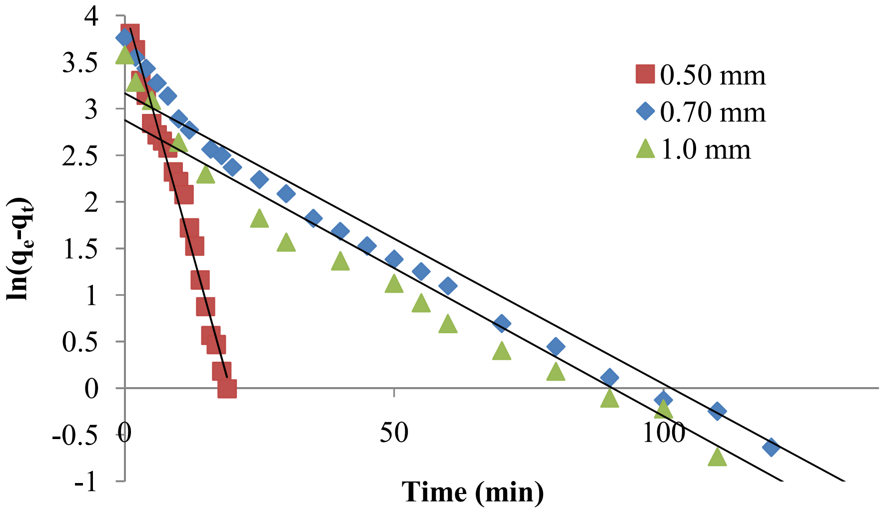

Figure 3.10 Pseudo-first order kinetic plots for Cs uptake by AMP-PAN for different particle sizes

For initial feed concentrations of 100, 300 and 500 mg/L, the rate constants were found to be 0.017, 0.028 and 0.03 min^{-1}, respectively and the corresponding capacities were calculated as 18.99, 37.86 and 43.66 mg/g. The first order rate constants were found to be 0.021, 0.030 and 0.028 min^{-1} for stirring speeds of 200, 400 and 600 RPM respectively. No significant effect was observed in the rate constants with increase in the particle sizes. It was observed that the regression coefficients (R^2) are varying between 0.94 and 0.99 for the parameters studied. In spite of the good R^2 values, the uptake could not be predicted with reasonable accuracy.

3.4.2. Pseudo-second order model

The kinetic data were further analyzed, using a pseudo second-order relation proposed by Ho and McKay [125], which is expressed as

$$\frac{dq_t}{dt} = K_2(q_e - q_t)^2 \qquad (3.8)$$

where, K_2 (g/mg/min) is the rate constant of the second-order sorption process. After integration and applying the boundary conditions, the Eq. (3.8) can be written as

$$\frac{t}{q_t} = \frac{1}{K_2 {q_e}^2} + \frac{1}{q_e} t \qquad (3.9)$$

where, q_e and q_t are the adsorption capacity (mg/g) at equilibrium and time t; K_2 is the rate constant for the pseudo second order adsorption reaction (g/mg/min). The value of q_e and the pseudo-second-order rate constant, K_2, can be calculated from the slope and intercept of the straight line obtained from the plot of t/q_t *versus* t.

Figures 3.11, 3.12 and 3.13 show the linear plots for different parameters studied and the determined model constants are given in Table 3.2.

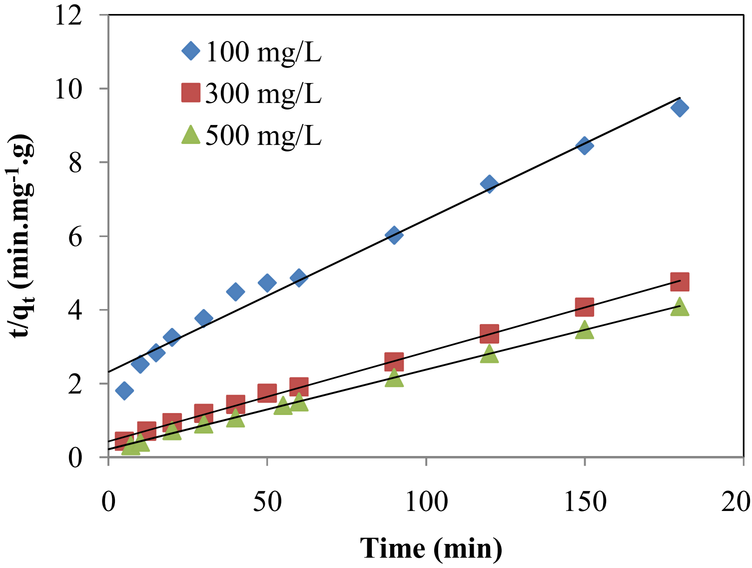

Figure 3.11 Pseudo second-order kinetic plots for Cs uptake of AMP-PAN for different feed concentrations

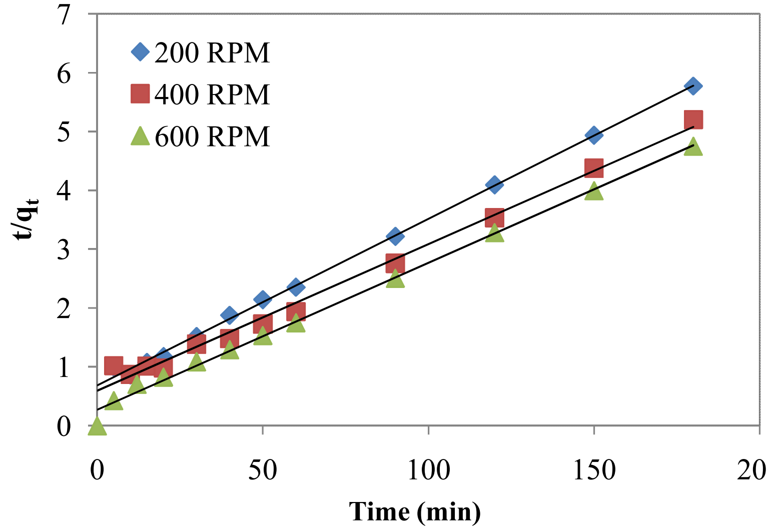

Figure 3.12 Pseudo-second order kinetic plots for Cs uptake of AMP-PAN for different stirring speeds

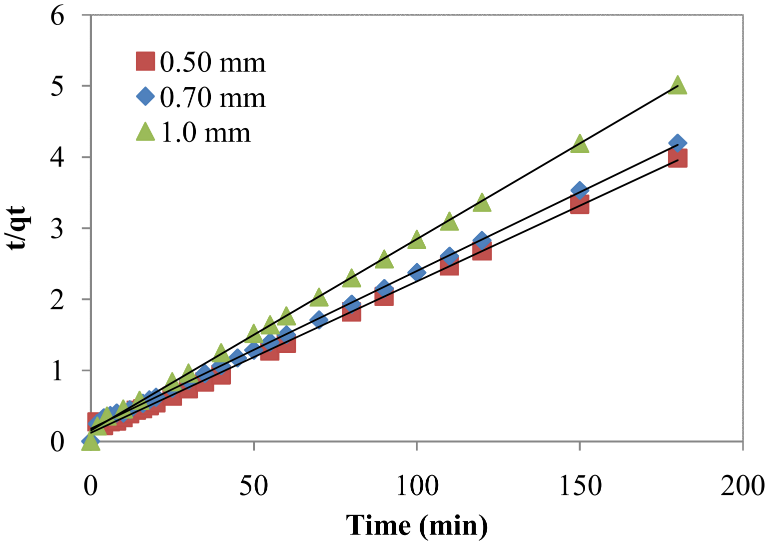

Figure 3.13 Pseudo-second order kinetic plots for Cs uptake of AMP-PAN for different particle sizes

The pseudo-second-order rate constants increased with increase in initial concentration and particle size. With increase in stirring speed form 200 to 600 RPM, no significant effect was observed in the rate constants. The regression coefficients were found in the range of 0.98 to 0.99 which shows a good fit. The predicted uptake capacities were comparable with the experimental values. Thus, the Cs ion exchange kinetics on AMP-PAN are well represented by the pseudo second order model.

3.4.3. Intra particle diffusion model

The intra-particle diffusion model proposed by Weber and Morris [126] is given as:

$$q_t = K_{id} t^{\frac{1}{2}} + I \qquad (3.10)$$

where, K_{id} is the intra-particle diffusion rate constant (mg/g min$^{0.5}$) and I provides the information about the thickness of the boundary layer. If the plot of q_t versus $t^{1/2}$ is a straight line passing through origin, the intra-particle diffusion can be considered as the rate limiting step, otherwise, some complex mechanism may be involved.

The plots of q_t versus $t^{1/2}$ are multi-linear as shown in Figures 3.14, 3.15 and 3.16 for different operating conditions. It is seen that q_t vs $t^{1/2}$ is linear and passes through the origin in the first 30 minutes and subsequently follows a linear profile with an intercept. Thus for the initial period of 30 minutes, it is film diffusion controlled and subsequently particle diffusion controlled. The magnitude of the intercept for the second linear profile is an indication of the film thickness [127]. The third linear portion attributes to the final equilibrium.

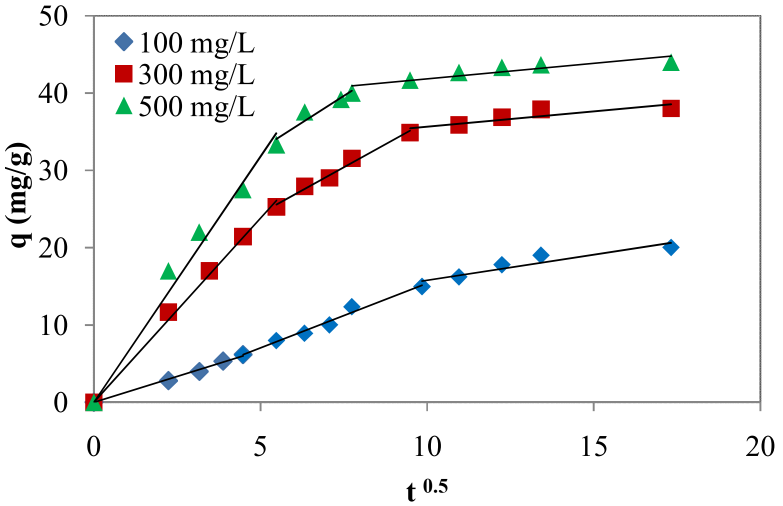

Figure 3.14 Intraparticle diffusion model for Cs uptake of AMP-PAN for different feed concentrations

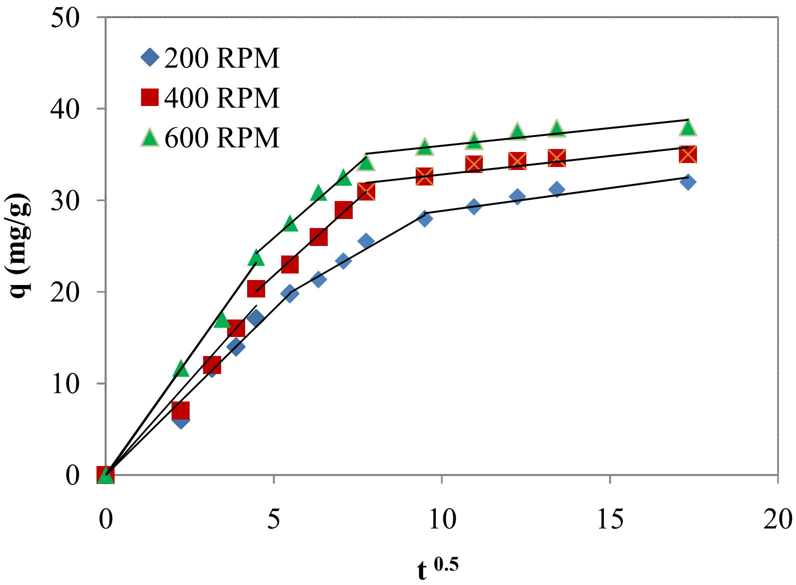

Figure 3.15 Intraparticle diffusion model for Cs uptake of AMP-PAN for different stirring speeds

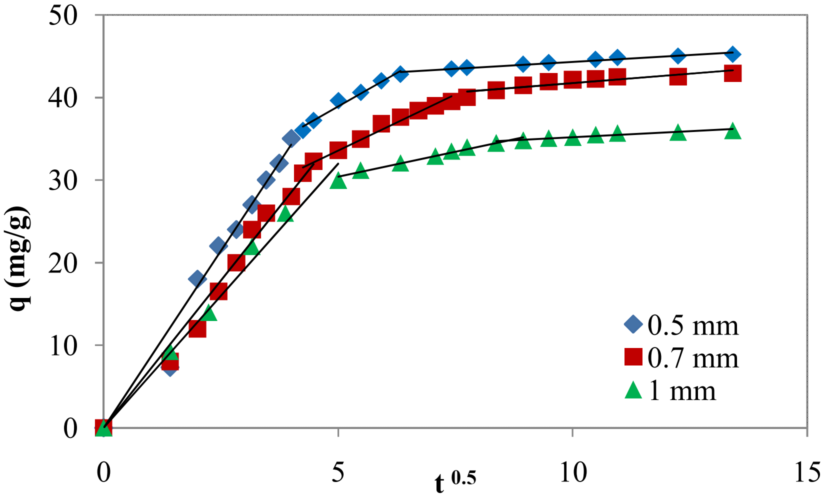

Figure 3.16 Intraparticle diffusion model for Cs uptake of AMP-PAN for different particle sizes

Table 3.2 Kinetic parameters for Cs sorption on AMP-PAN

Initial conc. (mg/L)	RPM	Particle size (mm)	q_{exp} (mg/g)	Pseudo First order kinetic model			Pseudo second order kinetic model			Intra particle diffusion model	
				K_1 (min^{-1})	q_e (mg/g)	R^2	q_e (mg/g)	K_2 (g/mg.min)	R^2	K_{id} (mg/g h)	R^2
100	600	0.5	18.99	0.017	18.52	0.99	23.26	0.0008	0.98	1.67	0.98
300	600	0.5	37.86	0.023	28.11	0.98	41.67	0.0013	0.99	3.19	0.97
500	600	0.5	43.66	0.030	30.91	0.98	47.62	0.0020	0.99	3.23	0.97
300	200	0.5	31.16	0.021	25.25	0.98	35.71	0.0011	0.99	2.11	0.97
300	400	0.5	34.60	0.031	30.23	0.99	41.67	0.0010	0.99	3.21	0.99
500	600	0.7	42.47	0.032	23.97	0.94	45.45	0.0028	0.99	2.72	0.97
500	600	1.0	35.20	0.031	17.34	0.95	38.46	0.0045	0.99	1.09	0.98

The intra particle diffusion rate constants, $K_{id,}$ were determined from the slope of the second portion of the corresponding plots and the values are given in Table 3.2. The intra-particle diffusion rate constants increased with increase in initial concentration and stirring speed. Since both parameters increase the concentration gradients and decrease the boundary layer thickness on the surface of the ion-exchanger, the rate constants might have increased. As the particle size reduces, K_{id} increases, which may be due to the decrease in the overall resistance for diffusion for smaller particles.

3.5. Column studies

Fixed bed studies are carried out to study the effect of different operating parameters on the breakthrough, exhaustion, uptake and behavior of the unsaturated zone. The most efficient sorption performance is obtained when the shape of the breakthrough curve is as sharp as possible [128]. The shape is dependent upon equilibrium, rate of ion exchange and operating conditions. For this analysis, breakthrough and exhaustion are respectively taken as $C/C_0 = 0.05$ and 0.95 throughout this work.

3.5.1. Effect of influent concentration

The effect of influent Cs concentration on breakthrough is shown in Figure 3.17. The breakthrough curves were obtained for different influent Cs concentrations ($C_0 = 500$, 700 and 1000 mg/L) at 5 mL/min flow rate (Q) and 14.5 cm bed height (H). Breakthrough occurred after 170 min for 500 mg/L initial cesium concentration, while the breakthrough occurred at 120 and 95 minutes for 700 and 1000 mg/L. Increase in cesium concentration resulted in a faster breakthrough due to early exhaustion of the bed.

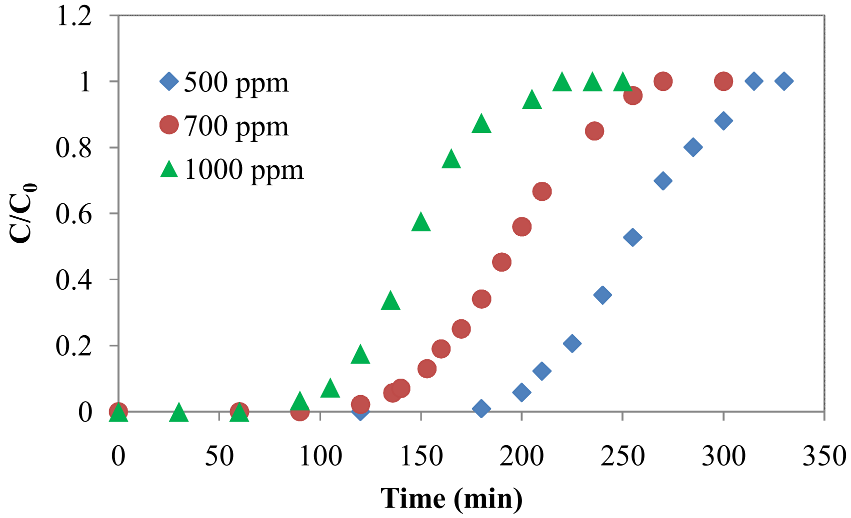

Figure 3.17 Breakthrough curves for different influent concentrations
Q = 5 mL/min; H =14.5 cm

From analysis of the samples of the effluent, the Cs uptake of the resin after complete exhaustion was found to be 28.7, 34.55 and 37.19 mg/g for influent concentration of 500, 700 and 1000 mg/L, respectively. Uptake increased with increase in the influent concentration due to the higher concentration gradient.

For the same flow rate and bed height, when the influent concentration of Cs was increased, sharper breakthrough curves were obtained and a steep breakthrough curve was obtained at 1000 mg/L. This is due to increase in the concentration gradient, which affects the ion exchange rate.

3.5.2. Effect of Bed Height

Amount of ion exchange resin in the column and consequently, availability of ion exchange sites increases linearly with the height of the column. Effect of bed height on breakthrough curve was studied by operating the column at three different bed heights (H = 14.5, 18.2, and 21cm) by charging 20, 25 and 30 g of resin, respectively. A feed solution of 700 mg/L of Cs was passed through the fixed-bed column at a constant flow rate of 5 mL/min. As can be seen from Figure 3.18, the volume of solution treated increased with the increase in bed height, due to increased availability of exchange sites.

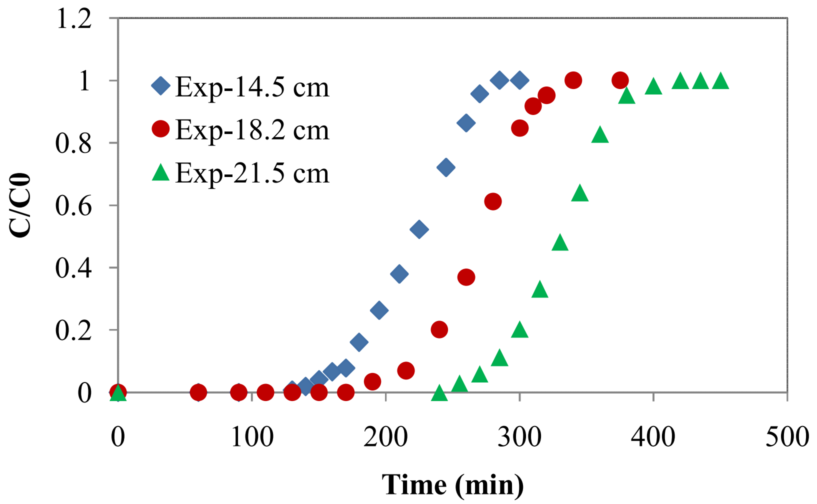

Figure 3.18 Breakthrough curves for different bed heights
C_0 = 700 mg/L; Q = 5 mL/min

The breakthrough time increased from 120 to 270 min, when the bed height was increased from 14.5 to 21.5 cm. Even though exhaustion time increased with increase in the bed height, time taken between breakthrough and exhaustion was same for different bed heights, indicating that the extent of unsaturated zone is not varying. The slopes of the breakthrough curves were found to be similar for the studied bed heights. An increase in column length (other parameters being kept constant) increases both the breakthrough and the overall capacity. If equilibrium is favorable, the boundary attains a constant pattern and the breakthrough curve shifts to the right without change in the shape [128].

The Cs uptake capacity was found to be 34.55, 35.28 and 36.58 mg/g for bed heights of 14.5, 18.2 and 21.5 cm, respectively. As already explained, the volume of bed occupied by the unsaturated zone remained constant, when the bed height is increased, consequently the fraction of unsaturated zone in the total volume of bed decreased. This increased the utilization of the bed and resulted in more uptake capacity.

3.5.3. Effect of Feed Flow Rate

To study the effect of flow rate, columns were charged at flow rates of 5, 10 and 15 mL/min with initial Cs concentration maintained at 700 mg/L in 4N HNO_3. The bed depth and column diameter were 14.5 and 2 cm, respectively. Since the flow rate is varying, breakthrough curves in terms of volume processed are shown in Figure 3.19. The experimental breakthrough times for flow rates 5, 10 and 15 mL/min were found to be 120, 55 and 25 min, respectively and the exhaust times were observed to be 220, 136 and 110 min.

Earlier breakthrough and exhaustion were observed with increase in flow rate. The uptake capacity of the ion exchanger decreased from 34.55 to 31.5 and 30.58 mg/g when the flow rate is increased from 5 to10 mL/min and 15 mL/min. This reduction is due to insufficient contact time in the bed. Flow rate of 5 mL/min corresponds to 6.5 bed volumes per hour and any increase in this resulted in inefficient operation. At higher flow rates, slope of the curve decreased showing high volume of unsaturated zone as a result of insufficient contact.

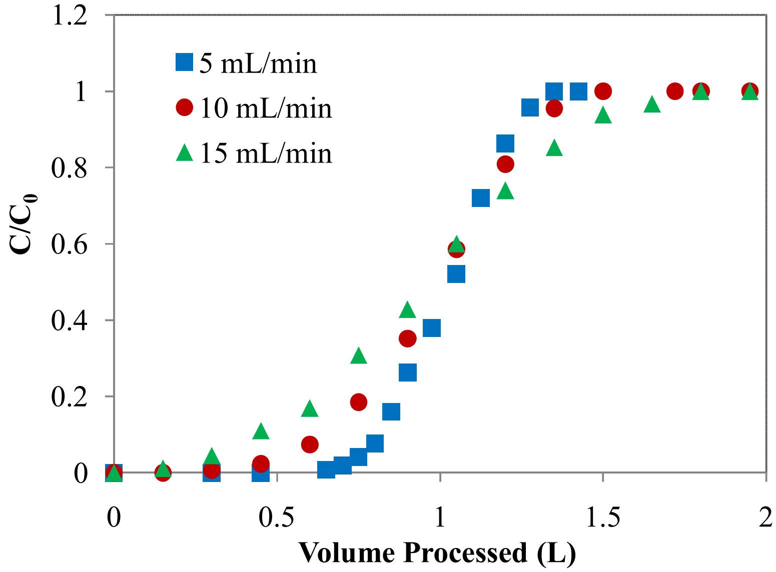

Figure 3.19 Breakthrough curves for different flow rates of feed
C_0 = 700 mg/L; H = 14.5 cm

3.5.4. Analysis of Mass Transfer Zone

The performance of fixed bed columns strongly relates to the length and shape of the mass transfer zone (MTZ) that develops during the dynamic contact of solid and liquid. In the region of MTZ, the sorbate concentration at the outlet changes from 5 to 95 % of its inlet value. This region indicates the area where sorption practically takes place in fixed beds [114]. It also indicates the type of diffusion resistances governing the sorption process. Smaller height of the mass transfer zone indicates faster kinetics and lower diffusion resistance.

The slope of the breakthrough curve determines the extent to which the capacity of a fixed bed can be utilized. Thus, the shape of the curve is very important in determining the length of the mass transfer zone. Fractional capacity is defined as the ratio of the quantity of solute eliminated to the potential capacity of elimination of adsorbent, within the mass transfer zone. This is given by

$$\boldsymbol{F = \frac{\int_{t_b}^{t_e}(C_0 - C_i)dt}{C_0(t_e - t_b)}} \tag{3.11}$$

The height of the MTZ is calculated by

$$\boldsymbol{H_{MTZ} = \frac{h(t_e - t_b)}{t_b + F(t_e - t_b)}} \tag{3.12}$$

where, H_{MTZ} is the height of the mass transfer zone (cm); h is the height of the ion exchange bed (cm); t_e is the exhaustion time; t_b is the breakthrough time and F is the factional capacity.

The smaller the height of MTZ, the faster is the rate of ion exchange and the more rapid is the saturation of bed [129].

The rate of movement of the MTZ is a function of adsorption capacity of the adsorbent and is directly related to the height of MTZ. The rate of movement of MTZ is given by

$$\boldsymbol{U_z = \frac{H_{MTZ}}{t_z} = \frac{H_{MTZ}}{t_e - t_b}} \tag{3.13}$$

where t_z is the time required for the movement of MTZ down its own length in the column.

The percentage of saturation of the column is given by

$$\%\, \boldsymbol{Saturation = \frac{h + (F-1)H_{MTZ}}{h}\, X100} \tag{3.14}$$

All these parameters were calculated for different operating conditions and the values are summarized in Table 3.3. Effects of operating parameters discussed in sections 3.5.1, 3.5.2 and 3.5.3 can be better understood based on MTZ concept.

With increase in initial concentration, H_{MTZ} decreased, indicating faster ion exchange. Because of higher concentration gradient, fractional capacity, rate of movement of MTZ as well as percentage saturation increased. This has also affected U_z strongly as can be seen from Table 3.3.

Table 3.3 Height of mass transfer zone for different process parameters

Conc. (mg/L)	Flow rate (mL/min)	Bed height H (cm)	t_B (min)	t_S (min)	F	MTZ (cm)	t_Z (min)	U_Z (cm/min)	% Saturation
500	5	14.5	170	320	0.520	8.77	150	0.058	70.96
700	5	14.5	120	220	0.669	7.75	100	0.078	82.26
1000	5	14.5	95	160	0.665	6.87	65	0.106	84.25
700	10	14.5	55	135	0.455	12.69	80	0.159	52.34
700	15	14.5	25	110	0.436	19.84	85	0.233	22.85
700	5	18.2	180	280	0.685	7.44	100	0.074	87.35
700	5	21.5	270	370	0.708	7.16	100	0.072	90.28

With increase in bed height, there is no substantial change in F or U_z or H_{MTZ}. However, as the volume fraction of bed occupied by the MTZ decreased with increase in bed height, percentage saturation increased. With increase in flow rate, H_{MTZ} increased and there by U_z, as the exchange become slow, due to insufficient contact time. F and percentage saturation decreased for the same reason.

3.5.5. Application of various dynamic models

For the design of column exchange process, breakthrough curves for different operating conditions are required. In the absence of experimental data, these curves can be generated if a suitable model is available and the model constants are known. It is difficult to model the dynamic behavior of ion exchange in a fixed bed system to describe accurately the concentration profiles in solid and liquid phases, which vary with both time and space. Solving of the differential equation based models of proposed rate mechanisms is a cumbersome process and they cannot be solved for all the operating conditions.

Simple models which would predict the breakthrough behavior of an ion exchange column are suitable for analyzing the column studies. Many such models have been developed for predicting the break through curves in fixed bed studies. The analysis of the breakthrough curve was done using three of these models, viz., Thomas model, Yoon Nelson model and Bohart-Adam model.

The average percentage error is calculated using

$$\textbf{APE (\%)} = \frac{\sum_{i=1}^{N}\left|\frac{\frac{C}{C_{0exp}} - \frac{C}{C_{0model}}}{\frac{C}{C_{0exp}}}\right|}{N} X100 \tag{3.15}$$

where, N is the number of experimental data.

3.5.5.1. Thomas model

Thomas model is based on the assumption that the process follows Langmuir kinetics with no axial dispersion; the rate driving force follows second order reversible reaction kinetics [130]. The expression of the Thomas model for a column operation is given as follows:

$$\frac{C}{C_o} = \frac{1}{1+\exp\left[\frac{K_{Th}q_0\,m}{Q} - K_{Th}C_o t\right]} \tag{3.16}$$

The linearized form of the Thomas model is

$$\ln\left(\frac{C_o}{C} - 1\right) = \frac{K_{Th}q_0 m}{Q} - K_{Th}C_o t \tag{3.17}$$

where, K_{Th} is the Thomas rate constant (L/min.mg); q_0 is the maximum solid-phase concentration of solute (mg/g); m is the amount resin in the column (g); V_{eff} is the effluent volume (L); Q is the flow rate (L/min); C is effluent concentration (mg/L) and C_0 is influent concentration (mg/L).

Thomas model was applied to the data at C/C_0 values between 0.05 and 0.95 for different operating conditions. The values of K_{Th} and $q_0$were obtained from the plot of $\ln(C_0/C-1)$

versus time and given in Table 3.4. It can be seen that R^2 values ranged from 0.981 to 0.998, indicating the goodness of fit of Thomas model.

Table 3.4 Thomas model parameters for Cs uptake of AMP-PAN for different experimental conditions

Flow rate Q (mL/min)	Initial conc. C_o (mg/L)	Bed height, H (cm)	Thomas constant, K_{Th} (mL/min mg) $\times 10^{-2}$	q_0 (model) (mg/g)	R^2	q_{exp} (mg/g)	APE
5	500	14.5	9.35	31.80	0.99	28.70	0.38
5	700	14.5	7.38	36.12	0.99	34.55	5.96
5	1000	14.5	5.53	40.88	0.98	37.19	0.20
10	700	14.5	9.60	34.50	0.99	31.50	0.73
15	700	14.5	9.91	32.99	0.99	30.58	7.23
5	700	18.2	7.70	37.06	0.98	35.28	2.69
5	700	21.5	8.10	38.12	0.99	36.58	1.19

The values of q_0 calculated from Thomas model (equation 3.17) were comparable to the experimentally determined values, q_{exp}. The experimental uptake capacity was determined after completion of experiment by thoroughly washing the resin with DM water to remove any liquid remaining in the bed in the interstitial space between the resin beads. The uptake capacity (q_0) increased from 31.8 to 40.88 mg/g, whereas Thomas rate constant (K_{Th}) decreased from 9.35×10^{-2} to 5.53×10^{-2} with increasing the influent concentration from 500 to 1000 mg/L. The rate constant was observed to be increasing with increasing the flow rate. The uptake capacity decreased with increasing flow rate, due to low contact time. The rate constant as well as the uptake capacity increased with increase in bed height. Similar observations were made by D.M. Saad et al. [131] in their study on the adsorption of U on phosphonated cross-linked polyethylenimine. The model or theoretical breakthrough curves for Cs ion exchange on AMP-PAN were obtained using the parameters K_{Th} and q_0 determined from the available experimental data for different operating conditions. The experimental and model breakthrough curves were shown in Figures 3.20, 3.21 and 3.21. The breakthrough curves confirm the applicability of this model in describing the experimental data.

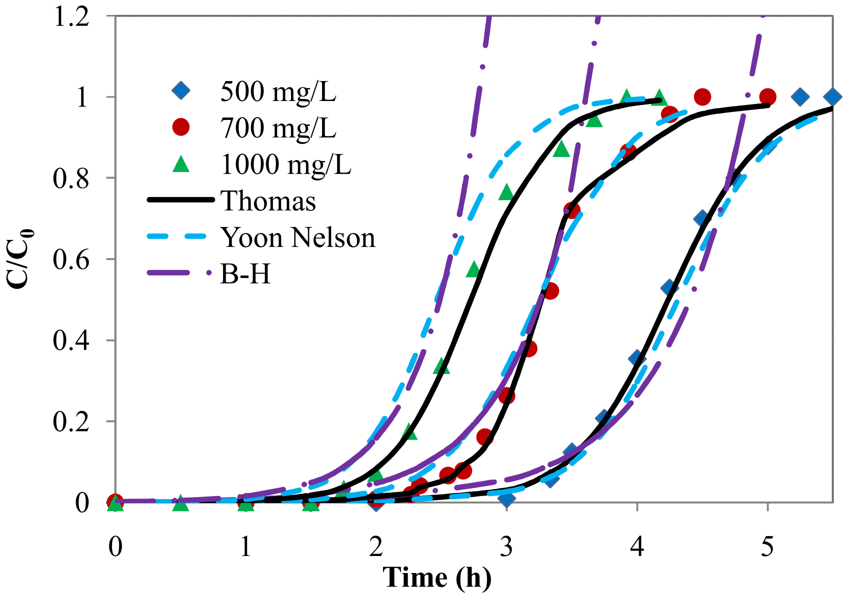

Figure 3.20 Comparison of experimental and model breakthrough curves for different feed concentrations

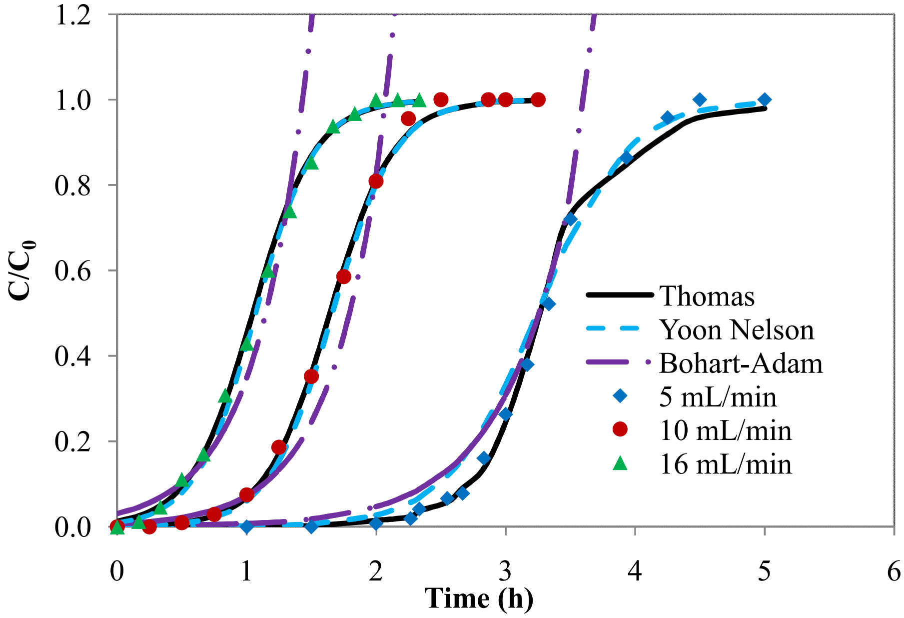

Figure 3.21 Comparison of experimental and model breakthrough curves for different feed flow rates

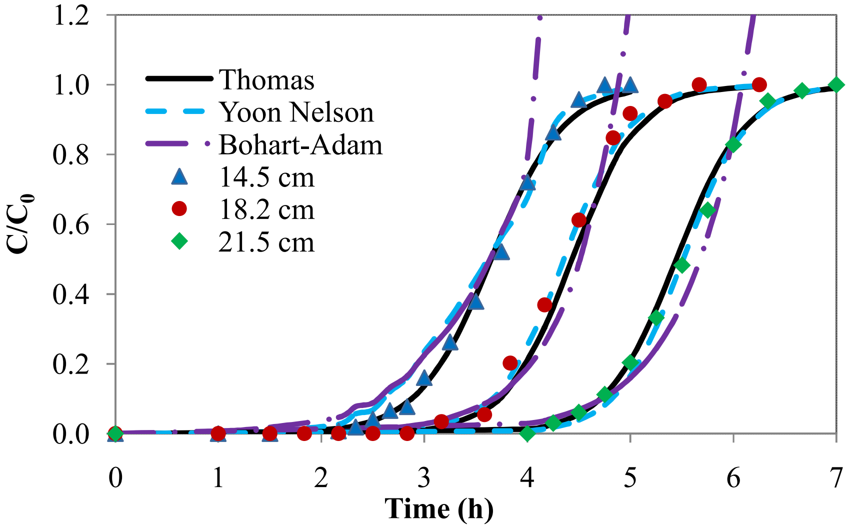

Figure 3.22 Comparison of experimental and model breakthrough curves for different bed height

3.5.5.2. Yoon-Nelson model

This model was based on the assumption that the rate of decrease in the probability of adsorption for each adsorbate molecule was proportional to the probability of adsorbate adsorption and the probability of adsorbate breakthrough on the adsorbent [131]. The Yoon-Nelson model is not only less complicated than other models, but also requires no detailed data concerning the characteristics of sorbate, the type of adsorbent, and the physical properties of sorption bed [115].

The Yoon-Nelson equation regarding a single component system was expressed as

$$\ln\frac{C}{C_0-C} = K_{YN}t - \tau K_{YN} \qquad (318)$$

where, K_{YN} is the rate constant (h^{-1}) τ the time required for 50% sorbate breakthrough and t is the time (h).

For a symmetric breakthrough curve the quantity of solute sorbed at time τ equals half of the removal capacity, and it is calculated relative to the initial concentration and flow rate. The uptake capacity q can be calculated as

$$q = \frac{C_0 . Q . \tau}{m} \qquad (3.19)$$

where, m is the mass of the resin (g), Q the flow rate (mL/min).

From a linear plot of ln[C/(C_0-C)] against sampling time (t), values of K_{YN} and τ were determined from the intercept and slope of the plot.

The values of K_{YN} and τ determined for different operating conditions are listed in Table 3.5. It was observed that the rate constant K_{YN} increased from 0.046 to 0.056 min^{-1} and the 50% breakthrough time τ decreased from 258 to 148 min with increasing Cs inlet concentration from 500 to 1000 mg/L. When the bed height increased from 14.5 to 21.5 cm, τ increased while the values of K_{YN} decreased. As the flow rate increased, K_{YN} increased and τ decreased. Table 3.5 indicates that the model and experimental uptake capacities were comparable and the regression coefficient (R^2) varies between 0.986 and 0.995. The model curves were compared with the experimental curves as shown in Figures. 3.18, 3.19 and 3.20 and the model parameters are given in Table 3.5. This model provided a good fit of the experimental data for all the effects studied with good correlation coefficients.

Table 3.5 Yoon-Nelson model parameters for Cs uptake of AMP-PAN for different experimental conditions

Flow rate Q (mL/min)	Initial conc. C_o (mg/L)	Bed height H (cm)	Yoon-Nelson rate constant (K_{YN}) x 10^{-2} (min^{-1})	τ (min)	q_{model} (mg/g)	R^2	q_{exp} (mg/g)	APE
5	500	14.5	4.6	258.69	32.33	0.99	28.70	12.7
5	700	14.5	5.1	194.62	34.05	0.99	34.55	1.4
5	1000	14.5	5.6	148.01	37.00	0.99	37.19	0.50
10	700	14.5	6.9	99.79	34.30	0.99	31.50	8.9
15	700	14.5	7.2	64.25	33.73	0.99	30.58	10.3
5	700	18.2	5.0	261.35	36.58	0.98	35.28	3.7
5	700	21.5	4.8	330.57	38.24	0.98	36.58	4.6

3.5.5.3. Application of the Bohart-Adam model

This model assumes that the adsorption rate is proportional to both the residual capacity of the sorbent and the concentration of the sorbing species [132]. The mass transfer rates obey the following equations [115].

$$\frac{\partial q}{\partial t} = -K_{BA}qC \qquad (3.20)$$

$$\frac{\partial C}{\partial Z} = -\frac{K_{BA}}{U_0}qC \qquad (3.21)$$

where, K_{BA} is the rate constant (L $mg^{-1}h^{-1}$). Some assumptions were made for the solution of these differential equation systems:

- the concentration field is considered to be low;
- for t→∞, q→N_0, where N_0 is the sorption capacity(mg L^{-1}).

When the differential equation systems are solved, the following equation was obtained with parameters K_{BA} and N_0:

$$ln\left(\frac{C_0}{C} - 1\right) = \frac{K_{BA}N_0}{U_0} - K_{BA}C_0t \qquad (3.22)$$

where, C is the effluent concentration (mg L^{-1}), C_0 the influent concentration (mg L^{-1}), K_{BA} the sorption rate coefficient ($Lmg^{-1}h^{-1}$), N_0 the sorption capacity (mg L^{-1}), Z the bed height (mm), U_0 the linear velocity (mm h^{-1}) and t is the time (h).

The model constants K_{BA} and N_0 can be determined from a plot of $\ln[(C/C_0) -1]$ against t for different operating conditions. The parameters of Bohart-Adams model determined from the experimental data are tabulated in Table 3.6. The rate coefficient (K_{BA}) decreased with increasing the concentration and decreased with increase in flow rate and bed height. It was also observed that the uptake capacity of the ion exchange resin increased with increasing flow rate, which contradicted the experimental findings. The simulated breakthrough curves are given in Figures 3.20, 3.21 and 3.22. The breakthrough curves predicted by the Bohart-Adam model are not complete curves and do not show the saturation point. The model could not predict the breakthrough capacity and percentage saturation reasonably.

Table 3.6 Bohart-Adam model parameters for Cs uptake of AMP-PAN for different experimental conditions

Flow rate Q (mL/min)	Initial conc. C_o (mg/L)	Bed height H (cm)	K_{BA} (L $mg^{-1}h^{-1}$) X 10^{-3}	N_{BA} (mg/L)	q_{model} (mg/g)	R^2	q_{exp} (mg/g)	APE
5	500	14.5	3.14	15961.38	23.94	0.91	28.70	58.69
5	700	14.5	2.69	16722.26	25.08	0.96	34.55	41.67
5	1000	14.5	2.36	18326.26	27.49	0.96	37.19	64.55
10	700	14.5	3.47	19185.85	28.77	0.92	31.50	48.66
15	700	14.5	3.48	21132.87	31.69	0.94	30.58	51.42
5	700	18.2	2.71	17922.93	26.88	0.93	35.28	59.01
5	700	21.5	2.41	18932.51	28.40	0.94	36.58	52.46

3.5.6. Regeneration of AMP-PAN

Cesium elution from the cesium saturated bed of AMP-PAN using 3.5M NH_4^+ and 0.27M NH_4^+ are shown in Figures 3.23 and 3.24. NH_4^+ replaced the loaded Cs on the AMP-PAN in the column and the effluent had Cs along with NH_4^+ and the corresponding anions of the regenerative salts (like SO_4^-, Cl^-, NO_3^-).

With 72 bed volumes of 3.5 M NH_4^+ solution, 88 % of cesium was eluted from the column. In case of 0.27M NH_4^+, only 57% of cesium was eluted with 400 bed volumes. High concentrations of eluant recovered more Cs in lesser bed volumes due to high concentration gradients. The effluent stream contains high concentrated NH_4^+ compared to Cs^+. Cesium affinity to AMP-PAN is very high and therefore complete elution of cesium is difficult to obtain. For complete recovery of cesium, using chemical methods, the practice is to dissolve AMP-PAN in alkaline medium and recover cesium from this solution by another ion exchanger.

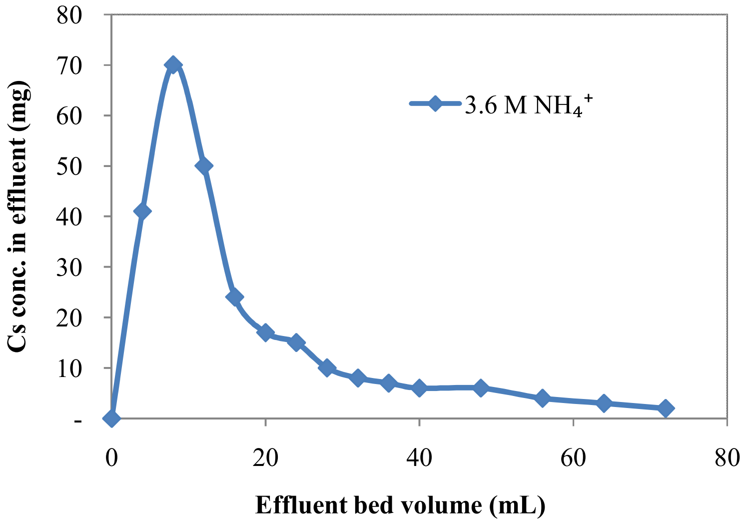

(a)

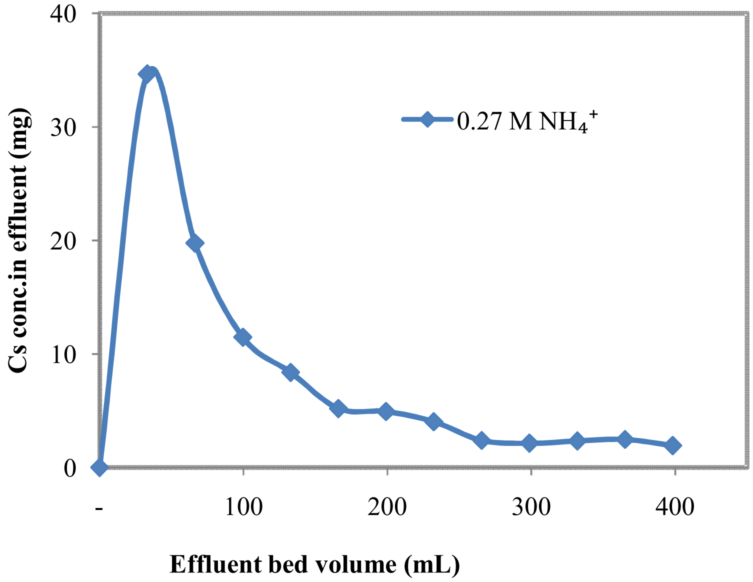

(b)

Figure 3.23 Elution profile of Cs from AMP-PAN in column for different eluant concentrations (a) 3.6 M NH_4^+ (b) 0.27 M NH_4^+

3.6. Conclusions

AMP-PAN was tested for its selectivity for Cs from the simulated High Level Waste containing the Cs, Sr and Na. High distribution coefficients were obtained for Cs compared to other ions. No significant change was observed in distribution coefficient with increase in acidity. Characterization of the AMP-PAN using FTIR indicates that the

Cs sorption was mainly due to the ammonium ions. XRD pattern of AMP-PAN confirmed the crystalline nature of AMP on PAN support.

Equilibrium isotherms for Cesium ion exchange on AMP-PAN were obtained and tested with well known equilibrium models like Langmuir and Freundlich models. Both the Langmuir and Freundlich models predicted the equilibrium nature of Cs on AMP-PAN, with Langmuir isotherm giving a better fit. Pseudo second order kinetic model predicted the Cs exchange on AMP-PAN better than Pseudo first order. Particle size, feed concentration and stirring speed affected the ion exchange kinetics of Cs on AMP-PAN. Both particle diffusion and film diffusion were observed to be the controlling factors for Cs sorption by AMP-PAN. The kinetics of Cs sorption on AMP-PAN can be increased by reducing the particle size and improving the turbulence.

The dynamic behavior of Cs ion exchange on AMP-PAN was examined in column at different operating conditions like influent concentration, flow rate and bed height. Early breakthroughs were obtained with increase in the feed concentration, increase in flow rate and decrease in bed height. Similarly the uptake capacities increased with increasing feed concentration and increasing bed height but decreased with increasing flow rate. Height of MTZ, which is an effective parameter for assessing the affinity of ionexchanger and rate of ion exchange, is determined for various operating parameters. Height of MTZ was not affected by variation in height of bed, decreased with increase in initial concentration and increased with increase in flow rate.

Mathematical models of Thomas, Yoon-Nelson and Bohart-Adam were applied to the experimental data obtained from column studies to predict the breakthrough curves and to determine the kinetic parameters. The prediction of whole breakthrough curve is effective with Thomas and Yoon-Nelson models. Bohart–Adam model was not able to predict the breakthrough curve. Comparing the values of R^2 of the breakthrough curves, both the

Thomas and Yoon -Nelson models can be used to describe the behavior of Cs ion exchange on AMP-PAN in a fixed-bed column. The behavior of the determined coefficients of the models for different operating conditions can be used to scale up the process. Cesium elution from the AMP-PAN using ammonium salts reduced its stability which limits its further reusability. It also suffers from the difficulty of separation for pure cesium from high concentrations of anions.

Current-Voltage characteristics and limiting current density

4

This chapter explains the concept of concentration polarization and the occurrence of limiting currents on account of concentration polarization. The current-voltage characteristics of electrodialysis cell determine the limiting current, below which the cell should operate to avoid the occurrence of concentration polarization. The effects of electrolytes' flow rates and concentration of the eluant used in the EDIX process for the recovery of Cs from AMP-PAN on the I-V characteristics are studied. An empirical equation for the limiting currents as a function of electrolytes' flow rates and eluant concentration is also suggested.

4.1. Introduction

Electrodialysis ion exchange is a hybrid electrochemical separation process, which attracted considerable attention in recent times. In electrodialysis, high current densities are desirable to achieve fast deionization with the lowest possible effective membrane area. But high operating currents are restricted by the occurrence of concentration polarization phenomena. Thus, electrodialysis is not economical for treating dilute solutions because of the high electrical resistance. When dilute compartments are packed with ion exchange material, they behave as conductors due to the presence of functional groups, which serve as bridges between the ion exchange membranes [133]. This enhances the transport of cations or anions under the application of electric potential and minimizes the concentration polarization [134-137]. Thus, introduction of ion exchange resins in electrodialysis cell reduces the power consumption considerably and increase the ion transport through the membranes.

4.1.1. Concentration polarization

Concentration polarization is a well-known phenomenon occurring at the interface between an ion exchange membrane and an electrolyte solution, when current passes through it. Due to the effect of counter ion present in the membrane, the permeate ion moves through the ion exchange membrane at a faster rate than through the solution. Consequently, a depletion of electrolyte is created in the aqueous layer adjoining the membrane face and a concentration gradient develops in the film that adjoins the membrane. This phenomenon is called concentration polarization.

Concentration polarization on the desalting membrane surface in electrodialysis was investigated by various researchers by analyzing the current–voltage (I-V) relationship [138-140]. A typical current-voltage relationship of an electrodialysis system, as shown in Figure 4.1 consists of three distinct regions: ohmic region, limiting current region and over limiting region [141-143].

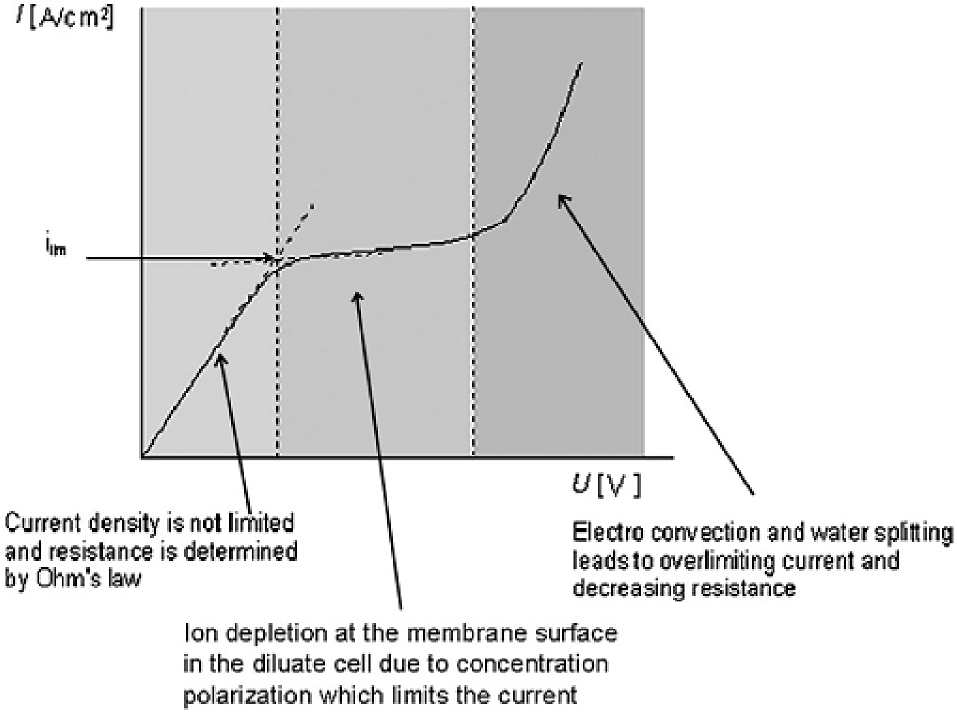

Figure 4.1 Typical current versus voltage curve of an electrodialysis stack operated at constant solution flow velocities and feed and diluate concentrations

The ionic transport both in the ohmic and limiting current regions can be explained by concentration polarization near ion-exchange membranes. The overlimiting current density is caused by electro-convection and is, at least partially, caused by the transport of H^+ and OH^- ions, which are generated at the membrane/solution interface by water dissociation. Water dissociation affects the current utilization and can lead to a drastic pH value decrease in the diluate and increase in the concentrate solution. The reasons for electro-convection are still not yet completely understood.

Concentration polarization can be partially controlled by circulating the salt solutions at high flow rates through the cell. The magnitude of concentration polarization is a function of various parameters including the applied current density, the feed flow velocity parallel to the membrane surface, the cell design and the membrane properties [144-146].

4.1.2. Limiting current density

Onset of concentration polarization in electrodialysis cell results in depletion of electrolyte at the membrane surface. The point at which the ion concentration at the membrane surface becomes zero corresponds to the maximum transport rate of ions through the boundary layer. The current per unit area of membrane at this point is called the limiting current density. Because of this depletion of the salt at the membrane surface, the voltage drop dissipated in transporting ions across the boundary layer is higher than through the membrane. Once the limiting current density is reached, any further increase in voltage applied across the membrane will not increase ion transport or current through the membrane. Normally the extra power is dissipated by side reactions, such as dissociation of the water in the cell into ions. Beyond this point there is an increasing resistance in the cell and the pH of the solution is altered and the changes in pH may lead to the precipitation of insoluble hydroxides on the surface of the membrane [147].

The limiting current density (i_{lim}) is obtained when the ion electrodiffusion transfer through a diffusion boundary layer near an ion exchange membrane is saturated and the boundary electrolyte concentration becomes small in comparison with its bulk value. The limiting current density in electrodialysis based on Nernst-diffusion model [148, 149] is represented as equation 4.1.

$$\boldsymbol{i}_{\boldsymbol{lim}} = \frac{\boldsymbol{FCzD}}{\boldsymbol{\delta}\,(\boldsymbol{t_m}-\boldsymbol{t_s})} \tag{4.1}$$

where, C is concentration of the diluate, D the diffusion coefficient, F the Faraday constant, z the valence, δ the boundary layer thickness, t_s and t_m are the ion transport numbers in the solution and the membrane respectively.

Korngold [134] suggested an equation for limiting current density with ion exchange resin in electrodialysis chamber, taking into account the lower surface contact between the solution and membrane

$$\boldsymbol{i}_{\boldsymbol{lim}} = \frac{\boldsymbol{FCzD}}{\boldsymbol{\delta}(\,\boldsymbol{t_m}-\boldsymbol{t_s})}\,\frac{\boldsymbol{A_s}}{\boldsymbol{A_t}} \qquad (4.2),$$

where, A_s is the membrane surface in direct contact with solution and A_t is the total surface of membrane.

It is difficult to determine the limiting currents directly by using the above equations either in electrodialysis or in electrodeionisation. A basic empirical equation given below relates the limiting current to the flow velocity and concentration and is widely accepted as it gives reasonable results within practical limits.

$$\boldsymbol{i}_{\mathbf{lim,emp}} = \boldsymbol{aCu^b} \tag{4.3}$$

where, u is the linear velocity, $i_{\mathrm{lim,emp}}$ is the empirical limiting current density. The coefficients *a* and *b* in the equation depend on hydrodynamics and design parameters of the cell [150].

4.2. Influence of flow rate on I-V characteristics

With different flow rates (5, 20, 100, 200 mL/min) of catholyte and anolyte for a constant flow rate of 20 mL/min of middle compartment solution, the current-voltage characteristics were studied. Equal flow rates of anolyte and catholyte were maintained so as to keep the pressure same on both sides of the middle compartment. Figure 4.2 shows the current-voltage relationship for different flow rates of anolyte and catholyte.

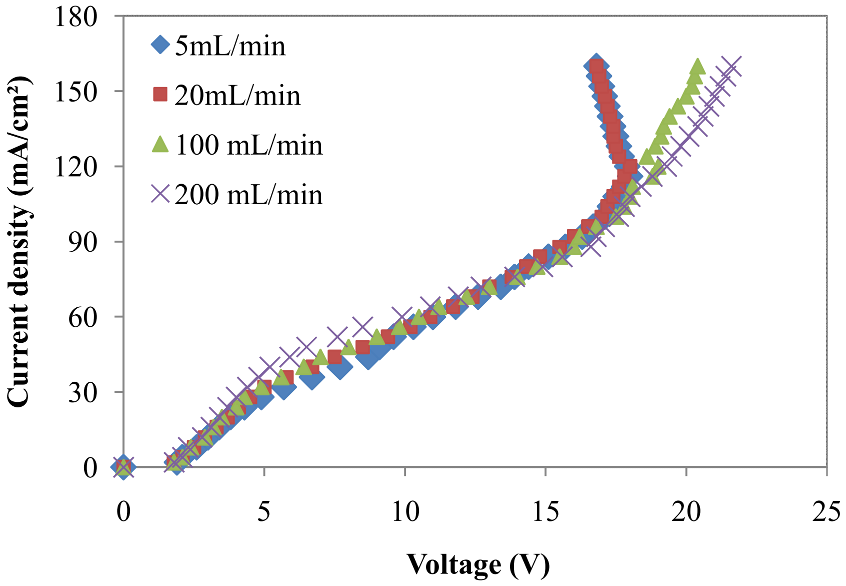

Figure 4.2 I-V relationship for different electrolytes' flow rates

Three main regions were seen in I-V relation as in conventional electrodialysis system. When the voltage was increased, current density was observed to be zero up to 1.8 V. The voltage applied up to 1.8 V was utilized in charging the electrodes and the membranes. A similar phenomenon was observed by Alvarado et.al [151] in their experiments for removal of chromium from wastewater. In the first region, current density increased linearly with applied voltage; this is termed as ohmic region in conventional electrodialysis. Maximum value of the current in this region is the limiting current, which is the maximum current that can be employed in an electrodialysis process. For all the flow rates studied, the ohmic region was observed up to about 5 V and in the ohmic region current densities increase with increasing anolyte and catholyte flow rates. The ohmic region is characterized by migration of ions through the ion exchange membranes and resin under an electric field. When voltage is increased beyond the limiting current density, concentration polarization becomes more pronounced and salt depleted boundary layer forms at the solution membrane interface. Decrease in the concentration at the boundary layer increases the resistance and flow of ions becomes diffusion controlled.

In the second region (5-17 V) a sharp decline of slope is not observed unlike in case of conventional electrodialysis. This might be due to the presence of ion exchange resin in the middle compartment, which had increased the conductivity of the compartment and consequently reduced the constant plateau region partially. In the third region, slope of the curve increased slightly greater than the second region. In this region, excessive gas generation at the cathode and anode was observed due to electrode reactions. A decrease in voltage is observed for lower flow rates (5 and 10 mL/min) in over limiting range (>120 mA/cm^2). This might be due to dissociation of water molecules at the membrane surface.

The I-V characteristics were studied, for different middle compartment solution flow rates (5, 20, 100, 200 mL/min) for constant (200 mL/min) anolyte and catholyte flow rates. Figure 4.3 shows current - voltage relationship for different middle compartment solution flow rates at constant 200 mL/min flow rates of anolyte and catholyte. For all the flow rates the electrode and membrane charging region appeared up to 1.8 V. The relation for 5 and 20 mL/min had all the three regions explained in 3.1.1. Ohmic region appeared till 5.5 V (current density 33 mA/cm^2) and 5.2 V (current density 40 mA/cm^2) for 5 and 20 mL/min flow rates respectively. Second region was observed from 5.5 to 21.5 V and 5.2 to 16.6 V for 5 and 20 mL/min flow rates respectively. Further increase in voltage resulted in over limiting region. For higher flow rates of 100 and 200 mL/min the characteristics were completely different from the characteristics at lower flow rates. The length of the second region, known as constant plateau region in conventional electrodialysis, decreased with increase in the flow rate of middle compartment solution and it disappeared at high flow rates of 100 and 200 mL/min. The constant plateau in the second region in case of electrodialysis is due to concentration polarization at the membrane-solution interface, which leads to boundary layer formation. Introduction of ion exchange resin, in case of EDIX, increases the conductivity in the middle compartment. Higher middle compartment flow rates resulted in decrease in the thickness of boundary layer and disappearance of the second region.

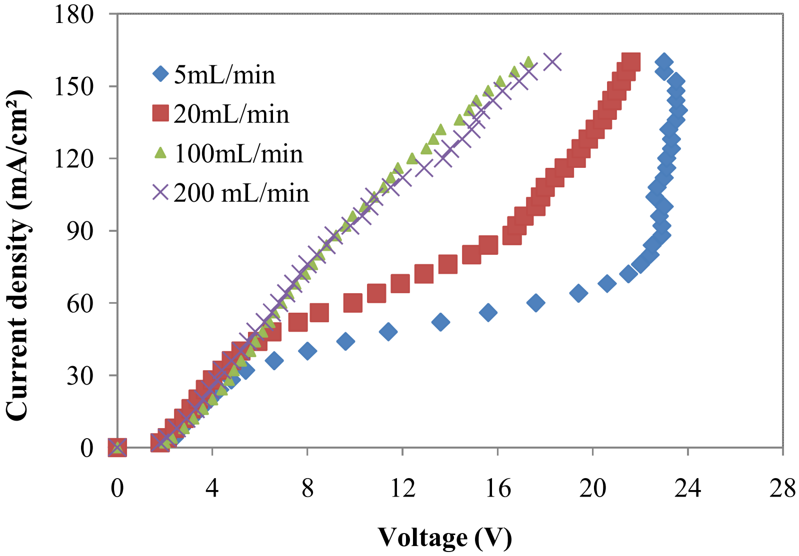

Figure 4.3 I-V characteristics for different middle compartment solution flow rates

The I-V relations were transformed to Cowan plots by plotting the middle compartment resistance against inverse of the current. From the Cowan plots, limiting currents were determined from the point of intersection of the tangents drawn to the increasing and decreasing resistance curves [152]. It was seen that when the middle compartment solution flow rate is increased, limiting currents increased up to 0.531 m/s (100 mL/min), but with further increase in flow rate, remained constant up to 1.062 m/s (200 mL/min). This can be observed in Figure 4.3 by the merging characteristics for these two flow rates. The increase in LCD up to 100 mL/min is due to the increase in the conductivity of the middle compartment. The conductivity of a flow cell was analyzed by Yeon et al [153] by breaking it into three different parts, conductivity through alternating layers of particles and interstitial solution, conductivity through the resin and conductivity through the solution. Increase in flow rate of the solution increases the conductivity through the solution. It also increases the conductivity through alternating layers of particles and interstitial solution, by decreasing the boundary layer thickness. At 0.531 m/s (100 mL/min), onset of bed expansion was observed and it was more pronounced for 1.062 m/s (200 mL/min). Figure 4.4 shows a plot of i_{lim}/C against linear velocity on a double logarithm graph, for varying electrolyte and middle compartment flow rates.

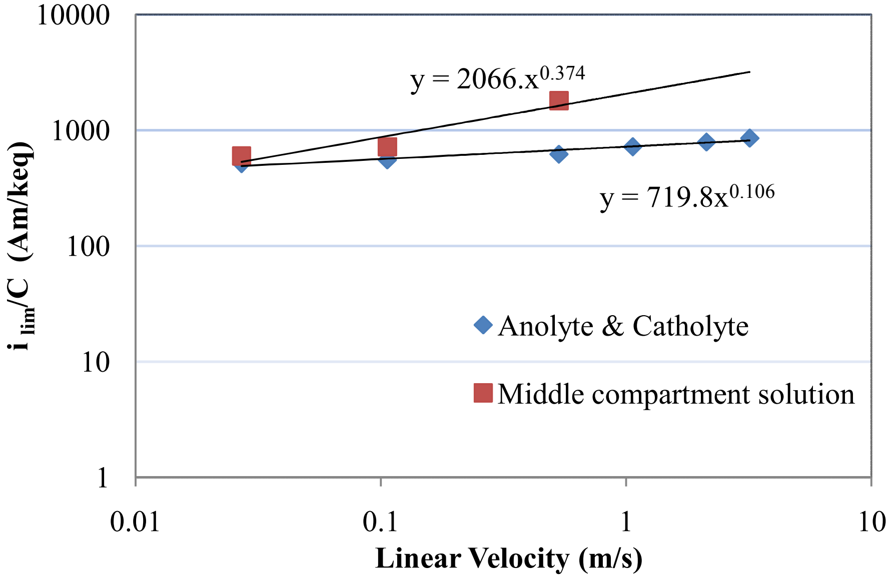

Figure 4.4 Determination of coefficients a and b

Limiting currents increased with increase in the flow rate. Higher flow rates might have decreased the boundary layer thickness, which limits the diffusion of ions to the membrane surface. In practice, electrodialysis systems are operated at currents substantially below this limiting value, whereas electrodeionization (EDI) systems with ion exchange resin in the middle compartment are operated at overlimiting currents. Enhanced water splitting at overlimiting currents increases the regeneration rate of the EDI systems, in which H^+ and OH^- ions are used for regeneration [154]. In this study, AMP-PAN has to be regenerated with ammonium ions and hence the presence of H^+ did not aid the regeneration. Due to this reason, the system needs to be operated only within limiting current range. From Figure 4.4, the coefficients *a* and *b* of equation (4.3) were estimated to be 716.6 $As^{b}m^{1-b}$/keq and 0.125 respectively, in the linear velocity range of electrolytes between 0.027 and 3.185 m/s at constant middle compartment solution flow rate of 20 mL/min. At a constant electrolytes flow rate of 200 mL/min, *a* and *b* were evaluated to be 2066 $As^{b}m^{1-b}$/keq and 0.374 for varying middle compartment flow rate. Higher values of *a* and *b* for middle compartment solution indicate higher dependency of LCD on middle compartment flow compared to electrolyte flow.

4.3. Influence of anolyte concentration on I-V characteristics

With different concentrations of regenarant (anolyte) solution (1000 ppm, 5000 ppm, 10000 ppm, 25000 ppm, 50000 ppm of NH_4^+) for constant (200 mL/min) flow rates of anolyte, catholyte and 20 mL/min of middle compartment solution flow rate, the I-V characteristics were studied.

As recovery of cesium from AMP-PAN depends on the regenarant concentration, anolyte concentration was varied keeping the catholyte and middle compartment solution concentrations constant at 0.1 N HNO_3. Current-voltage characteristics for different anolyte concentrations are shown in Figure 4.5. Three regions were observed in these plots similar to the plots above. Ohmic region, limiting region and over limiting region were observed with increasing the anolyte concentration from 0.028 to 0.694 M. As the concentration increased, slope of the limiting region increased, while its length decreased. At higher concentrations, more ions were available to transport current in the boundary layer, which could minimize the concentration polarization at the membrane solution interface.

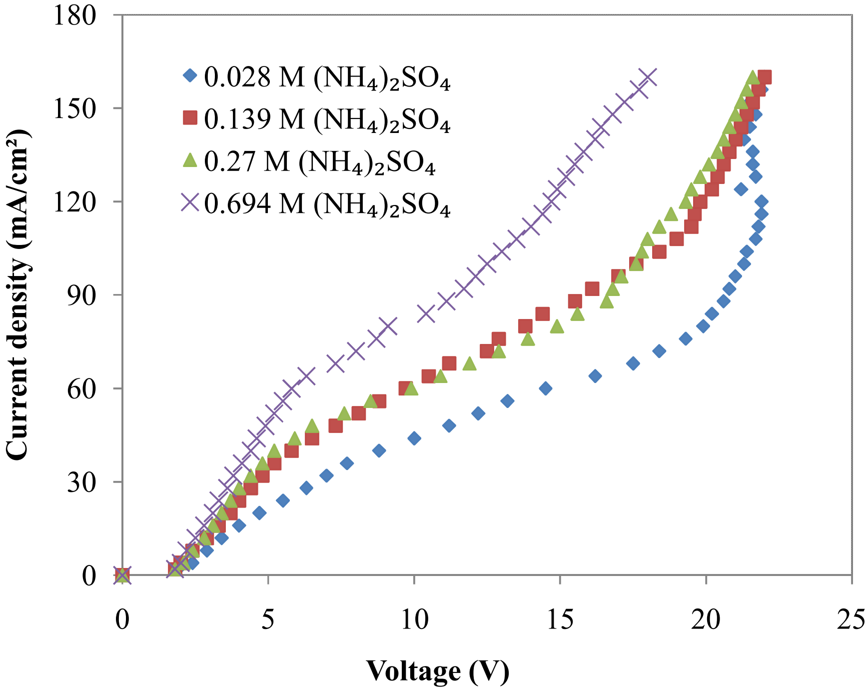

Figure 4.5 I-V characteristics for different $(NH_4)_2SO_4$ concentration

From Figure 4.5 it can be seen that the ohmic region appeared up to 5 V for all the concentrations studied. Limiting currents determined from Cowan plots for different electrolyte flow rates and anolyte concentrations are shown in Figure 4.6. It was observed that the limiting currents increased linearly with increasing anolyte concentration for all the flow rates studied and confirmed the linear relationship between limiting current and concentration, as given by equation 4.3. The linear relationship between LCD and concentration showed a discrepancy at lower concentrations. Presence of resin in the middle compartment might have increased the conductivity of the compartment, resulting in movement of ions even at a low anolyte concentration.

Figure 4.7 shows a plot for i_{lim}/C Vs u for different anolyte concentrations for determining the coefficients *a* and *b* of equation 4.3. The estimated values of *a* and *b* are shown in Figure 4.8. The coefficient *a* decreased with increasing the anolyte concentration from 0.028 to 0.139 M and then only a slight decrease was observed. The coefficient *b* was almost constant at lower concentrations and slightly increased for highest concentration studied (0.694 M). The coefficient *a* is related to ion transport through ion exchange membranes and the coefficient *b* is related to cell geometry and hydrodynamic conditions [150]. Results of the present study are in conformity with this observation.

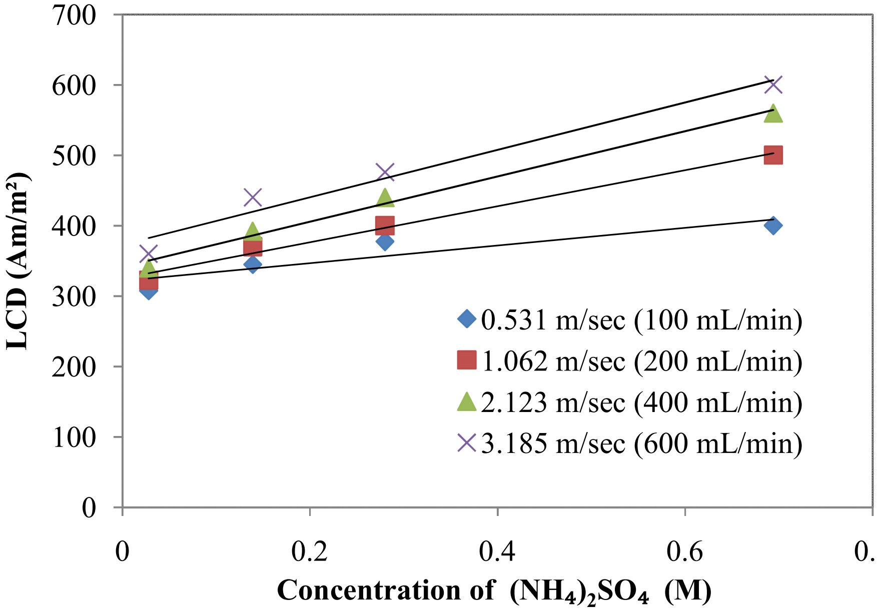

Figure 4.6 Limiting currents for different anolyte concentration

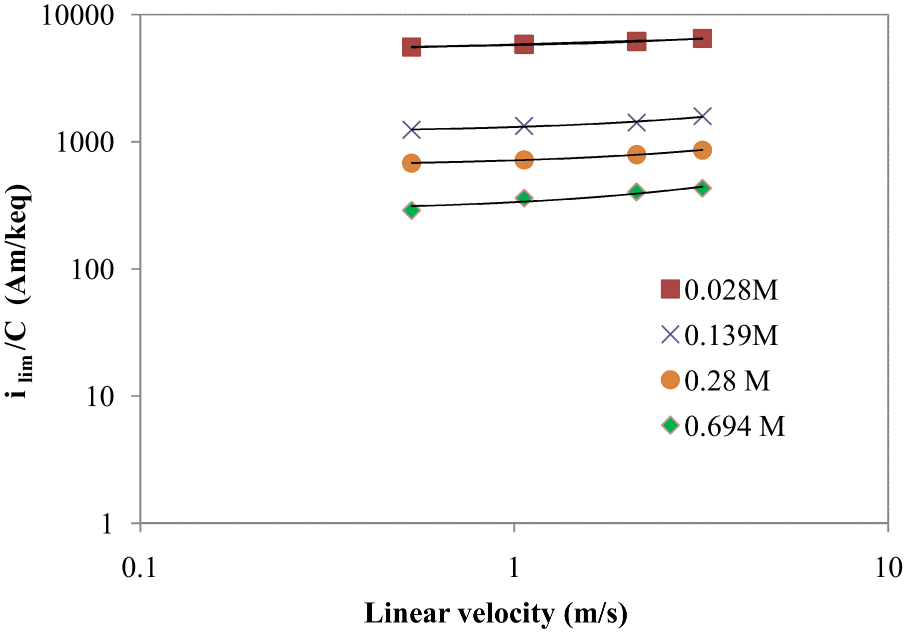

Figure 4.7 i_{lim}/C vs. linear velocity u for various anolyte concentrations

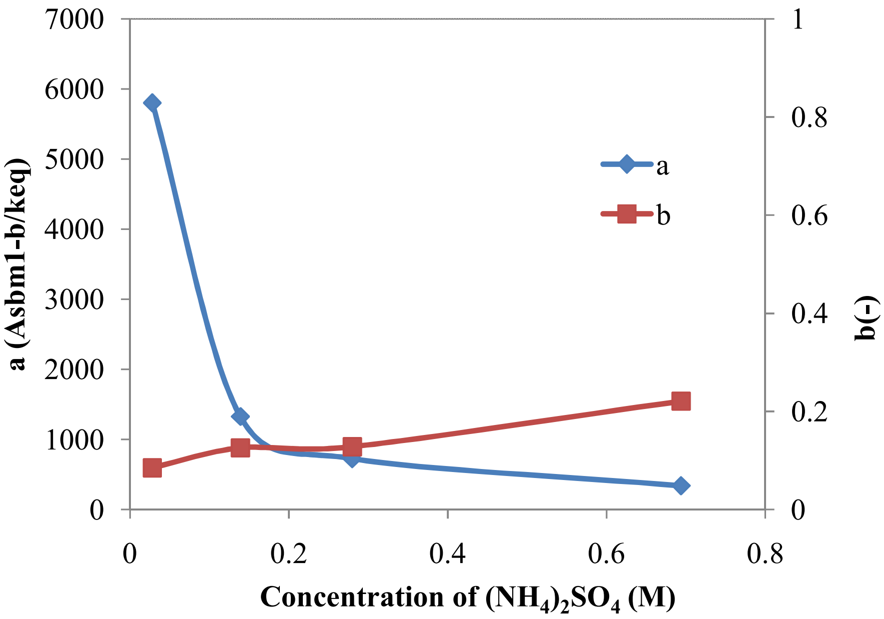

Figure 4.8 Coefficients a and b as a function of anolyte concentration

4.4. Operation of EDIX process at over limiting currents

Continuous operation of EDIX was carried out for 10 hours to study the dynamic behavior of the system. The flow rates of the electrolytes in all the three compartments viz., anolyte (10000 ppm NH_4^+), middle compartment solution (0.1 N HNO_3) and catholyte (0.1 N HNO_3) were maintained at 5 mL/min. The solutions were passed on once through basis and were not recycled, thus maintaining the concentrations constant. Current densities were varied from 20 to 60 mA/cm^2. pH of the solutions passing through the three compartments was monitored on hourly basis. Figure 4.9 shows the I-V characteristics for continuous operation. From Cowan plots, limiting current density was found to be 40 mA/cm^2.

To study the effect of current density, the cell was operated below and above this limiting value. Cesium recovery is shown in Figure 4.10 for 10 hours of operation. It was observed that the cesium recovery increased with increasing the current density up to 30 mA/cm^2 and subsequently decreased. Currents equal to or more than LCD result in concentration polarization and operation at about 80% of LCD gives high recovery.

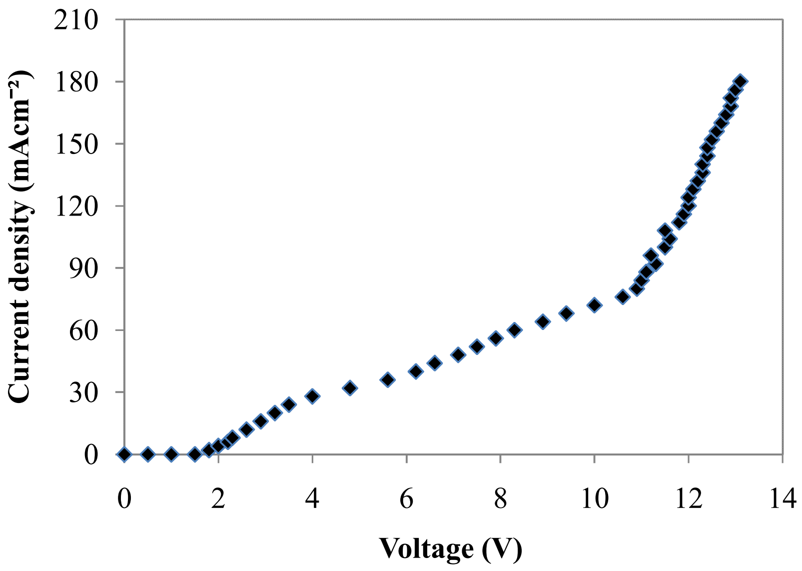

Figure 4.9 I-V curve for determination of limiting current in continuous EDIX

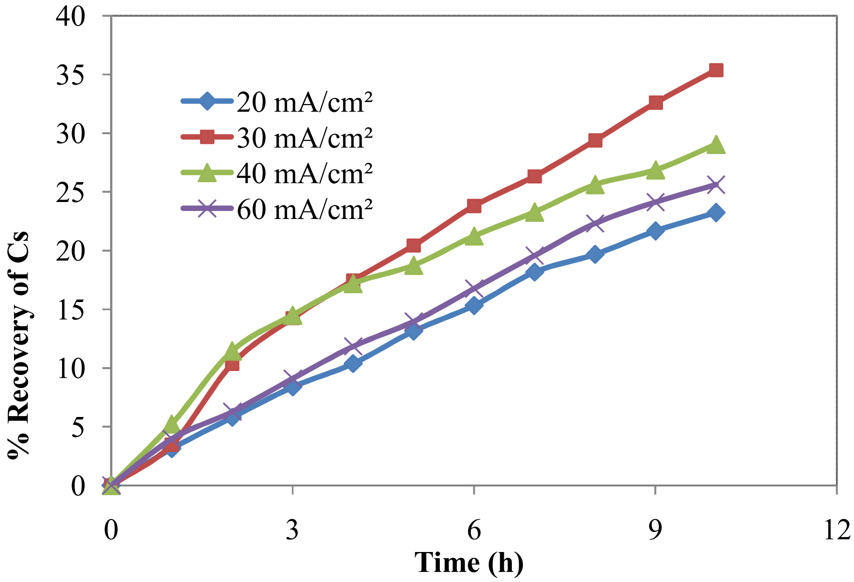

Figure 4.10 Recovery of cesium in catholyte at different current densities

To study the effect of water dissociation at overlimiting currents, pH of all the three compartments was monitored and presented in Figures 4.11, 4.12 and 4.13. The pH of the catholyte is almost constant, when current densities 20 and 30 mA/cm^2 were applied (Figure 4.11). When overlimiting currents were applied, pH of the catholyte suddenly increased to beyond 8 from pH of 1. It may be noted that the operation is continuous and the catholyte is passed on once through basis at the rate of 5 mL/min. At these currents, a salt depleted boundary layer forms at the solution membrane interface. Increase in applied current density increases the voltage drop across the cell, which further increases the secondary reactions at the electrodes. H_2 and O_2 are generated at the cathode and anode respectively. The electric potential to initiate water dissociation to H^+ and OH^- is 1.23 V. The rate of water dissociation is proportional to the current [155]. With increase in the current density, the water dissociation increases the catholyte pH and decreases the anolyte pH. Sudden increase of pH at higher current densities was also observed by Song et al [156] for continuous electro deionization system packed with an anion exchange textile.

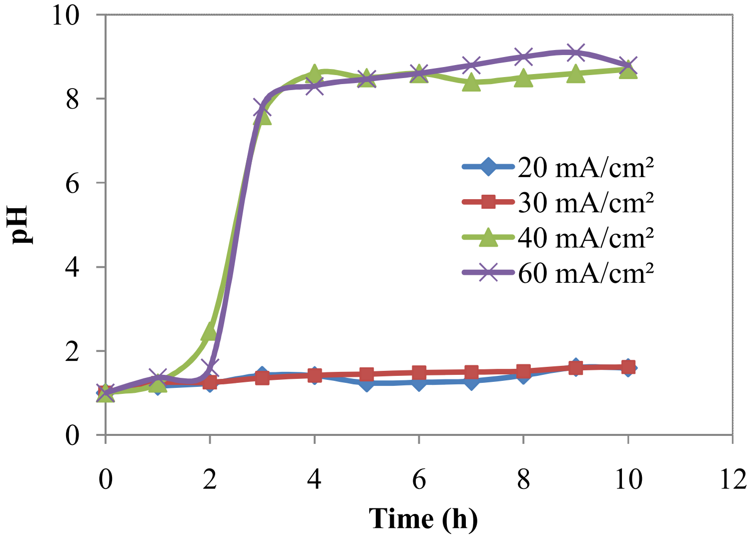

Figure 4.11 Variation of the catholyte pH for different current densities

pH of the anolyte decreased from 5 to 2.9 in the first one hour and then slightly decreased with time when current density of 20 mA/cm^2 was applied (Figure 4.12). At higher currents, anolyte pH further decreased, as pH of the electrolytes depends on the reactions occurring at the electrodes.

For all the current densities studied, pH of the middle compartment solution increased in the first hour and almost remained constant (Figure 4.13). The initial increase in the pH of the solution might be due to transfer of protons from middle compartment solution while the electrodes and membranes were getting charged. With increasing current densities, pH of the solution increased slightly due to the increase in proton/ cation transfer from the middle compartment to the cathode compartment.

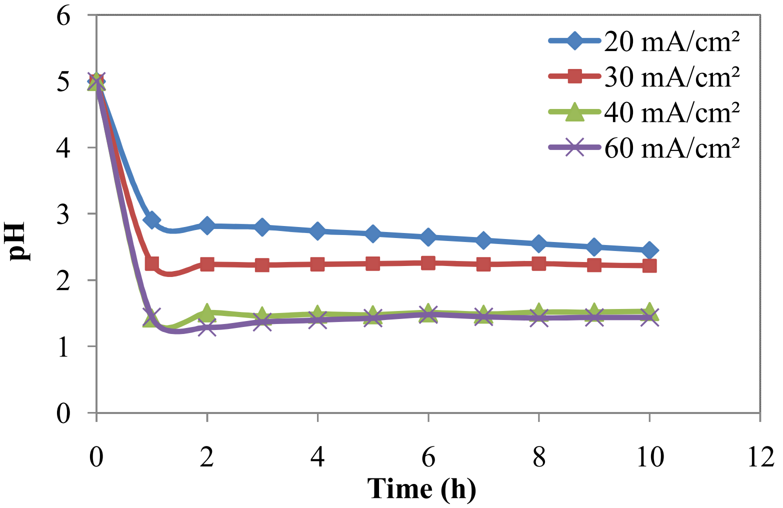

Figure 4.12 Variation of anolyte pH for different current densities

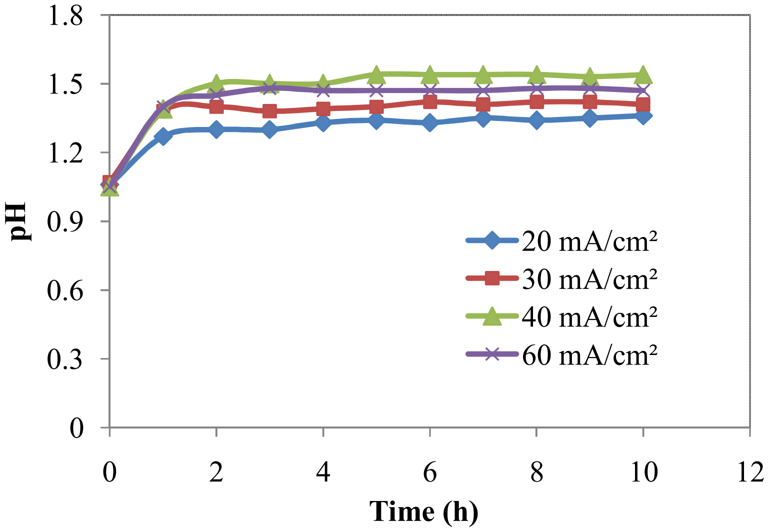

Figure 4.13 Variation of middle compartment solution pH for different current densities

4.5. Conclusions

Current-voltage characteristics were determined in EDIX process for the recovery of Cs from AMP-PAN for different process parameters, which showed three regions as in conventional electrodialysis. Limiting currents were determined from the I-V curves by transforming them into Cowan plots. It was observed that limiting currents increased with increasing flow rates and concentrations of electrolytes. Coefficients a and b to be used in the empirical equation for determining the limiting currents (equation 4.3), were estimated to be 716.6 $As^{b}m^{1-b}$/keq and 0.125 respectively for varying electrolyte flow rates and 2066 $As^{b}m^{1-b}$/keq and 0.374 for varying middle compartment flow rate. Higher values of a and b indicate higher dependency of LCD on middle compartment flow compared to electrolyte flow. Merging of the regions in I-V plots was observed for high middle compartment flow rates. Anolyte concentration had a pronounced effect on the value of a but little effect on b, as b is related to cell geometry and hydrodynamic conditions.

For the continuous flow system, the LCD is found to be 40 mA/cm^2. Operation at and above this current density resulted in low recovery of Cs from the resin and hence, operation at about 80% LCD is recommended. Monitoring the pH of catholyte yielded important information about the operating current density. Operating in the over limiting range turned the acidic catholyte to alkaline due to water splitting at the membrane-solution interface and secondary reactions at the electrodes. As AMP-PAN sorbed with cesium ions needs to be regenerated with NH_4^+ , H^+ generation due to water splitting did not aid the recovery of Cesium.

Investigation of EDIX for Cesium recovery from AMP-PAN

5

A hybrid electrodialysis ion exchange (EDIX) process is investigated for the recovery of Cs from AMP-PAN. Two different modes of operation are studied in which eluant used for Cs replacement, is passed through different compartments of the electrodialysis cell. Effects of various parameters like current density, eluant concentration, etc on Cs recovery are studied. Nernst-Plank equation is applied to describe the mechanism of the process. The feasibility of Cs recovery from AMP-PAN by EDIX is discussed.

5.1. Introduction

Electrodialysis (ED) is the most popular technique for electrically-driven processes in industry, as it separates undesired ions from dilute aqueous solutions at a low operational cost without generating residues [157-159]. This technology, which combines the principles of dialysis and electrolysis, was first applied for the demineralization of syrup in 1890. An initial work that described this technology in a scientific journal was published in 1930 [160]. Since its inception, the capabilities of this hybrid technology have been demonstrated in several areas, encompassing desalination, organic compound separation, radioactive wastewater treatment, acid and caustic production, ultrapure water production and general ionic separation. Although ED qualifies as an excellent technology for applications that span a broad range of processes, a specific concentration limit must be adhered to in order to optimize energy efficiency. When ions are separated from the feed solution, there is an inherent drawback of concentration polarization because of which, a high cumulative resistance within the cell is built up, decreasing the cell efficiency. In order to eliminate this disadvantage, a solid conductive ion medium has been introduced into the dilute compartment in the form of ion exchange resins. Thus, ED and ion exchange technologies were combined, permitting the achievement of high quality ion separation with improved efficiency. This new hybrid system was subsequently named as electrodeionization (EDI) or a hybrid Electrodialysis Ion exchange (EDIX).

5.2. Different modes of operation of EDIX for recovery of Cs from AMP-PAN

Two different modes of operation were studied for investigating the efficacy of EDIX for recovery of Cs from AMP-PAN.

5.2.1. Mode-I

In mode-I, the eluant $(NH_4)_2SO_4$ is passed through anode compartment and is subsequently called anolyte. The other electrode compartment was run with dilute acid (0.1-0.5N HNO_3) to reduce any precipitation on electrode surface. In the middle compartment, where ion exchange resin is loaded, 0.1N HNO_3 is circulated mainly to keep the ion exchange resin in acidic nature. The schematic of the operation of the cell in mode-I is shown in Figure 5.1.

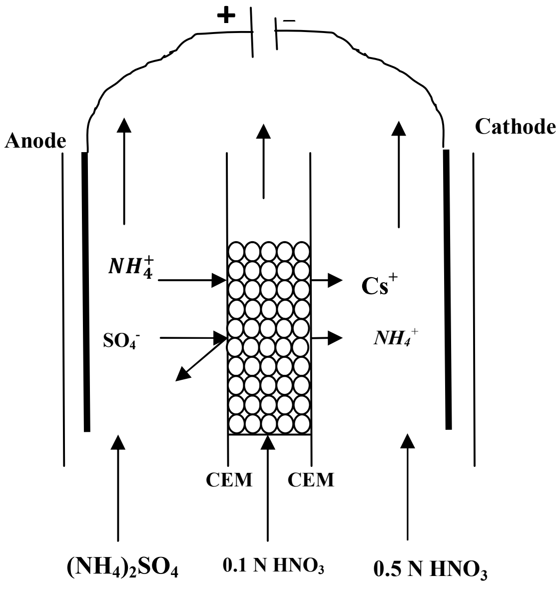

Figure 5.1 Operation of EDIX in mode-I

Anode compartment: $2H_2O \rightarrow O_2 + 4H^+ + 4e^-$

$(NH_4)_2SO_4 \rightarrow 2\ NH_4^+ + SO_4^{2-}$

Middle compartment: $R\text{-}Cs^+ + NH_4^+ \rightleftharpoons R\text{-}NH_4^+ + Cs^+$

Cathode compartment: $4H_2O + 4e^- \rightarrow 2H_2 + 4OH^-$

$Cs^+ + OH^- \rightleftharpoons CsOH$

$NH_4^+ + OH^- \rightleftharpoons NH_4OH$

In this mode, eluant ($(NH_4)_2SO_4$) containing NH_4^+ ions in the anode compartment migrate on application of electric potential towards cathode. Since cathode is negatively charged, it attracts only positive charged ions. On its way towards cathode, NH_4^+ ions pass through the middle compartment where Cs sorbed AMP-PAN is loaded. Since Cs^+ is replaced for NH_4^+ during sorption, while regeneration, NH_4^+ replaces Cs^+ on the resin. Once NH_4^+ replaces Cs^+, the exchanged Cs^+ is available for migration toward cathode. Thus Cs on the AMP-PAN is recovered in cathode compartment by application of electric potential.

5.2.2. Mode-II

Other than mode-I, the only possible way of operation is passing the eluant through the middle compartment containing ion exchange resin. In the remaining electrode compartments, dilute acids are circulated. The schematic of the operation of the cell in mode-II is shown in Figure 5.2. Here, ammonium ions in the eluant which is passing directly through the AMP-PAN in the middle compartment replace cesium ions and cesium ions are readily available in the middle compartment which will be convected by the eluant itself through the outlet of the middle compartment. On application of electric potential, the available cesium ions in the middle compartment are able to migrate towards cathode where they can concentrate. Without application of electric potential, the eluted cesium ions in the middle compartment cannot migrate to cathode compartment and only be convected by the eluant.

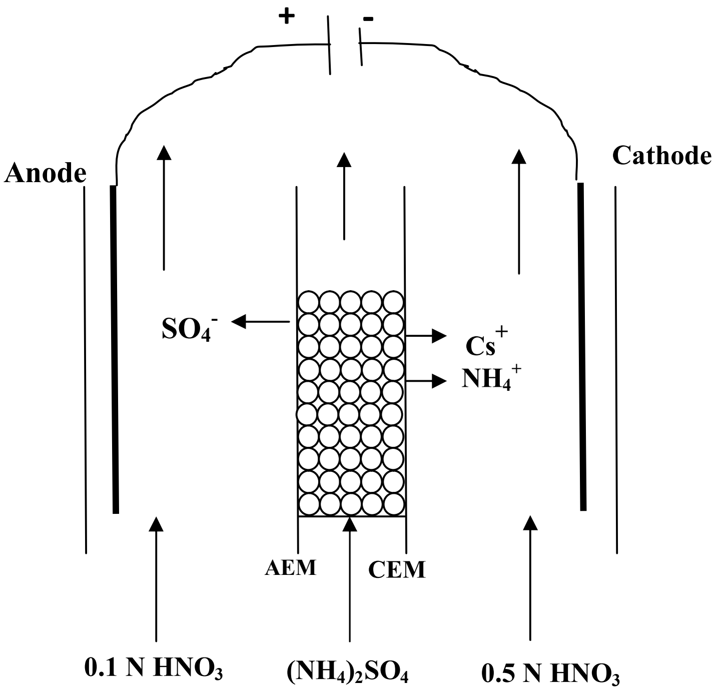

Figure 5.2 Operation of EDIX in mode-II

5.3. Porous plug model

The current flow in ion exchange resin beds is complex, since the beds are a mixture of two phases of different properties, namely resin and interstitial liquid. Several theories have been proposed for the transport phenomena involved—such as conduction of heat or electrical current in mixtures [161]. However, most of the theories are based on the assumptions of either a regular lattice-type arrangement or a completely random distribution of the components.

Wyllie suggested an approach for the ion exchange beds where the distributions of the resin particles constitute an irregular and discontinuous phase and the liquid is a continuous one [162]. The model estimates electrochemical properties from empirical and geometrical parameters. This "porous-plug" model is based on the assumption that the electrical current passes through three different paths within the bed. The first path is through alternating layers of particles and interstitial solution, the second is through particles in contact with each other, and the third is the channel through the interstitial solution [163]. For the model, the conductivity of the resin bed is depicted by Figure 5.3.

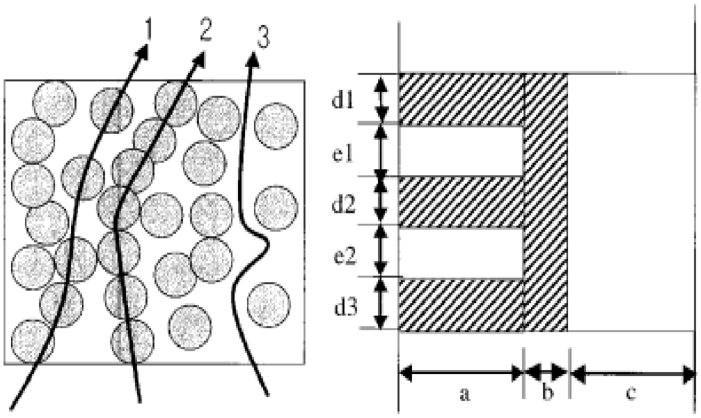

Figure 5.3 The "porous-plug" model, Left: schematic representation of the three paths which the current can take. Right: the simplified model consisting of three conductance elements in parallel. The geometrical parameters d and e are given by $d_1+d_2+d_3=d$; and $e_1+e_2=e$

5.4. Nernst- Plank equation

The Nernst-Plank relationship describing the transport of ions through a homogenous bed of ion-exchange resin was used by several researchers for electrodeionization [164-172].

$$\boldsymbol{N_i = \bar{D}_i \frac{d\bar{C}_i}{dx} + z_i\bar{C}_i\bar{u}_i grad\varphi + v\bar{C}_i} \tag{5.1}$$

where, values with an overbar belong to solid phase. The first term on the right hand side describes the diffusion of ion i with concentration $\bar{C}_i$ and diffusion coefficient $\bar{D}_i$. The second term is for the migration of ion i with valence state z_i and mobility $\bar{u}_i$. The bed potential gradient is denoted by gradφ. The third term describes the movement of pore liquid within the ion-exchange particles.

5.5. Ion transport in the presence of an electrical field

On application of electric field across an electrodialysis cell, It has been reported that diffusion and convection effects are negligible compared to migration effects. Nernst-Plank equation applied for ion transport in electrodeionization cells reduces to the migration term.

$$\mathbf{\bar{N}_{Cs} = z_i \bar{C}_i \bar{u}_i grad\varphi} \quad (5.2)$$

The mobility of the ions in the particles, $\bar{u}_i$, is defined by

$$\bar{u}_i = \frac{\bar{D}_i F}{RT} \quad (5.3)$$

Consequently 5.2 becomes

$$\mathbf{\bar{N}_{Cs} = z_i \bar{C}_i \frac{\bar{D}_{i,eff} F}{RT} grad\varphi} \quad (5.4)$$

5.6. Empirical equation for migration

The migration of metal ions to the cathode compartment can be analyzed by the empirical model of resin regeneration proposed by P.B. Spoor et al [165] for electromigration of nickel. The model assumes first order kinetics with respect to metal ion concentration in the resin and predicts the flux of the metal ion in terms of the maximum amount of ions extracted from the resin, which can be determined experimentally. Using this model, the experimental curves are fitted to the following exponential equation to predict n_{Cs}, the amount of cesium present in the catholyte:

$$\mathbf{n_{Cs} = n_{Cs,max}(1 - e^{-k_m t})} \quad (5.5)$$

where, $n_{Cs,max}$ is the maximum amount of Cs present in the catholyte at the end of the experiment and k_m is the mass transfer coefficient, a model parameter.

The cesium flux from the bed can be calculated using the derivative of equation 5.5.

$$\mathbf{N_{Cs} = \frac{1}{A_{bed}} \frac{dn_{Cs}}{dt} = \frac{k_m n_{Cs,max}}{A_{bed}} e^{-k_m t}} \quad (5.6)$$

5.7. Calculation of effective diffusion coefficient

The effective diffusion coefficient of cesium in the bed, $\bar{D}_{Cs,eff}$ can be found out using the migration term of Nernst-Planck equation [165],

$$\mathbf{N^0_{Cs} = z_{Cs} \bar{C}^0_{Cs} \frac{\bar{D}_{Cs,eff} F}{RT} grad\varphi} \quad (5.7)$$

where, N_{Cs}^{0} and $\bar{\mathrm{C}}_{\mathrm{Cs}}^{0}$ are the possible cesium flux and concentration of Cs in solid phase at time t=0.

The effective diffusion coefficient, $\bar{D}_{Cs,eff}$ can be calculated from equations 5.6 and 5.7 as

$$\boldsymbol{\bar{D}_{Cs,eff} = \frac{n_{cs,max}\, k_m}{A_{bed}}\ X\ \frac{RT}{z_{Cs}F|\overline{Cs}^{+}|_0\nabla\varphi}} \tag{5.8}$$

where subscript t refers to time t. The effective diffusion coefficient, $\bar{D}_{Cs,eff}$ (m^2/s), is calculated at time t=0.

5.8. Ohmic resistance and Potential gradient of the packed bed

The electric resistance of the ion-exchange bed can be calculated using the equation below by subtracting resistances offered by the anolyte (R_a), catholyte (R_c), eluant (R_e) and both membrane resistances (R_m) from the total resistance of the cell (R_{cell}).

$$\mathbf{R_{bed} = R_{cell} - R_a - R_c - R_e - 2R_m} \tag{5.9}$$

where, R_{cell} is the cell resistance; R_a is the anolyte resistance; R_c is the catholyte resistance; R_m is the membrane resistance; and R_e is the eluant resistance.

Similar to the bed resistance, bed voltage drop also can be calculated as

$$\boldsymbol{\Delta \mathbf{E}_{bed} = \mathbf{E}_{cell} - (\mathbf{E}_a + |\mathbf{E}_c|) - \mathbf{R}_e\mathbf{I}_e - 2\mathbf{E}_m} \tag{5.10}$$

where, E_{cell} is the cell potential; E_a is the anode electrode potential; E_c is the cathode electrode potential; E_m is the membrane potential; and R_eI_e is the eluant ohmic drop calculated from the conductivity of the solution.

The average gradient can be expressed as the ratio of the ohmic drop in the bed, $\Delta \mathrm{E}_{\mathrm{bed}}$, over its thickness, δ_{bed} .

$$\Delta\emptyset = \frac{\Delta \mathrm{E}_{\mathrm{bed}}}{\delta_{\mathrm{bed}}} \tag{5.11}$$

$(E_a + |E_c|)$ was found to be 1.8 V from the current-voltage measurements [173] of the electrodialysis cell. The resistance of the membranes was neglected compared to the cell resistance.

5.9. Study of process parameters in Mode-I

Before applying voltage across the electrodialysis cell containing AMP-PAN in the central compartment, it was saturated with Cs by passing Cs solution through a glass column containing AMP-PAN. The Cs sorbed AMP-PAN is then transferred to the middle compartment of the electrodialysis cell. The details of the EDIX setup used and the flow rates of the electrolytes in the cell are given in Table 5.1.

Table 5.1 Details of EDIX setup

	Anode compartment	Middle compartment	Cathode compartment
Size	10 cm X 10 cm X 0.8 cm	10 cm X 10 cm X 0.5 cm	10 cm X 10cm X 0.8 cm
Circulating solution	10000 ppm $(NH_4)_2SO_4$	AMP-PAN + 0.1N HNO_3	0.1N HNO_3
Vol. of solution	1000 mL	1000 mL	1000 mL
Flow rate	200 mL/min	5mL/min	200 mL/min

5.9.1. Effect of loading capacity of Cs on AMP-PAN

The effect of loading of Cs on AMP-PAN was studied at constant current density of 20 mA/cm^2 for an eluant concentration of 0.27 M. The amount of Cs on AMP-PAN was varied from 8.82 to 31.25 mg/g of resin and recovery of Cs from the AMP-PAN was shown in Figure 5.4.

The recovery of Cs from AMP-PAN in the catholyte increased with time for all the studied loading capacities of the ion exchanger. It was seen that a high recovery of

84.87% was observed for a loading capacity of 8.82 mg/g and only 38.76% of Cs was recovered for a high loading of 31.25 mg/g, in 30 h of operation.

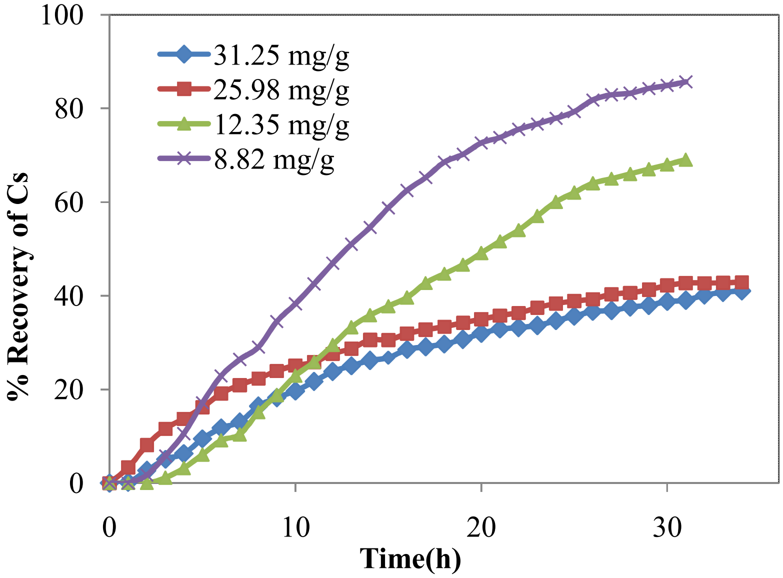

Figure 5.4 Influence of resin loading capacity on recovery of cesium
current density = 20 mA/cm^2, eluant conc. = 0.27 M

It was observed that cesium recovery percentage increased with decreasing the loading capacity of the adsorbent. The reason for such behavior is resulted by the fact that only cesium ions on the surface were recovered with ammonium ions under the effect of applied electric potential. For high loading capacities, AMP-PAN is fully exploited of its volume by Cs ions which are strongly bounded inside the micro pores of the resin particles as well as on the surface. Removal of these ions from deeply bounded sites requires long retention time or high eluant concentrations. In case of low loading capacities, only surface sites were exploited for exchange and hence available for exchange.

The effective diffusion coefficients for Cs migration to cathode compartment for different loading capacities of the resin were determined using equation 5.8 and the values were tabulated in Table 5.2. The diffusion coefficients were observed to increase with increasing loading capacity and similar is the case for mass transfer coefficients.

Table 5.2 Effective diffusion coefficients of Cs migration for different loading capacities of AMP-PAN

Capacity of resin (mg/g)	n_{max} (moles)	grad∅ (V/m)	K_m x10^{-5} (s^{-1})	D_{eff} x 10^{-10} (m^2/s)
8.82	1.52	2000	1.39	4.12
12.35	1.600	1600	1.50	5.63
25.98	1.667	1200	2.31	5.72
31.25	1.832	800	1.63	6.24

5.9.2. Effect of current density

Cesium recovery form AMP-PAN was studied by EDIX technique for an eluant concentration of 10000 ppm NH_4^+ (0.27M $(NH_4)_2SO_4$), varying the current density from 20 to 30 mA/cm^2. The limiting current density was found to be 35 mA/cm^2 for the studied conditions. The concentration of cesium recovered by migration in cathode compartment for the different applied current densities was shown in Figure 5.5.

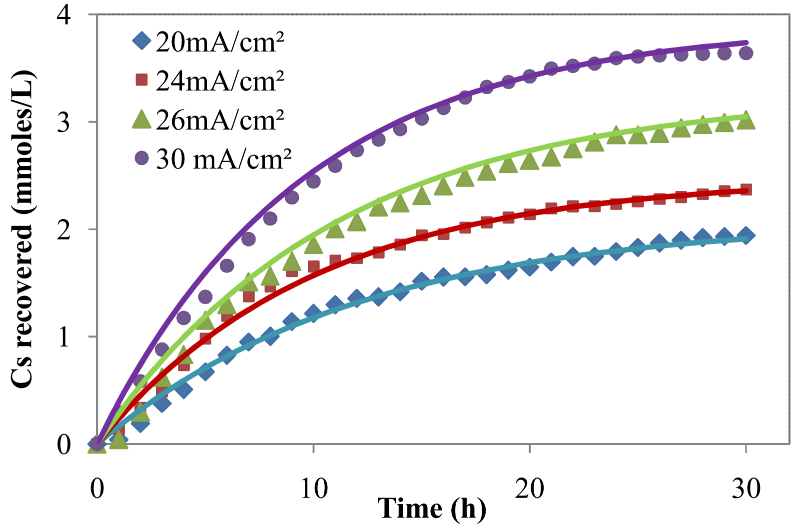

Figure 5.5 Cs recovery in catholyte for different current densities
Eluant Conc. = 0.27 M NH_4^+, loading capacity ≃ 30 mg/g

It was observed that Cs recovery increased with time for all the studied current densities. The recovery is rapid in the first 15 h and then only little increase in Cs recovery was observed upto 30 h of operation of the cell. From 15 h to 30 h of operation, only 10% of the total recovered Cs could be eluted from the AMP-PAN for all the studied current densities. The total recovery of Cs increased from 1.94 to 3.64 mmoles/L with increase in current density from 20 to 30 mA/cm^2. Further increase in current density was restricted by concentration polarisation. The percentage of Cs recovered from catholyte for different current densities was shown in Figure 5.6.

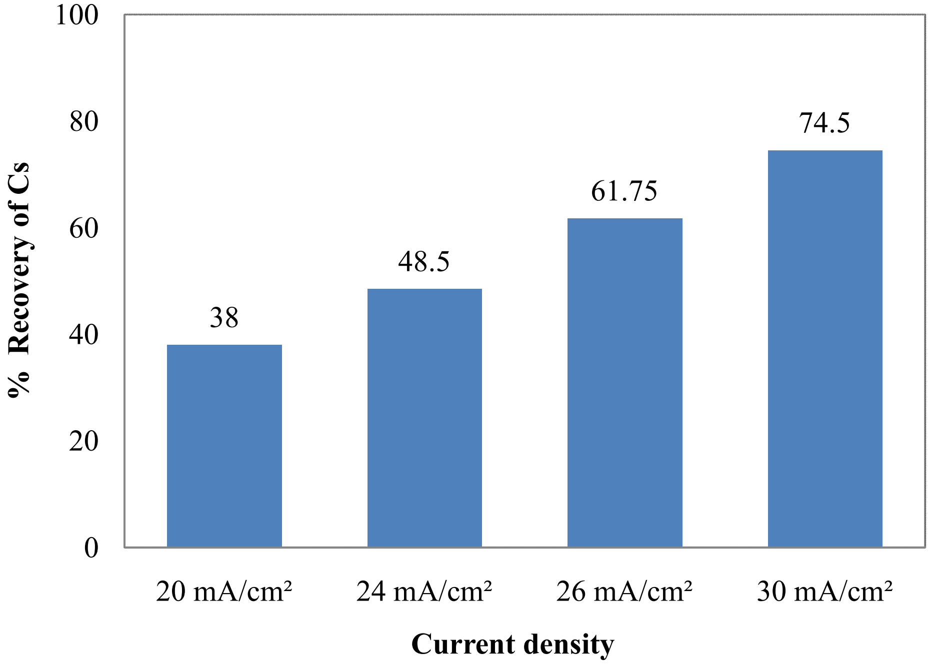

Figure 5.6 Total recovery of Cs from AMP-PAN for different current densities

With increase in applied current densities from 20 to 30 mA/cm^2, the total Cs recovered in catholyte increased from 38 to 74.5 %. The migration of ions in electrodialysis cell increases with increase in current, which had increased the Cs recovery percentage from AMP-PAN. Negligible amounts of Cs were observed in anode and middle compartment, which confirmed that there was no diffusion of Cs across the ion exchange membranes due to concentration gradients.

Application of Nernst-Planck equation to describe the recovery of Cs from AMP-PAN results in only migration term. The effective diffusion coefficient of Cs was determined at time t=0 using equation 5.8 for different current densities and tabulated in Table 5.3. It was observed that Cs migration diffusion as well as mass transfer coefficients increased with increase in current density.

Table 5.3 Effective diffusion coefficients of Cs migration for different current densities

Curretnt density (mA/cm^2)	n_{max} (moles)	gradØ (V/m)	k_m x 10^{-5} (s^{-1})	D_{eff} x 10^{-9} (m^2/s)
20	2.08	800	2.31	0.92
24	2.48	740	2.78	1.41
26	3.26	640	2.53	1.98
30	3.9	640	2.92	2.73

The behaviour of anolyte pH in the electrodialysis cell is shown in Figure 5.7 for different current densities. It was observed that anolyte pH decreased with time for all the current densities studied. The decrease in pH was more pronounced with increase in current density. Proton generation at the anode surface makes anolyte acidic in nature.

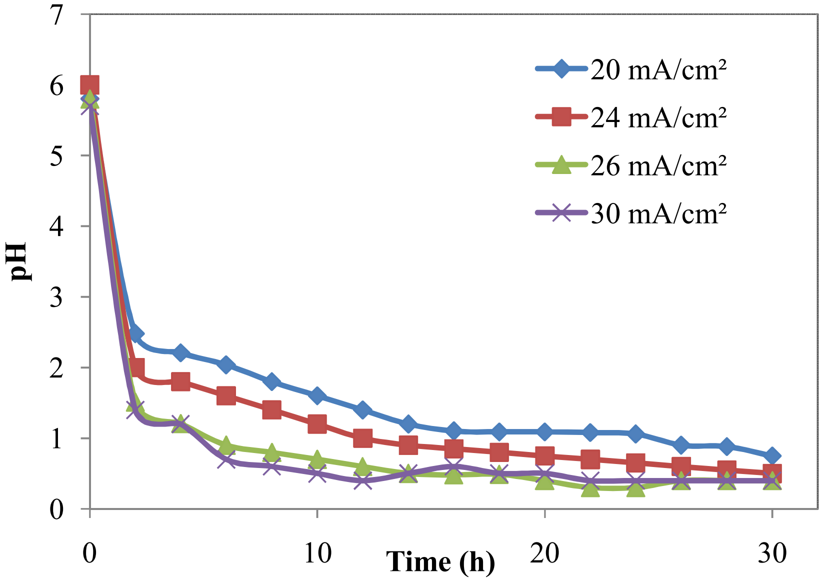

Figure 5.7 Anolyte pH for different current density

The pH of the middle compartment solution did not show significant variation with time for increase in current density as seen from Figure 5.8. Since the cell is operated under limiting current density, no water splitting was observed at the membrane surface.

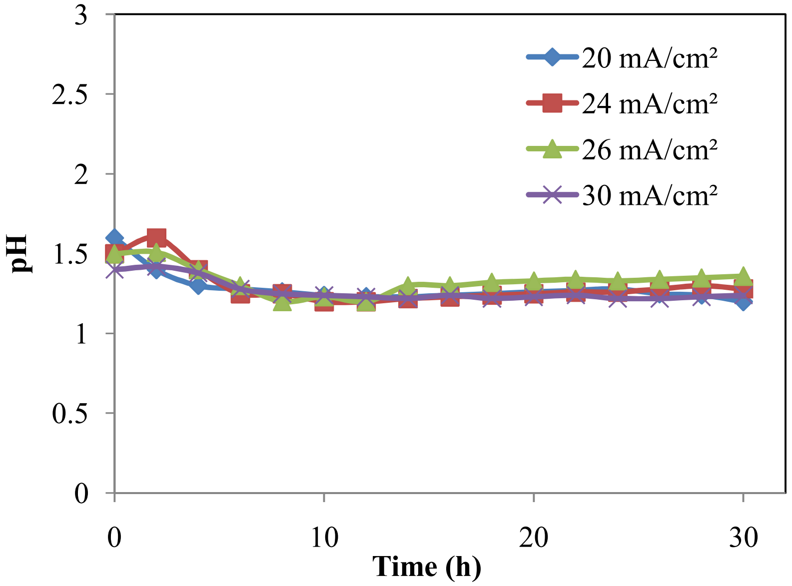

Figure 5.8 Middle compartment solution pH for different current densities

Variation of catholyte pH is presented in Figure 5.9. It was observed that the pH of catholyte slowly increased from 1 to 2 in 8 h of operation at constant current density of 20 mA/cm$^{2.}$ The increase in catholyte pH was due to hydroxide ion generation at cathode surface, the generation increasing with applied voltage. The pH of catholyte drastically increased from 2 to 8 in the ninth hour of operation of cell. The sudden jump in pH of catholyte is due to decrease in eluant concentration in anode compartment, which resulted in concentration polarisation in the electrodialysis cell.

To avoid concentration polarisation, the anolyte and catholyte were changed regularly for every 8 hours of operation. The onset of concentration polarisation resulted in high voltage drop across the cell, which further increased the electrode reactions. The rapid generation of hydroxyl ions at the cathode surface resulted in the sudden jump of pH from acidic to alkaline.

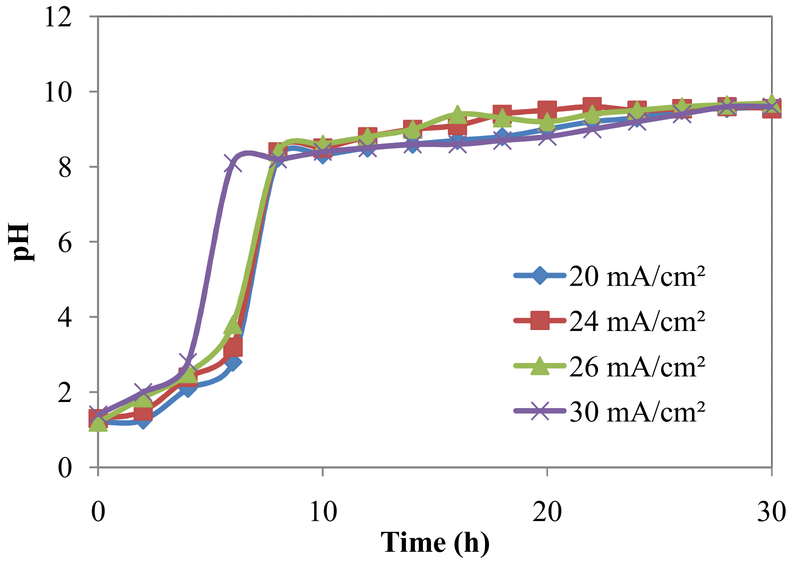

Figure 5.9 Catholyte pH for different current densities

5.9.3. Effect of eluant concentration

As discussed in section 4.3, the limiting current density increases with increase in eluant concentration. Thus high eluant concentrations enable EDIX operation at high current densities. The effect of eluant concentration on recovery of Cs from AMP-PAN was studied for two current densities, 20 mA/cm^2 and 40 mA/cm^2. Eluant concentrations of 0.27, 0.7 and 1.35 M were passed as anolyte at constant current density of 20 mA/cm^2. Effect of eluant concentrations of 1, 2 and 3 M $(NH_4)_2SO_4$ were studied at a higher current density of 40 mA/cm^2.

It was observed from Figure 5.10 that with increase in eluant concentration from 0.27 to 1.35 M $(NH_4)_2SO_4$ in the anode compartment, the transport of cesium by migration from AMP-PAN to the cathode compartment increased with time. As the eluant was recycling in the anode compartment, decrease in the concentration of the regenerative ions (NH_4^+) was observed with time. After eight hours of operation cesium elution was observed very low and hence the eluant was changed for every eight hours.

With increasing the eluant concentration from 0.27 to 1.35 M, the total recovery percentage increased from 42 to 62.35 % within 30 h of operation as shown in

Figure 5.11. As observed for different current densities, only 10 % of the total recovered was obtained in the last 15 h of operation.

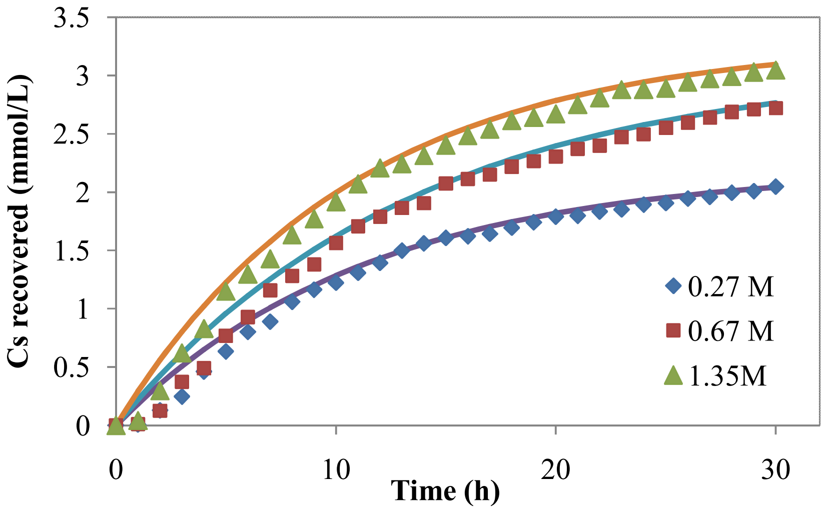

Figure 5.10 Cs recovered in catholyte for different eluant concentrations
current density = 20 mA/cm^2, loading capacity ≃ 30 mg/g

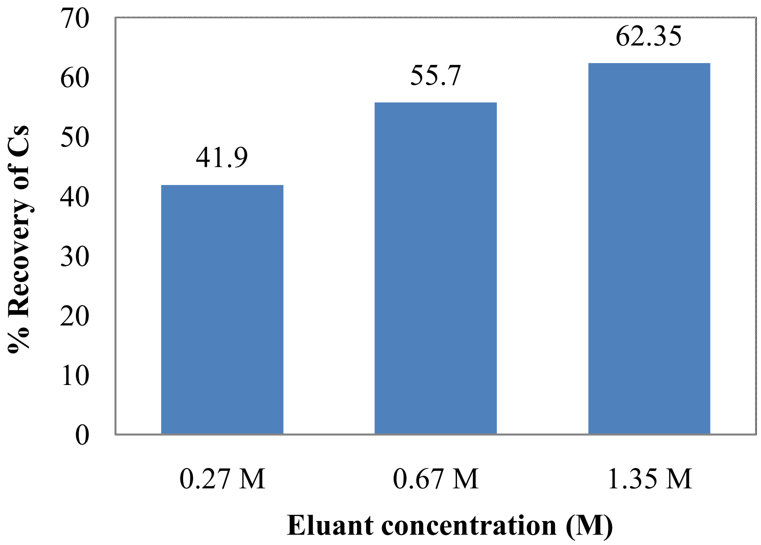

Figure 5.11 Percentage recovery of Cs for different eluant concentration

For a current density of 40 mA/cm^2 and different eluant concentrations (1, 2 and 3 M $(NH_4)_2SO_4$), the Cs recovery with time is shown in Figure 5.12. The concentration of Cs in catholyte increased from 2.2 to 3.22 mmol/L with increase in eluant concentration from 1 to 2 M and further increase in concentration decreased the Cs concentration to 2.32 mmol/L.

As shown in Figure 5.13, the recovery of Cs increased from 52.25 to 64.92 % with increase in eluant concentration from 1 to 2 M within 15 h of operation. Further increase in concentration resulted in lower recovery of about 49 %, which is less than that of 1 M eluant concentration. The incomplete dissociation of salt at higher concentration (3 M) resulted in a high voltage drop, which had increased the secondary reactions at the electrodes. The generation of protons at the anode might have decreased the recovery of Cs from the resin.

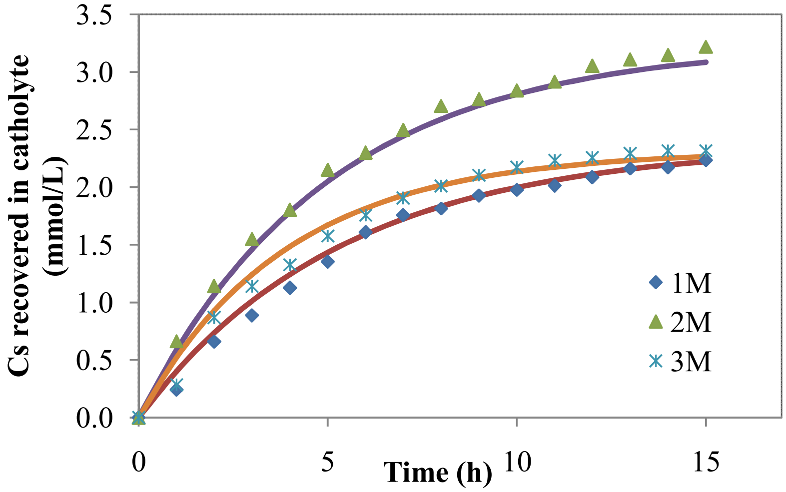

Figure 5.12 Cs recovered in catholyte for different eluant concentrations
current density = 40 mA/cm^2, loading capacity ≃ 30 mg/g

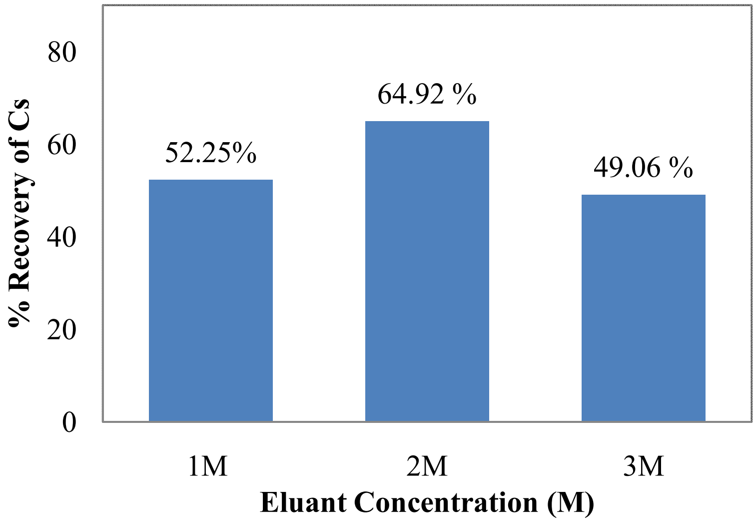

Figure 5.13 Percentage recovery of Cs for different eluant concentration
current density =40mA/cm^2

The migration diffusion coefficients of Cs were calculated for different eluant concentrations using Nernst-Planck equation and the determined values are presented in Table 5.4 and 5.5. The determined diffusion coefficients were found to increase with increase in eluant concentration for different current densities up to 2 M and further increase in eluant concentration up to 3 M resulted in a lower diffusion coefficient.

Table 5.4 Effective diffusion coefficients of Cs of migration for different eluant concentrations at current density of 20 mA/cm^2

Eluant conc. (M)	**n_{max} (moles)**	**grad$\emptyset$ (V/m)**	**$K_m \times 10^{-5}$ (s^{-1})**	**$D_{eff} \times 10^{-9}$ (m^2/s)**
0.27	2.08	800	2.314	0.929
0.675	2.72	780	2.057	1.11
1.35	3.04	750	2.579	1.62

Table 5.5 Effective diffusion coefficients of Cs migration for different eluant concentrations at current density of 40 mA/cm^2

Eluant conc. (M)	**n_{max} (moles)**	**grad$\emptyset$ (V/m)**	**$k_m \times 10^{-5}$ (s^{-1})**	**$D_{eff} \times 10^{-9}$ (m^2/s)**
1	2.42	740	4.82	2.41
2	3.35	640	5.48	4.35
3	2.45	840	5.91	2.66

5.10. Study of process parameters in Mode-II

5.10.1. Effect of current density

In an electrochemical separation process, current density plays a vital role. In the present EDIX process, application of current across the cell results in the migration of anions and cations through the middle compartment towards anode and cathode, respectively. The eluant containing 10000 ppm NH_4^+ flowing in the middle compartment replaces the cesium ions on the AMP-PAN resin, when it comes in contact with the resin. Some part of the total eluted cesium from the resin migrates towards the cathode compartment under the applied current and the remaining is convected by the eluant flowing through the middle compartment on once through basis. The recovery of cesium from cesium sorbed AMP-PAN was determined at different current densities ranging from 20 mA/cm^2 to 60 mA/cm^2. The amount of cesium recovered with time from the middle and cathode compartments was shown in Figure 5.14 and 5.15 for different current densities.

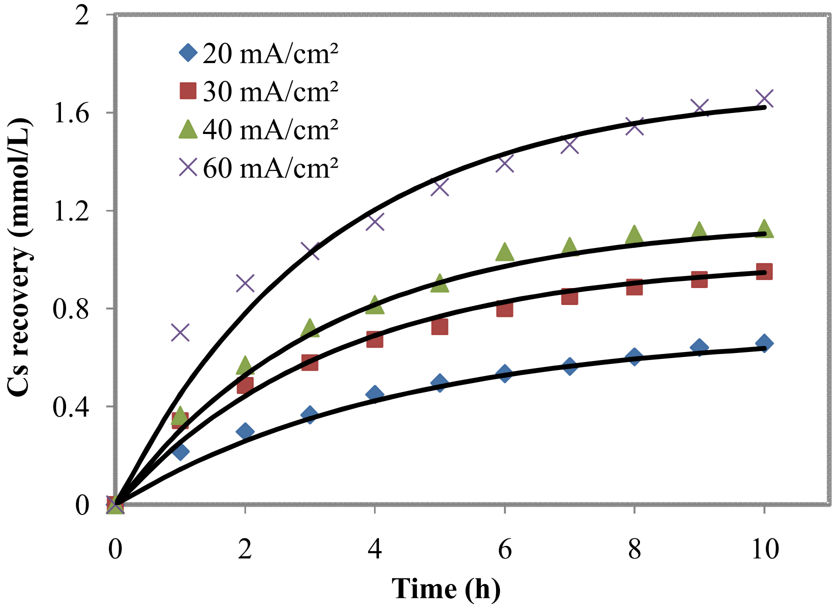

Figure 5.14 Cs recovered by migration for different current densities
NH_4^+ =0.27M

From Figure 5.14 it can be seen that migration of cesium to the cathode compartment increased with increase in the current density from 20 to 60 mA/cm^2, due to increased ion movement. The migrated cesium was about 0.6 millimoles for 20 mA/cm^2 and it increased to more than 1.6 millimoles for 60 mA/cm^2 in 10 h of operation.

From Figure 5.15, it can be seen that the total cesium convected by the eluant through the middle compartment decreased with increase in the current density. Increase in migration rate at higher current densities decreased the convection of cesium ions by the eluant. After 10 h of operation, both cesium migration and convection were found to be negligible.

As the middle compartment was separated from the anode compartment with an anion exchange membrane, which restricts the migration of cations towards anode, negligible amounts of cesium were found in the anode compartment.The total amount of cesium recovered along with the recovery from individual compartments is shown in Figure 5.16.

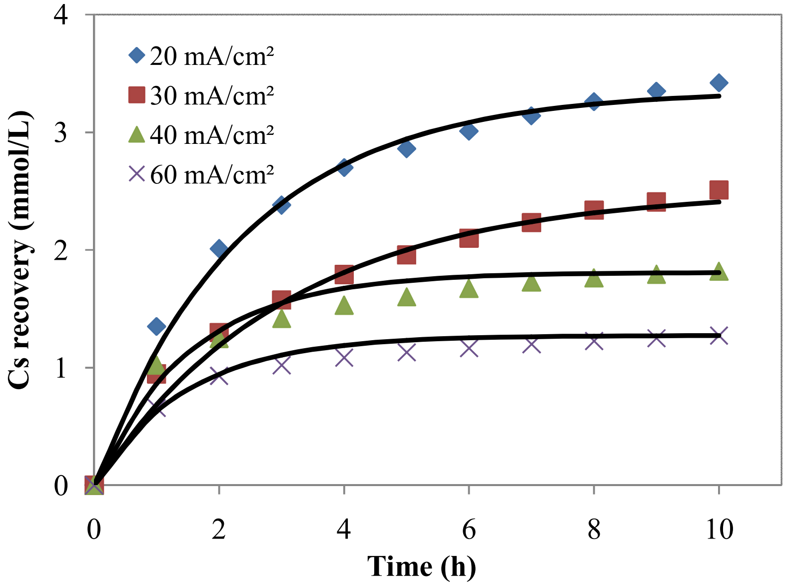

Figure 5.15 Cs recovered by convection for different current densities $NH_4^+ = 0.27M$

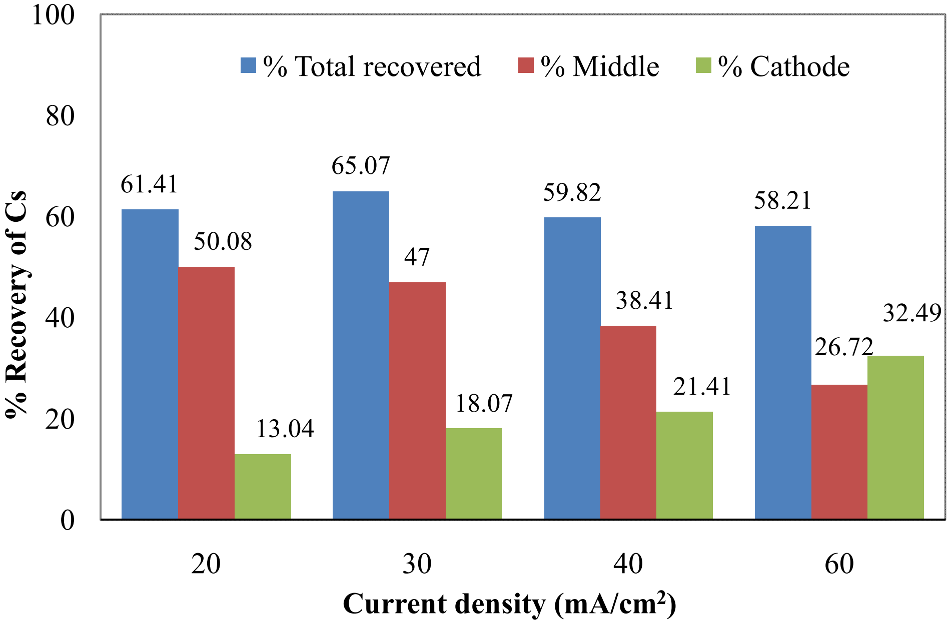

Figure 5.16 Total percentage of cesium recovered from all compartments for different current densities $NH_4^+ = 0.27$ M

With increasing current density from 20 mA/cm^2 to 30 mA/cm^2, the total recovery of cesium increased from 61.41 to 64.07% and further increase in current density from 40 to 60 mA/cm^2 resulted in decrease of recovery. Even though migration of cesium increased from 13.04 to 32.49 % with increase in current density, total recovery decreased.

In electromembrane processes, water splitting results in H^+ and OH^- formation, at the bipolar interface of the cation exchange resin and the anion ion exchange membrane. Water splitting is more intensive at the anion-exchange membrane [174]. The generation of H^+ at the anion ion exchange membrane increased the eluant conductivity as shown in Figure 5.17 after one hour of operation.

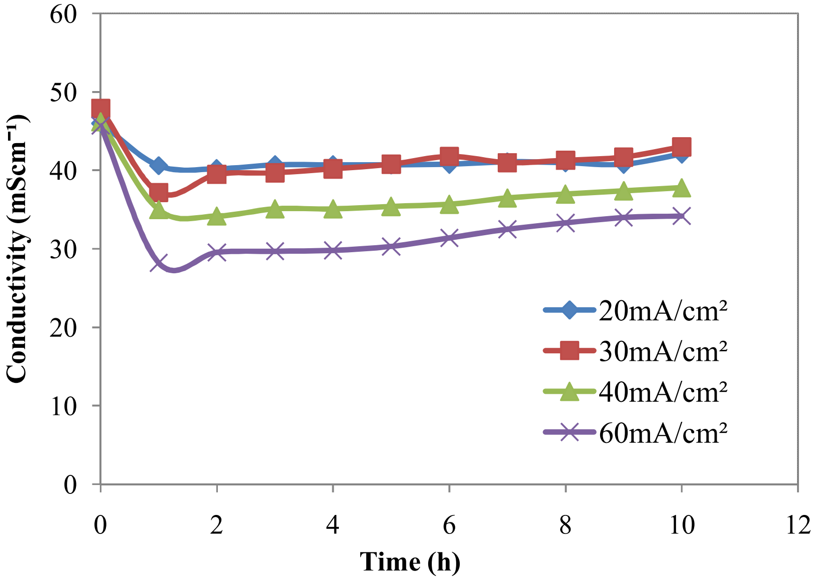

Figure 5.17 Variation of eluant conductivity for different current densities
NH_4^+ = 0.27 M

Since AMP-PAN is highly selective for Cs^+ in acidic medium and regeneration of the resin is possible only in alkaline medium, increase in H^+ ions in the eluant might have reduced the desorption of Cs from the resin. This resulted in decrease in total recovery at higher current densities. The increased presence of H^+ ions in the eluant increased the bed conductivity and consequently potential gradient over the bed decreased at higher current densities with time. This is also evident from the increase in voltage drop across the cell with increase in current densities (Figure 5.18). At any given current density, the cell voltage decreased slowly with increase in time of operation, the drop being more pronounced at higher current densities as shown in Figure 5.18. The secondary reactions at the anode and cathode result in the generation of H^+ and OH^- ions, respectively whose mobility is 5 to 10 times greater than that of salt ions. The generation of these ions resulted in the increase of anolyte and decrease of catholyte conductivities as shown in Figures 5.19 and 5.20.

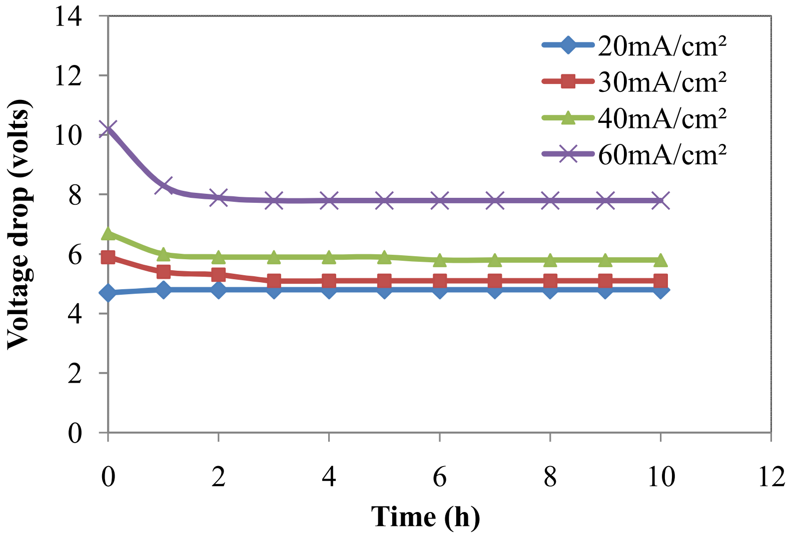

Figure 5.18 Variation of voltage drop for different current densities
$NH_4^+ = 0.27M$

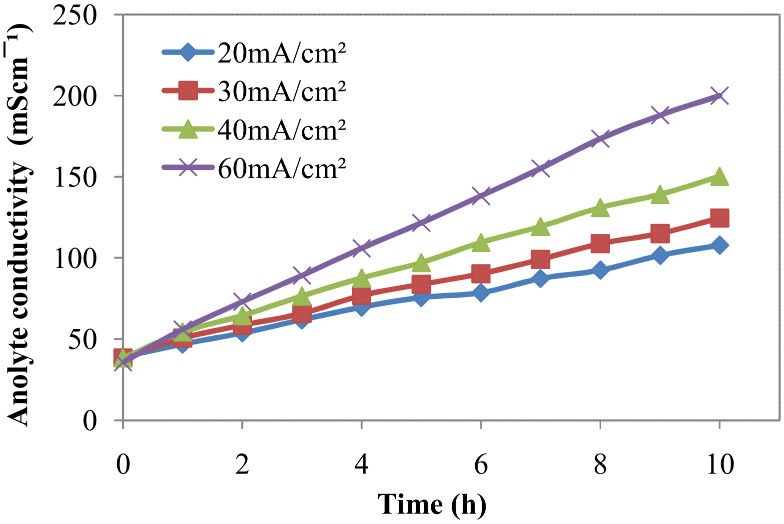

Figure 5.19 Variation of anolyte conductivity for different current densities
$NH_4^+ = 0.27M$

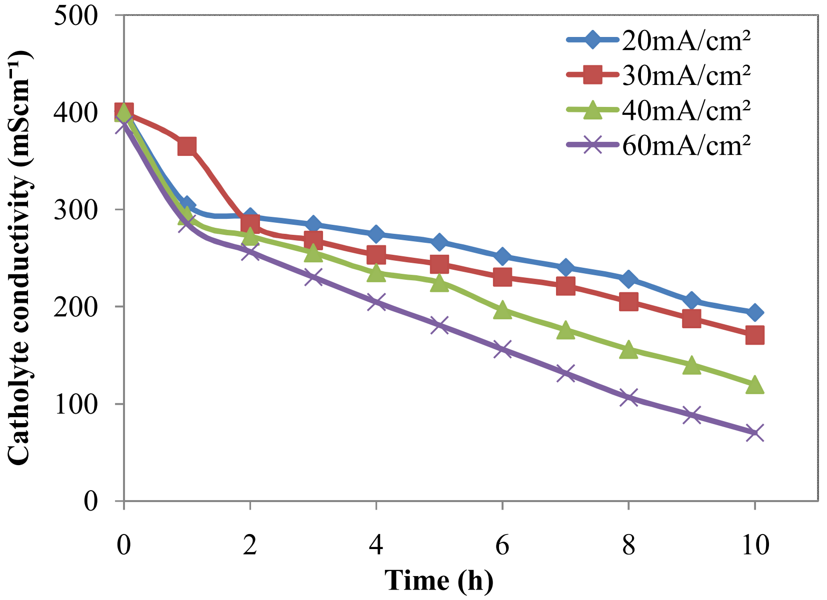

Figure 5.20 Variation of catholyte conductivity for different current densities
$NH_4^+ = 0.27M$

The migration diffusion coefficients of Cs were calculated for different current densities using equation 5.8 and the determined values are presented in Table 5.6. The determined diffusion coefficients were found to increase with increase in current densities up to 40 mA/cm^2 and further increase in current density decreased the diffusion as well as the mass transfer coefficients.

Table 5.6 Effective diffusion coefficients of Cs migration for different current densities

Current density (mA/cm^2)	**n_{max} (moles)**	**k_m X 10^{-5} (s^{-1})**	**grad∅ (V/m)**	**D_{eff} X 10^{-9} (m^2/s)**
20	0.71	6.313	600	1.002
30	1	8.145	800	1.135
40	1.16	8.443	1000	1.407
60	1.7	8.547	1680	1.262

The EDIX performance can be evaluated in terms of Cs$^+$ recovery in the catholyte and (ii) current efficiency yields of Cs$^+$ ions. The EDIX process for Cs recovery from AMP-PAN was effectively assessed by the difference between the initial and final concentration of cesium in the resin. On the other hand, the ratio of the quantity of cesium transferred to the cathode compartment and the charge passed during electrodialysis taking into account Faraday's constant, expresses the efficiency of cesium transport induced by the electrical field.

$$\mathbf{CE_{Cs+}^{catode}} = \frac{\mathbf{z_{Cu}\ F\ n_{Cs+}^{cathode}}}{\mathbf{Q}} \qquad \mathbf{(5.12)}$$

where, $n_{Cs+}^{cathode}$ is the number of moles Cs species in the cathode compartment and Q the electrical charge passed in the circuit at time t. For the present case of constant current operations, the electrical charge is given by: Q= I x dt.

As seen from the Fig. 5.21, the current efficiency was highest during the first hour of operation of the cell and later on it was decreasing with time for all the current densities studied. The initial current efficiency decreased from 23 % to 20% with decreasing applied current density from 60 to 20 mA/cm^2.

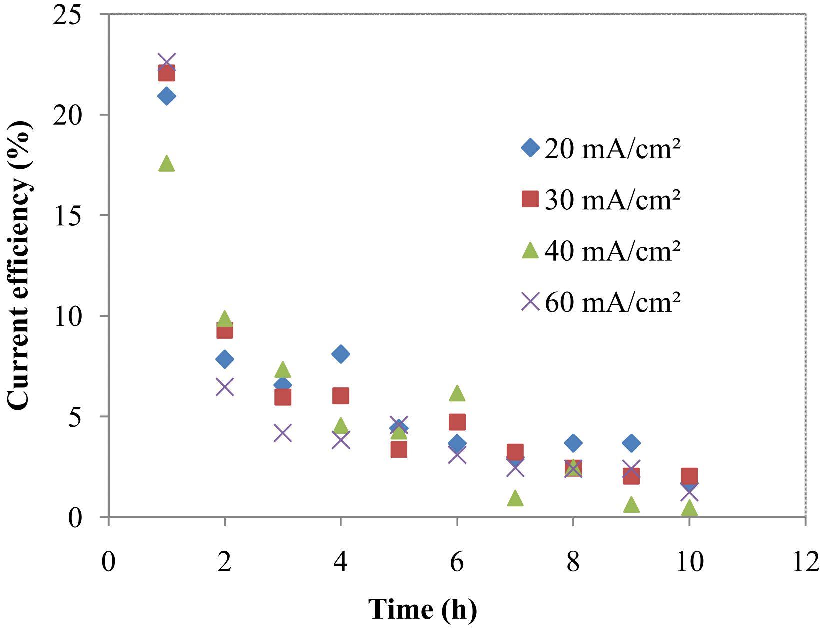

Figure 5.21 Variation of current efficiency with time for different current densities

5.10.2. Effect of eluant concentration

The recovery of cesium from AMP-PAN was investigated for different eluant concentrations at constant current density of 40 mA/cm^2. The concentration of eluant passing through the ion exchange resin in the middle compartment was varied from 1000 ppm to 25000 ppm. On application of current, the migration of cesium ions towards cathode was shown in Figure 5.22 for different eluant concentrations.

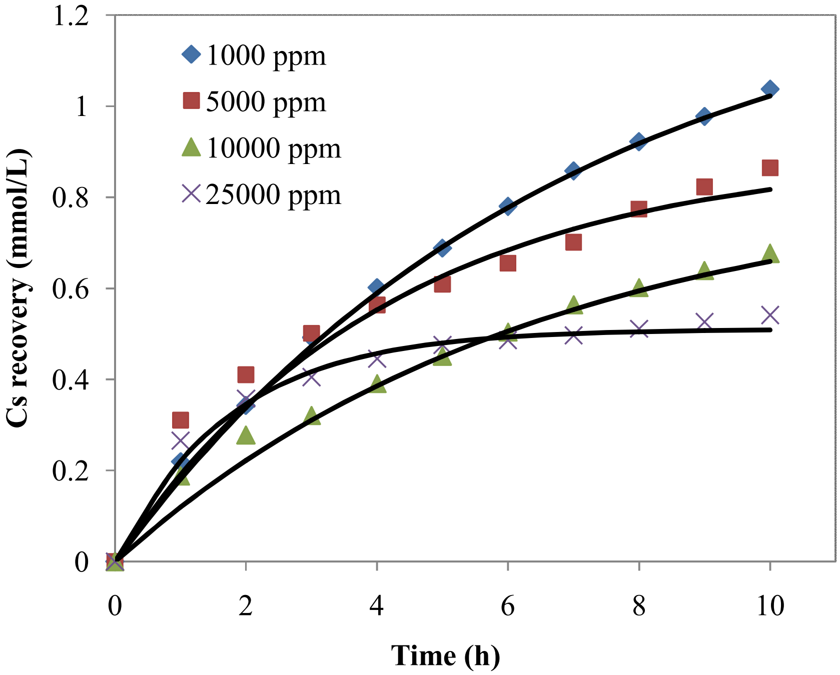

Figure 5.22 Cs recovered by migration for different eluant concentrations
Current density = 20mA/cm^2

Cs concentration in catholyte slowly increased with time when 1000, 5000 and 10000 ppm solutions were used. For 25000 ppm solution, negligible migration was observed after 4h. The total Cs recovered by migration decreased from 1.02 to 0.54 mmoles in 10 h of operation, when the eluant concentration increased from 1000 to 25000 ppm. The migration of cesium from the central compartment to the cathode compartment depends on the applied current and the available membrane area. When high eluant concentrations were used to recover the sorbed Cs from AMP-PAN, high concentration gradients led to more elution of Cs ions from the ion exchange resin. Since constant current is applied, out of these only a few ions were able to migrate and the remaining ions would be convected by the eluant flowing through the middle compartment. For low concentration of eluant (1000 ppm), the eluted ions were also low in quantity and most of them migrated due to the applied current.

“Porous-Plug” model [175-177] explains the passage of electric current through ion exchange media in terms of three different paths, viz., alternating layers of ion exchange resin and interstitial solution, the bridge connecting the ion exchange resin beads which are in contact with each other, and the channel through the interstitial solution. At low eluant concentrations, the conductivity of the solution is low and conductivity of the solid is high. Hence the preferred path for electric current is through the ion exchange resin and across the cation exchange membrane into the catholyte. Thus it results in high migration and low convection. As the concentration of the eluant increases, the roles are reversed and convection is preferred to migration. Also, it can be seen that increased eluant concentration increases the overall Cs recovery, as expected.

The amount of cesium recovered by convection from the middle compartment increased with increase in the eluant concentration from 5000 to 25000 ppm as shown in Figure 5.23. It reached equilibrium within 5h and subsequently no more cesium was convected from the middle compartment.

As observed from Figure 5.23, around 2.5 millimoles of cesium were recovered from the middle compartment outlet (by convection) in the first one hour and totally 3.5 millimoles were recovered at the end of 10 h, when 25000 ppm eluant was used for recovery of cesium. A negligible amount of cesium was observed in the outlet of the central compartment when 1000 ppm NH_4^+ was passed through the ion exchange resin, as most of the Cs was recovered by migration only. The overall percentage recovery of cesium from different compartments of the electrodialysis setup is shown in Figure 5.24. The total recovery increased from 21.77 to 77.58 % with increase in the eluant concentration from 1000 to 25000 ppm. For 1000 ppm, most of the total recovery is by migration and for 25000 ppm it was by convection. Increasing the eluant solution concentration enhanced the convection term in the Nernst-Plank equation, thus reducing the migration of Cs ions to cathode compartment.

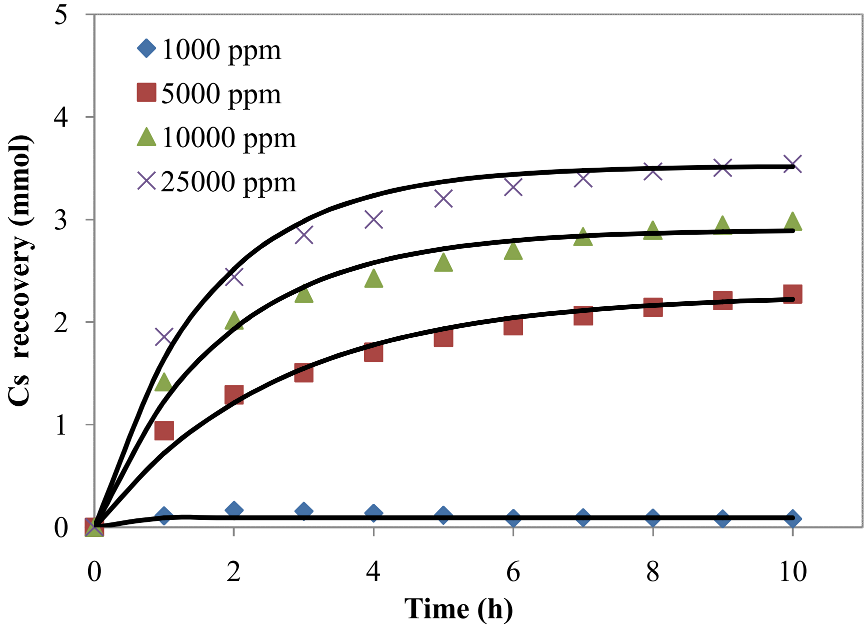

Figure 5.23 Cs recovered by convection for different eluant concentrations
Current density =20 mA/cm^2

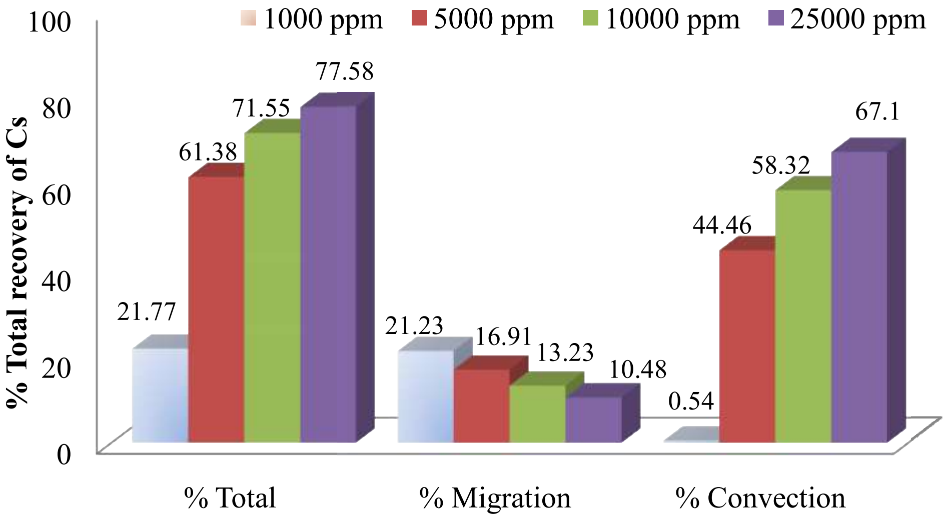

Figure 5.24 Cs recovered by convection for different eluant concentrations
Current density =20mA/cm^2

The diffusion coefficients were estimated from the data on migration of cesium with the help of equation 5.8. The migration diffusion coefficient was found to be the least for 1000 ppm (Table 5.7) in spite of its high % migration, as shown in Figure 5.24. The diffusion and mass transfer coefficients increased with increase in eluant concentration from 1000 to 25000 ppm.

Table 5.7 Effective diffusion coefficients of Cs migration for different eluant concentrations

Eluant conc. (mg/L)	n_{max} (moles)	$k_m \times 10^{-5}$ (s^{-1})	gradØ (V/m)	$D_{eff} \times 10^{-9}$ (m^2/s)
1000	1.31	4.067	2320	0.312
5000	0.89	6.944	840	0.973
10000	0.74	6.613	680	0.965
25000	0.52	13.888	660	1.443

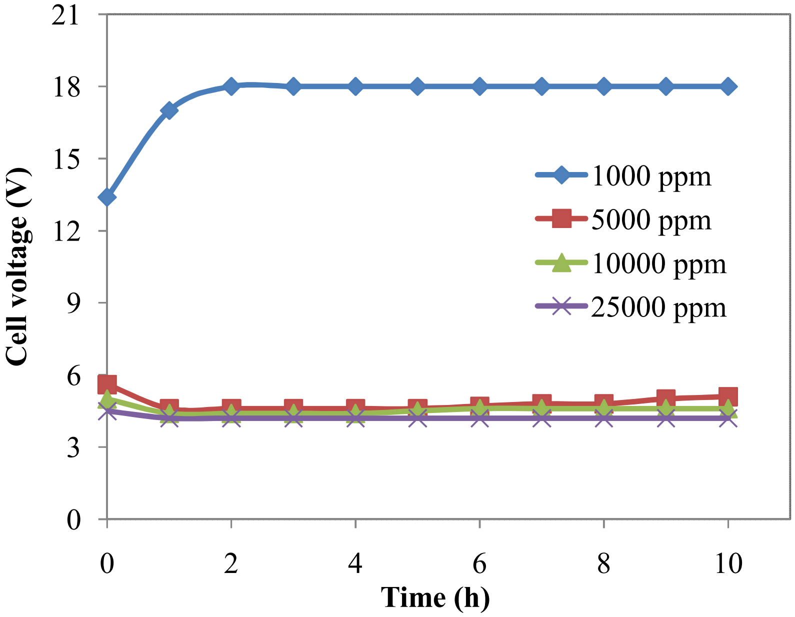

Figure 5.25 Cell voltage for different eluant concentrations
current density = 20 mA/cm^2

Figure 5.25 shows the cell voltage as a function of time for different eluant concentrations. A high voltage drop in case of 1000 ppm eluant resulted in a low diffusion coefficient. Low eluant concentration resulted in low conductivity of the compartment which had increased the resistance of the compartment. The high resistance at low eluant concentration resulted in high voltage drop across the packed bed. Increase in bed potential drop might have decreased the migration diffusion coefficient of Cs at low eluant concentration. Similar is the case for mass transfer coefficients.

5.10.3. Effect of catholyte concentration

Dilute acids or salts are used as electrolytes in electrodialysis systems. In the present investigation of ED for recovery of Cs from AMP-PAN, HNO_3 was used both as anolyte and catholyte. Since Cs was recovered in catholyte, the effect of concentration of catholyte is studied by varying the concentration from 0.1N to 1N, keeping the other parameters constant. The amount of Cs recovered by migration for different catholyte concentrations was shown in Figure 5.26. The rate of migration of Cs marginally increased with increase in concentration of catholyte. At the end of 10 h, almost 0.7 millimoles of Cs were recovered by migration for all the catholyte concentrations studied.

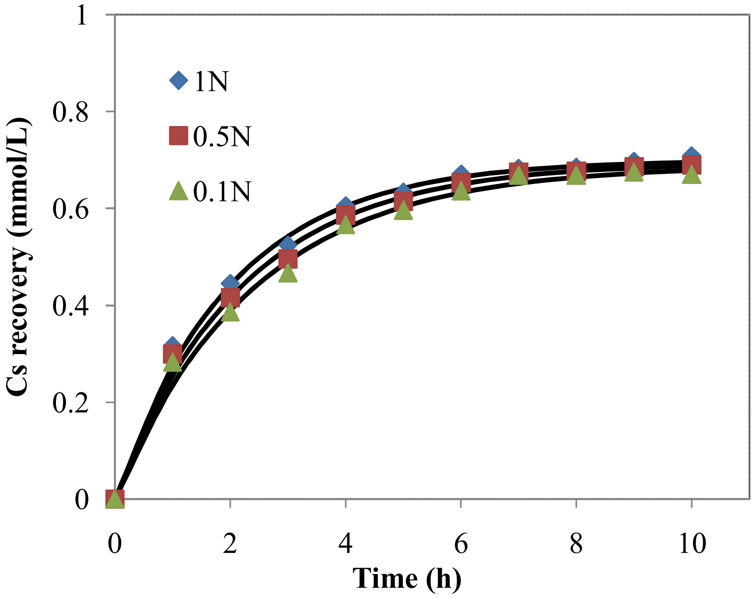

Figure 5.26 Recovery of Cs by migration for different catholyte concentrations
current density =20 mA/cm^2, NH_4^+ =10000 ppm

The Cs convected from the middle compartment by the eluant was found to increase slightly with increase in catholyte concentration as can be seen from Figure 5.27.

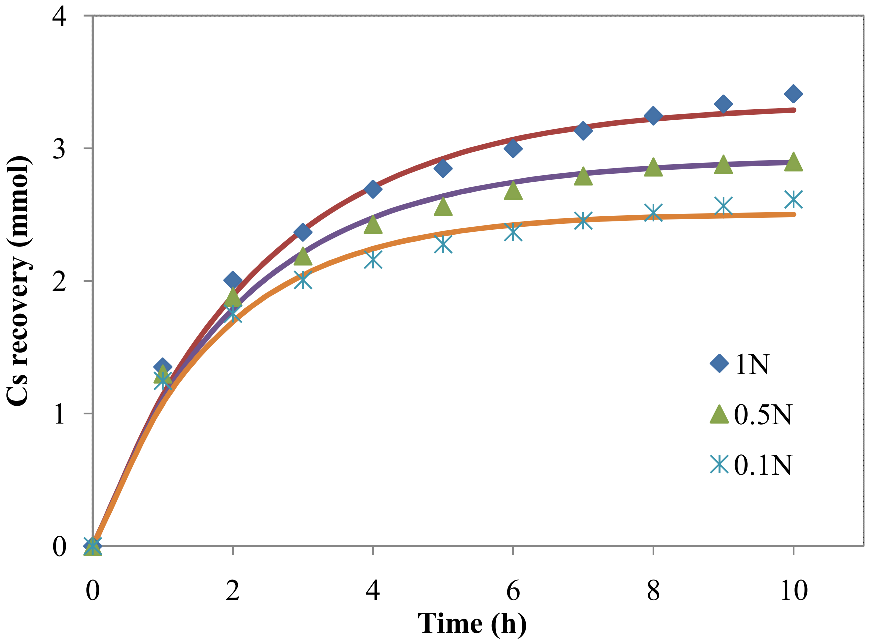

Figure 5.27 Recovery of Cs by convection for different catholyte concentration
current density =20 mA/cm^2, NH_4^+ = 0.27 M

The total recovery from all the compartments increased from 66.28 to 72.44 % with increase in catholyte concentration from 0.1 N to 1N (Figure 5.28). It was observed that as catholyte concentration was increased from 0.1 to 1N, the initial cell voltage decreased from 6 to 5.6 V, which is due to increase in the conductivity of catholyte. The decrease in cell voltage might have reduced the secondary reactions such as water splitting at the bipolar interface and water dissociation at the electrode surface. This would have resulted in the increase of Cs recovery, when catholyte concentration was increased. Moreover acidic catholyte reduces the precipitation of salts on the cathode surface apart from increasing the cesium recovery from AMP-PAN. The percentage of cesium recovered by migration was not significant with increase in the catholyte concentration which confirms the acidic nature of catholyte is just to keep the cathode compartment conductive and reduce salt precipitation.

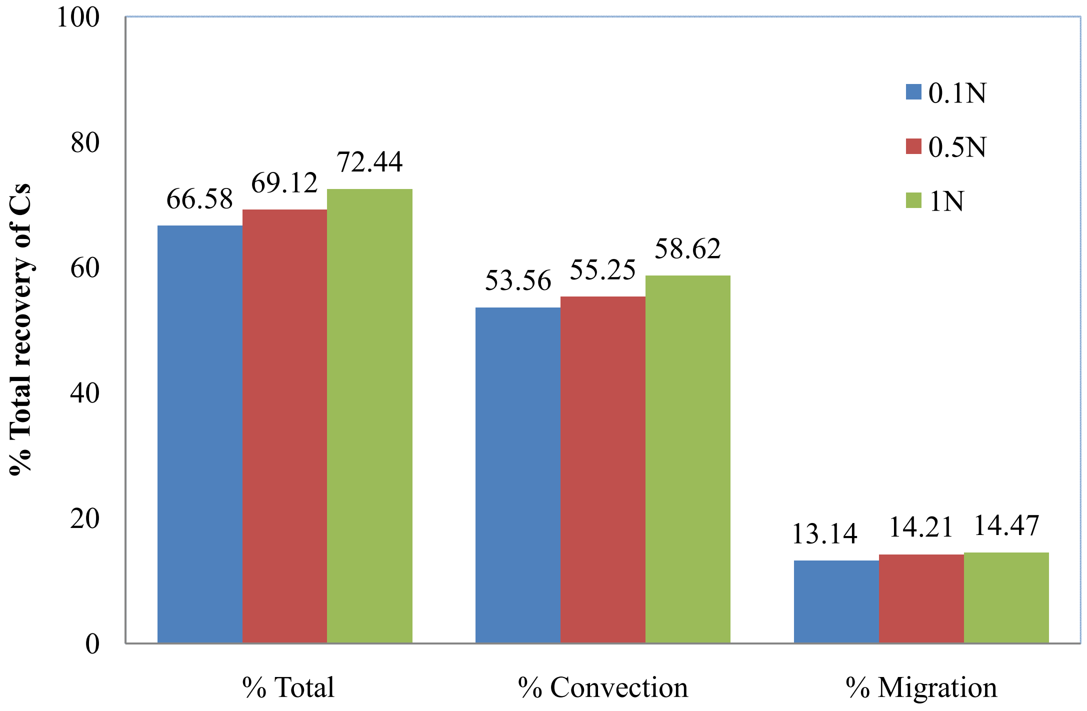

Figure 5.28 Percentage recovery of Cs for different catholyte concentrations
current density =20 mA/cm^2, NH_4^+ =0.27M

The migration diffusion coefficients were determined for cesium and tabulated in Table 5.8. The diffusion and mass transfer coefficients were found to be the increasing with increase in catholyte concentration from 0.1 to 1N due to decrease in the voltage drop across the cell.

Table 5.8 Effective diffusion coefficients of Cs migration for different catolyte concentrations

Catholyte conc. (N)	**n_{max} (moles)**	**k_m x10^{-5} (s^{-1})**	**gradØ (V/m)**	**D_{eff} x10^{-9} (m^2/s)**
0.1	2.61	11.6	680	6.43
0.5	2.9	12.7	640	8.31
1	3.41	13.8	600	11.3

5.11. Conclusions

Investigations were carried out for recovery of cesium from cesium loaded AMP-PAN, using a hybrid Electrodialysis-Ion exchange system. The eluant was passed as anolyte in mode-I and through a bed of AMP-PAN loaded in the central compartment in mode-II operation of an electrodialysis cell. Cs recovery from the system occurred in two ways, by migration into cathode compartment under the influence of applied voltage and by convection of Cs by the eluant through the central compartment. Effect of the operating parameters on the recovery of cesium by both the ways is experimentally determined and using Nernst Plank equation, diffusivities of cesium were estimated.

In mode-I, cesium recovery increased with increase in current density and eluant concentration. High recovery was observed for a low loading capacity of the resin. More than 84 % recovery was observed for 8.83 mg/g loading of AMP-PAN. Negligible recovery of Cs was observed with by convection.

In the second mode of operation, total recovery of cesium increased with increase in current density from 20 to 30 mA/cm^2, but decreased when current density is increased to 40 and 60 mA/cm^2, due to water splitting reactions. Current efficiencies increased with increase in current density within limiting current range. For an applied current density current efficiency decreased with time. Total recovery increased with eluant concentration, due to better elution, whereas increase in the catholyte concentration did not have a significant effect on the recovery. Recovery by convection decreased with the increase in current density, whereas it increased significantly with eluant concentration and slightly with catholyte concentration. Recovery by migration, which is the desirable phenomenon, increased with current density and decreased with increase in eluant concentration, whereas increase in the catholyte concentration did not have a significant effect. The maximum recovery of cesium obtained by migration in the present work is

32.49 % for 10 hours operation for a current density of 60 mA/cm^2, eluant concentration of 10000 ppm of NH_4^+ and catholyte of 0.1 N HNO_3.This corresponds to a total recovery of 58.21 % and hence more than half of the total recovery is by migration, which results in a stream with very low concentration of ammonia.

Summary and conclusions 6

This chapter summarizes the results of the studies aimed at the development of Electrodialysis-Ion exchange process for separation of cesium from simulated HLW using AMP-PAN. Application of AMP-PAN for cesium removal from HLW and investigation of EDIX for recovery of Cs in pure form from AMP-PAN were studied. The summary of results is presented in this chapter.

6.1. Scope of Cs recovery from AMP-PAN using EDIX

To separate Cs from HLW, AMP-PAN was selected because of its high affinity for Cs in acidic medium. Cs from simulated HLW was trapped by AMP-PAN and the trapped Cs from AMP-PAN was recovered by a hybrid Electrodialysis-Ion exchange system.

Equilibrium studies using simulated HLW showed high distribution of Cs compared to other ions on AMP-PAN. No significant effect on the selectivity of Cs was observed with change in the acidity of the simulated waste. Langmuir model was found to fit the equilibrium data well. The kinetics of Cs on AMP-PAN was explained well by pseudo second order model and both film and particle diffusions were found to be the controlling factors.

Dynamic sorption of Cs on AMP-PAN was studied for different operating conditions. Important parameters in column operations like breakthrough, mass transfer zone, bed saturation, rate of mass transfer zone, etc. were analyzed for different operating parameters like influent concentration, feed flow rate and bed height. Different mathematical models were applied for predicting the breakthrough and among them; Thomas and Yoon-Nelson models were able to predict the breakthrough well.

Recovery of Cs from AMP-PAN was investigated in an electrodialysis setup consisting of three compartments; cesium sorbed AMP-PAN loaded in the middle compartment was separated from the anode and cathode compartments by ion exchange membranes. Ammonium sulphate was used as eluant for the regeneration of AMP-PAN.

The limiting currents for different operating conditions were determined from current-voltage characteristics of the setup. The effects of electrolytes' flow rates and concentration of the eluant on current-voltage characteristics were determined. An empirical equation for the limiting currents as a function of electrolytes' flow rates and eluant concentration was also suggested. Increase in electrolytes' flow rates and eluant concentration increased the limiting currents.

Two modes of operation of the electrodialysis cell were studied. In the first mode, eluant was passed as anolyte and dilute HNO_3 was circulated in the middle compartment containing AMP-PAN to keep the resin in acidic form. The other catholyte compartment was also circulated with dilute HNO_3 to avoid any precipitation on cathode surface. In the second mode, both anode and cathode compartments were circulated with dilute HNO_3 separately and eluant was passed once through the resin filled in the middle compartment of the electrodialysis cell.

In mode-I, on application of potential the ammonium ions from the anode compartment migrate towards cathode through the middle compartment where they exchange with cesium ions on the resin and the exchanged cesium ions migrate towards cathode to get concentrated. In mode-II, ammonium ions elute the cesium ions from resin which migrate towards cathode and get concentrated in catholyte. In this mode of operation, Cs recovery from the system occurred in two ways, by migration into cathode compartment under the influence of applied voltage and by convection of eluant through the central compartment. In both modes of operation, some ammonium was also migrating along with Cs towards cathode which will convert to ammonia gas form due the generation of hydroxyl ions at the cathode surface.

Cesium recovery from AMP-PAN in the electrodialysis setup was studied for different operating parameters like current density, eluant concentration and loading capacities. Cesium recovery by migration is dominant in the first mode and convection is dominant in the second mode of operation. Cs recovered by migration would result in pure form of Cs without ammonium ions whereas the convected portion is a diluted ammonium solution containing Cs.

In the first mode of operation, cesium recovery by migration increased with time for all the studied parameters and recovery increased with increasing the current density and eluant concentration. Effect of the operating parameters on the recovery of cesium by both the ways is experimentally determined and using Nernst Plank equation, diffusivities of cesium were estimated.

In the second mode of operation, total recovery of cesium increased with increase in current density from 20 to 30 mA/cm^2, but decreased when current density is increased to 40 and 60 mA/cm^2, due to water splitting reactions at bipolar interfaces of anion exchange membrane and cation exchange resin. Total recovery increased with eluant concentration, due to better elution.

Recovery by convection decreased with the increase in current density, whereas it increased significantly with eluant concentration. Recovery by migration, which is the desirable phenomenon, increased with current density and decreased with increase in eluant concentration.

In both modes of operation, only 80 % of Cs could be recovered from the AMP-PAN. The recovered Cs solution contains Cs as well as ammonium ions. The hydroxyl ions generating at the cathode convert ammonium ions to ammonium hydroxide. Ammonium hydroxide is unstable and converts to ammonia gas in alkaline conditions.

6.2. Optimizing the parameters in the EDIX process

In mode-I, the limiting current density determines the current below which the cell should be operated. It depends on different parameters like cell design, electrolytes' flow rates and concentration, membrane properties, etc. It was observed that operating the cell at 80 % of LCD would be the optimum current. Increase in electrolytes' flow rates decrease the thickness of boundary layer adhering to the membrane surface. The middle compartment solution flow rate should be optimized to avoid bed expansion which had significant effect on the migration rate. In the present work, the optimum flow rate of middle compartment solution was between 20 and 100 mL/min. The eluant concentration is another factor to be optimized. Increase in the eluant concentration from 0.27 to 2 M increased the migration rate of Cs and further increase in concentration up to 3 M decreased the migration of Cs towards cathode. Increase in eluant concentration also increases the migration of ammonium ions as well along with Cs ions towards cathode. In order to reduce the ammonium migration to cathode as well as to increase recovery of Cs from AMP-PAN, the eluant concentration should be between 1 and 2 M. Even though high recovery rates were observed with decreasing the loading capacity of the ion exchange resin, it requires longer times of operation for complete removal which is not economical. Hence it was suggested to use full capacity of the resin and regenerate to the maximum possible extent within limited hours of operations. Since the Cs ion exchange on AMP-PAN is both film and particle diffusion controlled, complete regeneration requires longer times of operation.

In mode-II, increasing the current density and decreasing the eluant concentration favored the migration of Cs towards cathode. To minimize the convection of Cs by the eluant, the eluant concentration should be between 1000 to 5000 ppm and the operating current density should be 80 % of LCD. Acidity of catholyte is mainly to prevent the precipitation of salts on the electrode surface. However, the catholyte conductivity was decreasing with the generation of hydroxyl ions at the electrode surface. The generation of hydroxyl ions depends on the applied voltage and time of operation. In the present study, where the experiments were conducted up to 20 h and for the maximum voltage drop of about 10 V, 0.5 N HNO_3 of one liter was sufficient to keep the catholyte in acidic form.

6.3. Membrane and ion exchanger stability in EDIX

The continuous operation of the cell for longer hours up to 20 or 30 h resulted in heat dissipation which increased the solution temperature up to 50^oC. The ion exchange membranes were thermally stable up to 90^oC and chemically stable up to pH-10. Fouling of the membranes was observed when operating the cell beyond the limiting current density. AMP-PAN ion exchange resin was reported to be thermally stable up to 90^oC and chemically stable up to pH-9. The yellow colored AMP-PAN beads turned to white (due to dissolution of AMP), whenever over limiting currents were observed. Thus it resulted in better performance, when operated below limiting current or Ohmic region.

6.4. Scope of future studies

The observations from present work were that Cs can be separated from HLW preferentially using AMP-PAN and the sorbed Cs from the AMP-PAN could be recovered using EDIX. Only 80 % of the sorbed Cs could be recovered due to the high affinity of AMP-PAN for Cs and the recovered Cs is in pure form. The unrecovered Cs can be removed from the AMP-PAN by dissolving it in the alkaline medium and the obtained Cs can be converted to acid form which again can be loaded on a fresh AMP-

PAN. If the cycle continues, the amount of Cs recovered from HLW will be quite high with efficiencies >90%.

Investigation of other ion exchangers like zirconium phosphate which can be regenerated with H^+ ions to exploit the advantage of EDIX where H^+ and OH^- are generated in the cell without using acids for regeneration. Resorcinol formaldehyde which is selective for Cs in alkaline condition can also be studied for Cs recovery from alkaline waste using EDIX. The present work was done using simulated and inactive waste. The process can be demonstrated with actual HLW, after ensuring radiological procedures.

In the second mode of operation, the eluted Cs was convected by the eluant due to insufficient area or time for migration. This can be improved by increasing the residence time or increasing the membrane area of the cell. Only one side of the electrode surface was exploited for the operation. Instead of rectangular cell, employing an annular cell would improve the process efficiency. Various possibilities of cell design can also be studied for improving the kinetics of the process.

References

1. Load Generation Balance Report 2013–14 Central Electricity Authorities, Ministry of Power, and Government of India.
2. http://yearbook.enerdata.net/world-electricity-production-map-graph-and-data-in-2010.html.
3. http://www.tsp-data-portal.org/TOP-20-Generation#tspQvChart.
4. http://powermin.nic.in/power-sector-glance-all-india.
5. Integrated Energy Policy 2006 Report of the Expert Committee, Planning Commission, Government of India.
6. S.K.Jain, Nuclear Power –An alternative, BHAVINI Report.
7. S.A, Bharadwaj, Indian nuclear power programme – Past, present and future. Sadhana, 2013. 38: p. 775-794.
8. P.K. Wattal, Indian programme on radioactive waste management. Sadhana, 2013. 38: p. 849-857.
9. A. Anil Kakodkar, Nuclear Power in India: An Inevitable Option for Sustainable Development of a Sixth Humanity, World Nuclear Association Annual. 2002.
10. http://www.world-nuclear.org/info/Nuclear-Fuel-Cycle/Fuel-Recycling/Processing-of-Used-Nuclear-Fuel/.
11. P.K, Dey. N.K. Bansal, Spent fuel reprocessing: A vital link in Indian nuclear power program. Nuclear Engineering and Design, 2006. 236: p. 723-729.
12. http://www.pnausa.org/harmony-todd/nuclear-101-spent-fuel-reprocessing.
13. Actinide and Fission Product Partitioning and Transmutation - Status and Assessment report,OECD-NEA(1999), http://www.nea.fr/pt/docs/1999/neastatus99/Phase1_report.html.

14. A Technology Roadmap for Generation IV Nuclear Energy Systems", U.S. DOE Nuclear Energy Research Advisory Committee at the Generation IV International Forum, GIF-002-00, 2002, http://gif.inel.gov/roadmap/.
15. http://www.igcar.gov.in/cg/fcg/ppss/pyro.htm.
16. J. Serpa, M. Allibert, A. L. Terrier, R.Malmbeck, M. Ougier, J. Rebizant, J.P.Glatz Electroseparation of Actinides from Lanthanides on Solid Aluminum Electrode in LiCl-KCl Eutectic Melts. Journal of the electrochemial society, 2005. 152: p. 167-172.
17. K. Raj, K.K. Prasad, N.K. Bansal, Radioactive waste management practices in India. Nuclear Engineering and Design, 2006. 236: p. 914-930.
18. Classificiation of radioactive waste, IAEA general standards, General safety guide, No.GSG-1. 2009, International Atomic Energy Agency: Vienna.
19. N. Kocherov, M. Lammer, O. Schwerer, Handbook of Nuclear Data for Safeguards," International Atomic Energy Agency, INDC(NDS)-376, December 1997.
20. Chernobyl: Assessment of Radiological and Health Impacts (OECD Nuclear Energy Agency, 2002).
21. M.P. Unterweger, D.D. Hoppes, F.J. Schima, New and revised half-life measurements results. Nucl. Instrum. Meth. Phys. Res., 1992. 312: p. 349-352.
22. A. F. Holleman, E. Wiberg, Inorganic Chemistry. 2001: Academic Press.
23. K. Buesseler, M. Aoyama, M. Fukasawa, Impacts of the Fukushima Nuclear Power Plants on Marine Radioactivity. Environmental science and technology, 2011. 45: p. 9931-9935.
24. J.A. Dean, Lange' s Handbook of Chemistry, 13th edn., McGraw-Hill, New York. 1985.

25. J.C. Fanning, The solubilities of the alkali metal salts and the precipitation of Cs^+ from aqueous solution. Coordination Chemistry Reviews, 1995. 140: p. 21-36.

26. H. Rogers, J. Bowers, D.G. Anderson, An isotope dilution–precipitation process for removing radioactive cesium from wastewater. J.Hazard. Mat., 2012. 243: p. 124–129.

27. P.K. Mohapatra, S.A.Ansari, A. Sarkar, A. Bhattacharyya, V.K. Manchanda, Evaluation of calix-crown ionophores for selective separation of radio–cesium from acidic nuclear waste solution. Anal. Chim. Acta, 2006. 571: p. 308–314.

28. J. Rais, P. Selucky, M. Kyrg, Extraction of Alkali-Metals into Nitrobenzene in Presence of Univalent Polyhedral Borate Anions. Journal of Inorganic Nuclear Chemistry Ar.. 1976. 38: p. 1376.

29. J. Rais, J. Plesek, P. Selucky, Extraction of Cesium with Derivatives of Carborane into Nitrobenzene. Journal of Radioanalytical and Nuclear Chemistry, 1991. 148: p. 349-357.

30. J. Rais, B. Gruner, Extraction with Metal Bis(dicarbollide) Anions. Ion Exchange Solvent Extraction, ed. A.K.S. Y. Marcus. Vol. 17. 2004, New York: Marcel Dekker.

31. B. Gruner, J. Plesek, J. Baca, J.F. Dozol, V. Lamare, I. Cisarova, M. Belohradsky, J. Caslavsky, Crown ether substituted cobalto bis(dicarbollide) ion as selective extraction agents for removal of Cs^+ and Sr^{2+} from nuclear waste. New J. Chemistry, 2002. 26: p. 867–875.

32. D. Naoufal, B. Gruner, P. Selucky, B. Bonnetot, H. Mongeot, Solvent extraction of radioactive Cs+ by hydroborate anionic extractants of the [1-LB10H9]-type (L=amine or phosphine). J. Radioanal. Nucl. Chem., 2005. 266: p. 145–148.

33. Z. Valentova, P. Vanura, E. Makrlik, Solvent extraction of cesium from water into nitrobenzene using hydrogen dicarbollylcobaltate in the presence of PEG 400. J. Radioanal. Nucl. Chem., 2005. 267: p. 237–239.

34. A.G. Vendilo, D.I. Djigailo, S.V. Smirnova, II. Torocheshnikova, K.I. Popov, V.G. Krasovsky, I.V. Pletnev, 18 crown-6 and dibenzo-18-crown-6 assisted extraction of cesium from water into room temperature ionic liquids and its correlation with stability constants for cesium complexes. Molecules, 2009. 14: p. 5001–5016.

35. E. Makrlik, P.Vanura, P. Salucky, Extraction of microamounts of cesium by hydrogen dicarbollylcobaltate in the presence of dibenzo-21-crown-7. J. Radioanal. Nucl. Chem., 2006. 267: p. 703–705.

36. E. Makrlik, P. Vanura, P. Selucky, Extraction of microamounts of cesium into nitrobenzene by using sodium, ammonium and thallium dicarbollylcobaltates in the presence of benzo-15-crown-5. J. Radioanal. Nucl. Chem., 2008. 278: p. 131–135.

37. R.J. Lewis, Hazardous Chemicals Desk Reference. 2nd ed. V.N. Reinhold. 1991, NewYork.

38. E. Blasius, K. H. Niles, The Removal of Cesium from Medium-Active Waste Solutions I. Evaluation of Crown-Ethers and Special Crown Ether Adducts in the Solvent Extraction of Cesium. Radiochim Acta, 1984. 35: p. 173-182.

39. J.W. McDowell, G. N. Case, Selective Extraction of Cesium from Acidic Nitrate Solutions with didodecylnaphthalenesulfonic acid synergized with bis(tert-butylbenzo)-21-crown-7. Anal. Chem., 1992. 64: p. 3013.

40. M.L. Dietz, E.P. Horwitz, S. Rhoads, R. A. Bartsch, J. Krzykawski, Extraction of Cesium from Acidic Nitrate Media Using Macrocyclic Polyethers: The Role of Organic Phase Water. Solvent Extraction and Ion Exchange, 1996. 14: p. 1-12.

41. M.L. Dietz, E.P. Horwitz, M.P. Jensen, S. Rhoads, R. A. Bartsch, A. Palka, J. Krzykawski, J. Nam, Substituent Effects in the Extraction of Cesium from Acidic Nitrate Media with Macrocyclic Polyethers. Solvent Extraction and Ion Exchange, 1996. 14: p. 357-384.

42. E.A. Filippov, E.G. Dzenkun, A.K. Nardova, I.V. Mamakin, V.M. Gelis, V.V. Mityutin, Application of Crown ethers and Ferrocyanide-Based Inorganic Material for Cesium and Strontium Recovery from High-Level Wastes. in Waste Management 1992. Tucson, Arizona.

43. Y. Du, W.J. Chen, S.Y. Qin, Extraction of cesium from the irradiated nuclear waste by 4(5),4 -Bis[1-hydroxyalkylbenzo]-21-crown-7. Chin. Chem. Lett., 2004. 15: p. 1219–1222.

44. T.G. Levitskaia, L. Maya, G.J. Van Berkel, B.A, Moyer,, Anion partitioning and ion-pairing behavior of anions in the extraction of cesium salts by 4,5-bis(tert-ctylbenzo)dibenzo-24-crown-8 in 1,2–dichloroethane. Inorg. Chem., 2007. 46: p. 261–272.

45. E. P. Horwitz, W. W. Schulz, Solvent Extraction in the Treatment of Acidic High-Level Liquid Waste:. in Where Do We Stand? Metal-Ion Separation and Preconcentration: Progress and Opportunities. 1999. Washington D.C. ACS Symposium Series 716.

46. G.R. Choppin, M. K. Khankhasayev, H. S. Plendl, Chemical Separations in Nuclear Waste Management, in Battelle Press 2002, DOE/EM-0591: Columbus OH.

47. J.F. Dozol, R. Ludwig, Extraction of Radioactive Elements by Calixarenes. Ion Exchange and Solvent Extraction, 2010. 19: p. 195–318.

48. J. F. Dozol, N.Simon, V.Lamare, H.Rouquette, S.Eymard, B.Tournois, D.Demarc, R.M. Macicas, A Solution for Cesium Removal from High-Salinity Acidic or Alkaline Liquid Waste: The Crown Calix[4]arenes. Separation Science and Technology, 1999. 34: p. 877-909.

49. J. Guillon, J.M. Leger, P. Sonnet, C. Jarry, M. Robba, Synthesis of cone, partial-cone, and 1,3-alternate 25,27-bis[1-(2-ethyl)hexyl]- and 25,27-bis[1-(2-tert-butoxy) ethyl] calyx [4] arene crown-6 conformers as potential selective cesium extractants. J. Org. Chem, 2000. 65: p. 8283–8289.

50. V.S. Talanov, G.G. Talanova, R.A. Bartsch, New proton-ionizable, cesium-selective calyx [4] arene-bis (crown-6-ethers) with markedly enhanced extraction efficiency. Tetrahedron Lett., 2000. 41: p. 8221–8224.

51. V.S. Talanov, G.G. Talanova, M.G. Gorbunova, R.A. Bartsch, Novel caesium-selective, 1,3-alternate calix[4] arene-bis (crown-6-ethers) with proton-ionizable groups for enhanced extraction efficiency J. Chem. Soc.-Perkin Trans.2, 2002. 2: p. 209-215.

52. M.G. Gorbunova, P.V. Bonnesen, N.L. Engle, E. Bazelaire, L.H. Delmau, B.A. Moyer, New amino–functionalized 1,3-alternate calix[4] arene bis- and mono-(benzo-crown-6 ethers) for pH-switched cesium nitrate extraction. Tetrahedron Lett., 2003. 44: p. 5397-5401.

53. E. Bazelaire, M.G. Gorbunova, P.V. Bonnesen, B.A. Moyer, L.H. Delmau, PH-Switchable cesium nitrate extraction with calix[4]arene mono and bis(benzo-crown-6) ethers bearing amino functionalities Solvent Extraction and Ion Exchange, 2004. 22: p. 637–661.

54. B.W. Harmon, D.D. Ensor, L.H. Delmau, B.A. Moyer, Extraction of cesium by a calix[4]arene–crown–6 ether bearing a pendant amine group. Solvent Extraction and Ion Exchange, 2007. 25: p. 373-388.

55. N. Sieffert, G. Wipff, Comparing an ionic liquid to a molecular solvent in the cesium cation extraction by a calixarene: A molecular dynamics study of the aqueous interfaces. J. Phys. Chem. B, 2006. 110: p. 19497–19506.

56. N. Sieffert, A. Chaumont, G. Wipff, Importance of the liquid–liquid interface in assisted ion extraction: new molecular dynamics studies of cesium picrate extraction by a calix[4]arene. J. Phys. Chem.C, 2009. , 113: p. 10610–10622.

57. H.M. Luo, S. Dai, P.V.Bonnesen, Solvent extraction of Sr 2+ and Cs + based on roomtemperature ionic liquids containing monoaza–substituted crown ethers. Anal. Chem., 2004. 76: p. 2773–2779.

58. H.M. Luo, S. Dai, P.V. Bonnesen, A.C. Buchanan, J.D. Holbrey, N.J. Bridges, R.D. Rogers, Extraction of cesium ions from aqueous solutions using calix[4]arene-bis(tert-octylbenzocrown-6) in ionic liquids. Anal. Chem., 2004. 76: p. 3078–3083.

59. C. Xu, L.Y. Yuan, X.H. Shen, M.L. Zhai, Efficient removal of caesium ions from aqueous solution using a calix crown ether in ionic liquids: mechanism and radiation effect. Dalton Trans., 2010. 39: p. 3897–3902.

60. F. Xiaogui, J. Shan, W. Qiulin, C.Jing, S. Chongli, Thermal decomposition of Potassium Titanium Hexacyanoferrate(II) loaded with cesium in a fixed bed calciner. Chin. J. Chem. Eng., 2007. 15: p. 184-189

61. J. Lehto, R. Harjula, H. Mimura, Selective Removal of Cesium from Simulated High-Level Liquid Wastes by Insoluble Ferrocyanides. J. Nuc. Sci.and Technol, 1993. 28: p. 2479-2506.

62. P.A. Hass, A Review of Information on Ferrocyanide Solids for Removal of Cesium from solutions. Sep. Sci. Technol., 1993. 28: p. 2479-2506.

63. K. N. Brewer, D. J. Wood, P. A. Tullock, L. G. Olson, A. L. Olson T. A. Todd,, Evaluation and Testing of Inorganic Ion Exchange Sorbents for the Removal of Cesium-137 from Idaho Chemical Processing Plant Acidic Tank Waste. Sep. Sci. Technol., 2001. 36: p. 999-1016.

64. C. L. Neskovic, S. Ayrault, V. Badillo, B. Jimenez, E. Garnier, M. Fedoroff, D. J. Jones, B. Merinov, Structure of copper-potassium hexacyanoferrate (II) and sorption mechanisms of cesium. Journal of Solid State Chemistry 2004. 177: p. 1817–1828.

65. J. Orechovskh, P. Rajec, Sorption of cesium on composite sorbents based on nickel ferrocyanide. J. Radioanal. Nucl. Chem., 1999. 242: p. 387-390.

66. J. Lehto, R. Harjula, H. Mimura, Ion Exchange of Cesium on Potassium Nickel Hexacyanoferrate(II)s. J. Nucl.Sci. and Technol., 1997. 34: p. 484-489.

67. B. Bartos, B. Filipowicz, M. Łyczko, A. Bilewicz, Adsorption of 137Cs on titanium ferrocyanide and transformation of the sorbent to lithium titanate: a new method for long term immobilization of 137 Cs. J. Radioanal. Nucl. Chem., 2014. 302: p. 513–516.

68. J. Rais, B. Million V. Kourim, Exchange properties of complex cyanides—I: Ion exchange of caesium of ferrocyanides. J. Inorg. Nucl. Chem., 1964. 26: p. 1111-1115.

69. J. Lehto, R. Harjula, H. Mimura, Chemical and Thermal Stability of Potassium Nickel Hexacyanoferrate(II). J. Nuc.Sci. and Technol., 1997. 34: p. 582-587.

70. F. Sebesta, Composite Sorbents of Inorganic Ion-Exchangers and Polyacrylonitrile Binding Matrix. I. Methods of Modification of Properties of Inorganic Ion-Exchangers for Application in Column Packed Beds. J. Radioanal. Nucl. Chem., 1997. 220: p. 77-88.

71. R. G. Dosch, D. Gu, C. V. Philip, R. G. Anthony, Use of Silicotitanates for Removing Cesium and Strontium from Defense Waste. Ind. Eng. Chem. Res., 1994. 33: p. 2702-2705.

72. K.A. Venkatesan, V. Sukumaran, M.P. Antony, T.G. Srinivasan, Studies on the feasibility of using crystalline silicotitanates for the separation of cesium-137 from fast reactor high-level liquid waste. J. Radioanal. Nucl. Chem. , 2009. 280: p. 129–136.

73. N. R. Mann, T. A. Todd, Removal of Cesium from Acidic Radioactive Tank Waste Using IONSIV IE-91. Sep. Sci.Technol., 2005. 39: p. 2351-2371.

74. C. Dwivedi, S. K.Pathak, M. Kumar, S.C. Tripathi, P.N. Bajaj, Removal of cesium by spherical resorcinol–formaldehyde resin beads: Sorption and kinetic studies. J. Radioanal. Nuc. Chem., 2013. 297: p. 1–8.

75. Dwivedi, Charu Kumar, Amar Ajish, Juby K.Singh, Krishan Kant Kumar, Manmohan Wattal, Piaray Kishen Bajaj, Parma Nand, Resorcinol-formaldehyde coated XAD resin beads for removal of cesium ions from radioactive waste: synthesis, sorption and kinetic studies. RSC Advances, 2012. 2(13).

76. F. Sebesta, Composite ion-exchanger with ammonium molybdophosphate and its properties. J. Radioanal. Nucl. Chem., 1990. 140: p. 15-21.

77. T.J. Tranter, R.S. Herbst, T.A. Todd, A.L. Olson, H.B. Eldredge, Evaluation of ammonium molybdophosphate-polyacrylonitrile AMP-PAN as a cesium selective sorbent for the removal of 137 Cs from acidic nuclear waste solutions. 2002. 6: p. 107-121.

78. T.A.Todd, N.R. Mann, T.J. Tranter, F. Šebesta, J. John, A. Motl, Cesium sorption from concentrated acidic tank wastes using ammonium molybdophosphate-polyacrylonitrile composite sorbents. Journal of radioanalytical and nuclear chemistry, 2002. 254: p. 47-52.

79. K.N. Brewer, AMP-PAN Column Testing with Actual INEEL High Activity Wastes. Czech Journal of Physics, 1999. 49: p. 959-964.

80. A. I. Bortun, L.N. Bortun, A.A. Stepin, N.P. Pekhamkina, Cs-137 Sorption on Granular Inorganic Ion-Exchangers based on Titanium and Zirconium Hydroxophosphates. J. Radioanal. Nuc. Chem. , 1993. 174: p. 279-289.

81. T. Moller, A. Clearfield, R. Harjula, Preparation of hydrous mixed metal oxides of Sb, Nb, Si, Ti and W with a pyrochlore structure and exchange of radioactive cesium and strontium ions into the materials. Microporous and Mesoporous Materials, 2002. 54: p. 187-199.

82. J. Narbutt, A. Bilewicz, B. Bartos, Composite Ion-Exchangers - Prospective Nuclear Applications. J. Radioanal. Nuc. Chem., 1994. 183: p. 27-32.

83. Yamazaki, Inoue, Airano, Studies of hydrous Silicon-Titanium (IV) oxide Ion Exchanger. III. The rate of the isotopic exchange of Na(+) and Cs(+) ions between the exchanger in the relevant ionic form and aqueous solutions. Solvent Extraction Ion Exchange, 1995. 13: p. 157.

84. Puziy, Cesium and Strontium Exchange by the Framework Potassium Titanium Silicate K3Ti4O4(SiO4)3.4H2O, . J. Radioanal. Nuc. Chem., 1998. 237: p. 73-79.

85. K. Lv, L. P. Xiong, Y.M. Luo, Ion exchange properties of cesium ion sieve based on zirconium molybdopyrophosphate. Colloids and Surfaces A: Physicochem. Eng. Aspects 2013. 433: p. 37– 46.

86. G.S. Murthy, M.V. Sivaiah, S.S. Kumar, V.N. Reddy, R.M. Krishna, S. Lakshminarayana, Adsorption of cesium on a composite inorganic exchanger zirconium phosphate-ammonium molybdophosphate. Journal of radioanalytical and nuclear chemistry, 2004. 260(1): p. 109-114.

87. E. Glueckauf, Electrodeionization through a packed bed. Brithish Chemical Engineering, 1959. 4: p. 646-651.

88. D.B. Richard, J. D. Kerber, Concepts, Instrumentation and Techniques in Atomic Absorption Spectrophotometry. THE PERKIN-ELMER CORPORATION.

89. M. Birkholz, Thin Film Analysis by X-Ray Scattering, ed. V.V.G. Co., Weinheim: WILEY.

90. http://mmrc.caltech.edu/FTIR/FTIRintro.pdf.

91. D.A. Cowan, J.H. Brown, Effect of turbulence on limiting current in electrodialysis cells. Ind. Eng. Chem., 1959. 51: p. 1445–1448.

92. P.A. Hass, A review of infomation on ferrocyanide solids for the removal of cesium from solutions. Sep. Sci. Technol., 1993. 28: p. 2479-2506.

93. K. Shakir, M. Sohsah, M. Soliman, Removal of cesium from aqueous solutions and radioactive waste simulants by coprecipitateflotation. Sep. Sci. Technol., 2007. 54: p. 373–381.

94. E. Makrlík, P. Vaňura, Synergistic extraction of some univalent cations into nitrobenzene by using cesium dicarbollylcobaltate and dibenzo-30-crown-10. Journal of Radioanalytical and Nuclear Chemistry, 2013. 295(2): p. 911-914.

95. M.G. Jalhoom, I.A. Mani, J.A. Hassan, Extration of sodium and some fission produdts with crown ethers. 38(4): p. 219-222.

96. P. Rajec, K. Domianová, Cesium exchange reaction on natural and modified clinoptilolite zeolites. Journal of Radioanalytical and Nuclear Chemistry, 2008. 275(3): p. 503-508.

97. B. Yıldız, H.N. Erten, M. Kış, The sorption behavior of Cs + ion on clay minerals and zeolite in radioactive waste management: sorption kinetics and thermodynamics. Journal of Radioanalytical and Nuclear Chemistry, 2011. 288(2): p. 475-483.

98. A. Bilewicz, R. Dybczynski, J. Narbutt, Ion exchange of alkali metals on hydrous titanium dioxide in neutral and alkaline solutions. Journal of Radioanalytical and Nuclear Chemistry Articles, 1991. 148(2): p. 359-371.

99. V.N, L., M. N.A, R. A.V, Sorption of cesium on titanium and zirconium phosphates. 2003. 45(2): p. 149-151.

100. J. Narbutt, J. Siwinski, B. Bartos, A. Bilewicz, Studies on new titanium hexacyanoferrate sorbents for radiocesium removal from primary coolant of pressurized water reactors. Journal of Radioanalytical and Nuclear Chemistry Articles, 1986. 101(1): p. 41-49.

101. C. Loos-Neskovic, S. Ayrault, V. Badillo, V. Jimenez, B. Garnier, E. Fedoroff, M. Jones, D. J. Merinov, B. Structure of copper-potassium hexacyanoferrate (II) and sorption mechanisms of cesium. Journal of Solid State Chemistry, 2004. 177(6): p. 1817-1828.

102. J. Orechovská, P. Rajec, Sorption of cesium on composite sorbents based on nickel ferrocyanide. Journal of radioanalytical and nuclear chemistry, 1999. 242(2): p. 387-390.

103. T.A. Todd, V.N. Romanovskiy, A Comparison of Crystalline Silicotitanate and Ammonium Molybdophosphate-Polyacrylonitrile Composite Sorbent for the Separation of Cesium from Acidic Waste. Radiochemistry, 2005. 47(4): p. 398-402.

104. K.A. Venkatesan, V. Sukumaran, M.P. Antony, T.G. Srinivasan Studies on the feasibility of using crystalline silicotitanates for the separation of cesium-137 from fast reactor high-level liquid waste. Journal of Radioanalytical and Nuclear Chemistry, 2009. 280(1): p. 129-136.

105. C. Dwivedi, S. K. Pathak, M. Kumar, S.C. Tripathi, P.N. Bajaj, Removal of cesium by spherical resorcinol–formaldehyde resin beads: Sorption and kinetic studies. Journal of Radioanalytical and Nuclear Chemistry, 2013. 297(1): p. 1-8.

106. F. Sebesta, Composite ion exchanger with ammonium molybdophosphate and its properties. J. Radioanal. Nucl. Chem. , 1990. 140: p. 15-21.

107. F. Sebesta, Composite sorbents of inorganic ion-exchangers and polyacrylonitrile binding matrix I. Methods of modification of properties of inorganic ion-exchangers for application in column packed beds. J. Radioanal. Nucl. Chem., 1997. 220: p. 77-88.

108. Y. Park, Y.C. Lee, W.S. Shin, S.J. Choi, Removal of cobalt, strontium and cesium from radioactive laundry wastewater by ammonium molybdophosphate–polyacrylonitrile (AMP–PAN). Chemical Engineering Journal, 2010. 162(2): p. 685-695.

109. M. Suss, F.P., Investigation of the sorption ofcesium from acidic solutions by various inorganic sorbents. Radiochemica Acta, 1981. 29: p. 33-40.

110. A. Nilchi, R. Saberi, M. Moradi, H. Azizpour, R. Zarghami, Evaluation of AMP–PAN composite for adsorption of Cs+ ions from aqueous solution using batch and fixed bed operations. Journal of Radioanalytical and Nuclear Chemistry, 2012. 292(2): p. 609-617.

111. T.J. Tranter, R.S. Herbst, T.A. Todd, A.L. Olson, H.B. Eldredge, Application of a second order kinetic model for the preliminary design of an adsorption bed system using ammonium molybdophosphate–polyacrylonitrile for the removal of 137 Cs from acidic nuclear waste solutions. Advances in Environmental Research, 2003. 7(4): p. 913-923.

112. T. J. Tranter, R.S.Herbst, T. A. Todd, Determination of a solid phase mass transfer coefficient for modeling an asorption bed system using ammonium molybdophospahte-polyacrylonitrile (AMP-PAN) as a sorbent for the removal of 137 Cs from acidic nuclear waste solutions. Adsorption 2002. 8: p. 291-299.

113. C. J. Miller, A.L. Olson, C.K. Johnson, Cesium absorption from acidic solutions using ammonium molybdophosphate on a polyacrylonitrile support (AMP-PAN). Separation science and technology, 1997. 32(1-4): p. 37-50.

114. K. Naddafi, R. Nabizadeh, R. Saeedi, A. Mahvi, V. Hossein, Y. Forough. F. Yaghmaeian, A. Ghasri, S. Nazmara, Biosorption of lead(II) and cadmium(II) by protonated Sargassum glaucescens biomass in a continuous packed bed column. Journal of Hazardous Materials, 2007. 147(3): p. 785-791.

115. O. Hamdaoui, Dynamic sorption of methylene blue by cedar sawdust and crushed brick in fixed bed columns. Journal of Hazardous Materials, 2006. 138(2): p. 293-303.

116. O. Hamdaoui, Removal of copper(II) from aqueous phase by Purolite C100-MB cation exchange resin in fixed bed columns: Modeling. Journal of Hazardous Materials, 2009. 161(2-3): p. 737-746.

117. L. Boguslavsky, S. Margel, Poly(acrylonitrile) mcirospheres with a narrow size distribution: synthesis by sing-step swelling and properties. Glass Phys. Chem. , 2005. 31: p. 102–114.

118. M.H. Alizadeh, H. Eshtiagh-Hosseini, M. Mirzaei, A.R. Salimi, H. Razavi, Synthesis, X-ray crystallography characterization, vibrational spectroscopy, and DFT theoretical studies of a new organic-inorganic hybrid material. Struct. Chem., 2008. 19: p. 155–164.

119. A. Nilchi, M.R. Hadjmohammadi, S. Rasouli Garmarodi, R.Saberi, Studies on the adsorption behavior of trace amounts of 90Sr2, 140La3, 60Co2, Ni2 and Zr4 cations on synthesized inorganic ion exchangers. J. Hazard. Mater. , 2009 167: p. 531-535.

120. M. Feng, W. Li, Y. Zhao, C. Liu, Z. Chen, L.Yan, G. Tian, H. Wang, S. Li,Synthesis and characterization of a new activated carbon supported ammonium molybdophosphate composite and its cesium-selective adsorption properties. Radiochimica Acta, 2010. 98(1).

121. B. Ali Fil, R. Boncukcuoglu, A.E. Yilimaz, S. Bayar, Adsorption of Ni on ion exchange resin: Kinetics, equilibrium and thermodyanic studies. Korean J. Chem. Eng., 2012. 29: p. 1232-1238.

122. V. Ponnusami, S.Vikram, S.N. Srivastava, Guava(Psidium guajava) leaf powder: Novel adsorbent for removal of methylene blue from aqueous solutions. Journal of Hazardous Materials, 2008. 152: p. 276-286.

123. S. Wang, H. Li, Kinetic modeling and mechanism of dye adsorption on unburned carbon. Dyes and Pigments, 2007. 72: p. 308-314.

124. S. Lagergren, About the theory of so called adsorption of solutble substances. Kungliga Svenska Vetenskapsakademiens Handlingar 1898. 24: p. 1-39.

125. Y. Ho, G. Mckay, Pseudo-second order model for sorption processes. Process Biochem., , 1999. 34: p. 451–465.

126. W.J. Weber, J.C. Morris, Kinetic of adsorption on carbon from solution. J.Sanit. Eng. Div. Am. Soc. Civ. Eng., 1963(89): p. 31-60.

127. V. Sivasankar, S. Murugesh, S. Rajkumar, A. Darchen, Cerium dispersed in carbon (CeDC) and its adsorption behavior: A first example of tailored adsorbent for fluoride removal from drinking water. Chemical Engineering Journal, 2013. 214(0): p. 45-54.

128. F. Helfferich, Ion exchagne, Mc Graw-Hill, New York, 1962.

129. N. Hanen, O. Abdelmottaleb, Modeling of the dynamics adsorption of phenol from an aqueous solution on activated carbon produced from olive stones. J. Chem. Eng. Process Technol. , 2013. 4.

130. H.C. Thomas, Heterogeneous ion exchange in flowing system. J. Am. Chem. Soc. , 1944. 66 p. 1664–1666.

131. D.M. Saad, E. Cukrowska, H. Tutu, Column adsorption studies for the removal of U by phosphonated cross-linked polyethylenimine: Modeling and optimization. Appl. Water Sci., 2014.

132. G. Bohart, E.Q. Adams, Some aspects of the behavior of charcoal with respect to chlorine. J. Am. Chem. Soc., 1920. 42 p. 523–544.

133. L. Alvarado, A. Chen, Electrodeionization: Principles, Strategies & Applications. Electrochimica Acta, 2014. 132: p. 583-597.

134. E. Korngold, Electrodialysis processes using Ion exchange resins between membranes. Desalination, 1975. 16: p. 225-233.

135. N. Meyer, W.J.P., P.J. Van Geel, M. Adiga, Development of an electrodeionization process for removal of nitrate from drinking water. Part I. Single species testing. Desalination, 2005. 175 p. 153-165.

136. Y.S. Dzyazko, V.N. Belyakov, Purification of a diluted nickel solution containing nickel by a process combining ion exchange and electrodialysis. Desalination, 2004. 162: p. 179-189.

137. O. Arara, U.Y., N. Kabay, M. Yuksel, Various applications of electrodeionization (EDI) method for water treatment-A short review. Desalination, 2014. 342: p. 16–22.

138. C. Forgacs, N.I., J. Leibovitz, J. Sinkovic,, K.S. Spiegler, Polarization at ion-exchange membranes in electrodialysis. Desalination, 1972. 10: p. 181-214.

139. M. Taky, G.P., F. Lebon, C. Gavach Polarization phenomena at the interfaces between an electrolyte solution and an ion exchange, Part I. Ion transfer with a cation exchange membrane. J. Electroanal. Chem., 1992. 336: p. 171-194.

140. I. Rubinstein, L. Shtilman, Voltage against current curves of cation exchange membrane. J. Chem. Soc., Faraday Trans. II 1979(75): p. 231-246.

141. J.J. Krol, M. Wessling, H. Strathmann, Concentration polarization with monopolar ion- exchange membranes: current-voltage curves and water dissociation. J. Membr. Sci. , 1999. 162: p. 145-154.

142. J.H. Choi, H.J. Lee, S.H. Moon, Effects of electrolytes on the transport phenomena in a cation-exchange membrane. J. Colloid and Interface Sci., 2001. 238: p. 188-195.

143. Y. Kim, D.F. Lawler, Overlimiting current by interactive ionic transport between space charge region and electric double layer near ion-exchange membranes. Desalination, 2012. 285: p. 245-252.

144. Y. Ervan, I.G.Wensten, Study on the influence of applied voltage and feed concentration on the performance of electrodeionization. Songklanakarin J. Sci. Technol., 2002. 24: p. 955-963.

145. V. Fíla, K.B., The effect of convection in the external diffusion layer on the results of a mathematical model of multiple ion transport across an ion selective membrane. J. Appl. Electrochem., 2008. 38: p. 1241-1252.

146. K. Bouhidel, A.Lakehal, Influence of voltage and flow rate on electrodeionization (EDI) process efficiency. Desalination 2006. 193: p. 411–421.

147. J.S. Park, T.C.C., H.G.L. Coster, S.H. Moon, Characterization of BSA-fouling of ion-exchange membrane systems using a subtraction technique for lumped data. jounal of membrane science, 2005. 246(2): p. 137-144.

148. B.A. Cooke, Concentration polarization in electrodialysis. 1. The electrometric measurement of interfacial concentration. Electrochimica Acta, 1961. 3: p. 307–317.

149. N.W. Rosenberg, C.E.T., Limiting currents in membrane cell. industrial & Engineering Chemistry 1957. 49: p. 780–784.

150. H.J. Lee, H.Strathmann, S.H. Moon, Determination of the limiting current density in electrodialysis desalination as an empirical function of linear velocity. Desalination, 2006. 190 p. 43–50.

151. L. Alvarado, I.R. Torres, A. Chen, Integration of ion exchange and electrodeionization as a new approach for the continuous treatment of hexavalent

chromium wastewater. Separation and Purification Technology, 2013. 105: p. 55-62.

152. D.A. Cowan, J.H. Brown, Effect of turbulence on limiting current in electrodialysis cells. Industrial & Engineering Chemistry, 1959. 51: p. 1445–1448.

153. K.H. Yeon, J.H. Song, S.H. Moon, A study on stack configuration of continuous electrodeionization for removal of heavy metal ions from the primary coolant of a nuclear power plant. Water Research, 2004. 38(7): p. 1911-1921.

154. H.J. Lee, J.H. Song, S.H. Moon, Comparison of electrodialysis reversal (EDR) and electrodeionization reversal (EDIR) for water softening. Desalination, 2013. 314: p. 43-49.

155. A. Abou-Shady, C. Peng, O.J. Almerira, H. Xu, Effect of pH on separation of Pb (II) and NO3− from aqueous solutions using electrodialysis. Desalination, 2012. 285: p. 46-53.

156. J.H. Song, K.H. Yeon, S.H. Moon, Effect of current density on ionic transport and water dissociation phenomena in a continuous electrodeionization (CEDI). Journal of Membrane Science, 2007. 291(1-2): p. 165-171.

157. H. Strathmann, Electrodialysis, a mature technology with a multitude of new applications. Desalination, 2010. 264: p. 268-288.

158. T. Xu, C. Huang, Electrodialysis-based separation technologies-A critical review. AIChE Journal, 2008. 54: p. 3147-3159.

159. V.A. Shaposhnik, N.N. Zubets, I,P. Strygina, B.E. Mill, High demineralization of drinking water by electrodialysis without scaling on the membranes. Desalination, 2002. 145(1): p. 329-332.

160. V.A. Shaposhnik, K. Kesore, An early history of electrodialysis with permselective membranes. Journal of Membrane Science, 1997. 136: p. 35-39.

161. M.C. Sauer, P.F.S., K.S. Spiegler, M.R.J. Wyllie, Electrical conductance of porous plugs. Ind. Eng. Chem. , 1955. 47: p. 2187– 2193.

162. K.S. Spiegler, R.L. Yoest, M.R.J. Wyllie, Electrical potentials across porous plugs and membranes. Ion-exchange resin-solution systems. Discussions of the Faraday Society, 1956. 21.

163. F. Helfferich, Ion-exchange columns.Ion Exchange. 1962, New York: McGraw-Hill Book Company.

164. P.B. Spoor, W.R. Ter Veen, L.J.J. Janssen, Electrodeionization 1: migration of nickel ions absorbed in a rigid, macroporous cation-exchange resin. Journal of Applied Electrochemistry, 2001. 31(5): p. 523-530.

165. P.B. Spoor, W.R. Ter Veen, L.J.J. Janssen, Electrodeionization 2: The migration of nickel ions absorbed in a flexible ion-exchange resin. Journal of applied electrochemistry, 2001. 31(10): p. 1071-1077.

166. P.B. Spoor, L. Koene, W.R. Ter Veen, L.J.J. Janssen, Electrodeionisation 3: The removal of nickel ions from dilute solutions. Journal of applied electrochemistry, 2002. 32(1): p. 1-10.

167. P.B. Spoor, L. Koene, L.J.J. Janssen, Potential and concentration gradients in a hybrid ion-exchange/electrodialysis cell. Journal of applied electrochemistry, 2002. 32(4): p. 369-377.

168. P.B. Spoor, L. Koene, W.R. Ter Veen, L.J.J. Janssen, Continuous deionization of a dilute nickel solution. Chemical Engineering Journal, 2002. 85(2): p. 127-135.

169. Y.S. Dzyazko, Purification of a diluted solution containing nickel using electrodeionization. Desalination, 2006. 198(1-3): p. 47-55.

170. Y.S. Dzyazko, L.N. Ponomaryova, L.M. Rozhdestvenskaya, S.L. Vasilyuk, V.N. Belyakov, Electrodeionization of low-concentrated multicomponent

Ni2+containing solutions using organic-inorganic ion-exchanger. Desalination 2014. 342: p. 43-51.

171. A. Mahmoud, L. Muhr, S. Vasiluk, A. Aleynikoff, F. Lapicque, Investigation of transport phenomena in a hybrid ion exchange-electrodialysis system for the removal of copper ions. Journal of applied electrochemistry, 2003. 33(10): p. 875-884.

172. A. Mahmoud, A.F.A. Hoadley, An evaluation of a hybrid ion exchange electrodialysis process in the recovery of heavy metals from simulated dilute industrial wastewater. Water Research, 2012. 46(10): p. 3364-3376.

173. Ch. Mahendra, P.M.S. Satya Sai, C. Anand Babu, Current-voltage characteristics in a hybrid Electrodialysis- Ion exchange system for the recovery of Cesium ions from Ammonium Molybdophosphate-Polyacrylonitrile. Desalination, 2014. 353: p. 8-14.

174. V.V. Nikonenko, A.V. Kovalenko, M.K. Urtenov, N.D. Pismenskaya, J. Han, P. Sistat, G. Pourcelly, Desalination at overlimiting currents: State of the art and perspectives. Desalination 2014. 342: p. 85-106.

175. K.H. Yeon, S.H. Moon, A study on removal of cobalt from a primary coolant by continuous electrodeionization with various spacers. Sep. Sci. and Tech., 2003. 38 p. 2347-2371.

176. J.H. Song, K.H. Yeon, S.H. Moon, Transport characteristics of Co2+ through an ion exchange textiles in a continous electrodeionization (CEDI) system unsdr electro-regenreation. Sep. Sci and Tech. , 2004. 39: p. 3601-3619.

177. K.S. Spiegler, R.L. Yoest, M.R.J. Wyllie, Electrical potentials acrossporous plugs and membranes, ion-exchange resin-solution system. Discussions Faraday Soc. , 1956. 21: p. 174 –183.